2016

On Full Scale Slamming Testing of High-Speed Boats

Robert Skoglund Thodal
Lehigh University

On Full Scale Slamming Testing of High-Speed Boats

By

Robert S Thodal

Presented to the Graduate and Research Committee

of Lehigh University

in Candidacy for the Degree of

Doctor of Philosophy

In

Mechanical Engineering

Lehigh University

January, 2016

December, 22 2015

Approved and recommended for acceptance as a dissertation in partial fulfillment of the requirements for the degree of Doctor of Philosophy.

_____

Date

_____

Accepted Date

_____
Dr. Joachim L. Grenestedt, Dissertation Advisor, Committee Chairman
Professor
Department of Mechanical Engineering and Mechanics

Committee Members:

_____
Dr. D. Gary Harlow
Professor, Department Chair
Department of Mechanical Engineering and Mechanics

_____
Dr. Herman F. Nied
Professor
Department of Mechanical Engineering and Mechanics

_____
Dr. Justin Jaworski
Assistant Professor
Department of Mechanical Engineering and Mechanics

_____
Yue Yu
Assistant Professor
Department of Mathematics

Acknowledgements

I would like to thank all the faculty and staff of the Department of Mechanical Engineering and Mechanics. They have always been willing to offer their help and expertise throughout my undergraduate and graduate education.

I consider myself extremely fortunate to have worked with all the great people in the Lehigh Composites Lab. I owe thanks to my fellow students and friends including Jack Reany, Andrew Truxel, Scott Shirey, Brett Snowden, Jian Lv, Tianyi Liu, Kevin Curran, Jake Patterson and Scott Larson. I am in debt to Engineer Bill Maroun for his time and patience working with me over the years. Bill's ability to find creative solutions to engineering problems has been illuminating and instrumental in many of my achievements academically and otherwise.

I am especially grateful to my Ph.D advisor Professor Joachim Grenestedt. His knowledge and passion in the theory and execution of engineering have been an inspiration. The skills and experience I have gained from working under his guidance are the greatest strengths of my education.

Finally, I would like to thank the Office of Naval Research and program monitor Dr. Roshdy Barsoum for their support of my research.

Contents

1. Abstract 1
2. Introduction 3
3. Conclusions 15
4. Future Work 17
5. On Stiff Versus Compliant Bottom Panels of High Speed Craft 18
6. Experimental Study of Slamming on High-Speed Craft Operating in the Atlantic 27
7. Analysis of Bottom Panel Slamming Using the Wavelet Transform 64
8. Validation of High Fidelity CFD/FE FSI for Full-Scale High-Speed Planing Hull With Composite Bottom Panels Slamming 95
9. Works Cited 126
10. Vita 132

Tables

Table 5-1: Results from slamming tests in the Atlantic 23
Table 6-1:Bottom panel layup details (top to bottom, 0° parallel to keel). The materials used in the bottom were Owens Corning double bias glass fiber fabric DB240 (840 g/m2), Devold AMT carbon fiber fabrics DBL 700 (620 g/m2) and L(X) 440 (434 g/m2), and Divinycell H250 foam core ($250\ \mathrm{kg/m^3}$). 35
Table 6-2 Bay 4 panel eigenfrequencies 48
Table 6-3 NOAA wave buoy 44066 data, WVHT=Significant wave height, MWD= Mean wave direction of waves at dominant period, DPD= dominant wave period 50
Table 6-4 Comparison of Observed and Calculated Panel Vibration Frequencies for Bay 4 Panels (Mode 2) 59
Table 7-1: Dry modal frequencies 82
Table 7-2: Predicted wet mode eigenfrequencies 92
Table 8-1 Literature review for slamming studies 111
Table 8-2 Slamming load test facility bay 4 bottom panel layup 112
Table 8-3 Regular wave model parameters 112
Table 8-4 Average port/starboard 1/3 highest slamming events parameters (experiments) 112
Table 8-5 Frequencies associated with the first three modes of the starboard panel 112
Table 8-6 Frequencies associated with the first three modes of the port panel 112
Table 8-7 Average port/starboard slamming strains (CFD/FE) 113

Figures

Figure 2-1: Slamming of a V Bottom Hull....3
Figure 5-1: The Numerette slamming boat. The section behind the colored bow is the one presently studied....20
Figure 5-2: Port and starboard bottom panels, stainless steel longerons, bulkhead, and bottom sensors (pressure sensors, accelerometers, strain gages, LVDT's)....21
Figure 5-3:Speed and heading during recent tests in the Atlantic. 22
Figure 5-4:Sketch of where the measurements presented where taken.....22
Figure 5-5 Top: normal probability distributions of displacements and strains. Bottom: peak displacements and strains, ordered from largest to smallest. 24
Figure 5-6: FFT of port and starboard displacements....25
Figure 6-1: Slamming load test facility boat 31
Figure 6-2: Composite sandwich panel with strain gages 32
Figure 6-3:Strain gage paddles bonded to PVC foam core 33
Figure 6-4:Bottom panel strain gage locations and orientation....36
Figure 6-5 Steel structure strain gage locations 36
Figure 6-6: PXI Instrumentation....37
Figure 6-7: Compact DAQ Instrumentation 37
Figure 6-8 Static load test fixture....39
Figure 6-9 Static Load Test LVDTs 39
Figure 6-10 Static load test grid 39
Figure 6-11 Image from cockpit mounted camera taken during Atlantic testing 43
Figure 6-12 Bay 4 panel static stiffness ratios port/starboard 45
Figure 6-13 Bay 4 port accelerance FRF....46
Figure 6-14 Bay 4 Starboard accelerance FRF....46
Figure 6-15 Bay 4 port panel mode 1....47
Figure 6-16 Bay 4 port panel mode 2....47
Figure 6-17 Bay 4 port panel mode 3....47
Figure 6-18 Bay 4 port panel mode 4....47
Figure 6-19 Bay 4 port panel mode 5....47
Figure 6-20 Typical strain gage time history for sea testing 48
Figure 6-21 Strain response, single slamming event 49
Figure 6-22 Test tracks....50
Figure 6-23 Distribution of heading and speed 51
Figure 6-24 Test segments identified as head and following seas 51
Figure 6-25: Largest 3rd Peak Strain Waveforms and mean bay 4 port transverse strain in head seas 52

Figure 6-26: Largest 3rd Peak Strain Waveforms and mean bay 4 starboard transverse strain in head seas 52
Figure 6-27: Largest 3rd Peak Strain Waveforms and mean bay 4 port transverse strain in following seas 52
Figure 6-28: Largest 3rd Peak Strain Waveforms and mean bay 4 starboard transverse strain in following seas 52
Figure 6-29: Forward speed vs bay 4 port mean peak 3rd transverse strain in head and following seas 53
Figure 6-30: Forward speed vs bay 4 starboard mean peak 3rd transverse strain in head and following seas 53
Figure 6-31 Roll angle vs bay 4 port transverse strain 53
Figure 6-32 Roll angle vs bay 4 starboard transverse strain 53
Figure 6-33 LCG vertical acceleration vs bay 4 port transverse strain 54
Figure 6-34 LCG Vertical acceleration vs bay 4 starboard panel transverse strain 54
Figure 6-35 Vertical velocity vs peak bay 4 port transverse strain 55
Figure 6-36 Vertical velocity vs peak bay 4 starboard panel transverse strain 55
Figure 6-37 Peak transverse strains in bay 4 port and starboard panels in head seas 56
Figure 6-38 Peak transverse strains in bay 4 port and starboard panels in following seas 56
Figure 6-39 Bay 4 transverse strain head sea histogram 56
Figure 6-40 Bay 4 transverse strain following sea histogram 56
Figure 6-41 Bay 4 Panel Acceleration FFT 57
Figure 6-42 Bay 4 Panel Transverse Strain FFT 57
Figure 6-43 Transverse strain waveforms from highest 1% of slams in bay 4 port panel in head seas 58
Figure 6-44 Transverse strain waveforms from highest 1% of slams in bay 4 starboard panel in head seas 58
Figure 6-45 Peak transverse strains vs hydroelastic parameter R in bay 4 port bottom panel 60
Figure 6-46 Peak transverse strains vs hydroelastic parameter R in bay 4 starboard bottom panel 60
Figure 6-47 Characteristic velocity $\boldsymbol{c}$ vs peak transverse strains in bay 4 port bottom panel .. 60
Figure 6-48 Characteristic velocity $\boldsymbol{c}$ vs peak transverse strains in bay 4 starboard bottom panel 60
Figure 6-49 Rigid body-panel velocity differential vs peak transverse strains in bay 4 port bottom panel 61
Figure 6-50 Rigid body-panel velocity differential vs peak transverse strains in bay 4 starboard bottom panel 61
Figure 7-1:Slamming of a wedge shaped body 65
Figure 7-2: Numerette slamming test boat 75
Figure 7-3: Location of panel under test 76
Figure 7-4: Sandwich panel cross section with sensor locations 77

Figure 7-5: Test panel sensor locations 78
Figure 7-6: Test Panel 78
Figure 7-7: Dry accelerance frequency response function of mid panel accelerometer 80
Figure 7-8: Dry panel modes 81
Figure 7-9: Displacement, pressure, and acceleration time histories 83
Figure 7-10: Bay 4 mid panel acceleration and bay 2,3,4 mid panel transverse strain time histories 84
Figure 7-11: Pressure time histories at two locations 85
Figure 7-12: Fourier transform of mid panel acceleration 86
Figure 7-13: Continuous wavelet transform of mid panel acceleration signal 87
Figure 7-14: Cross sections of acceleration wavelet transforms at t=0.516s 87
Figure 7-15: Mode shapes observed at t=0.516s 89
Figure 7-16: Cross section of wavelet transform at t=0.7s 90
Figure 7-17: Mode shapes observed at t-0.7s 91
Figure 8-1: Slamming load test facility 113
Figure 8-2: Slamming load test facility sensor layout 113
Figure 8-3: CFD model of Numerette with detailed view of the sterndrive 114
Figure 8-4 FFT of panel pressure and strain (S1) 114
Figure 8-5 FFT of panel pressure and strain (S2) 114
Figure 8-6: FE model of a Bay 4 panel showing cored sandwich areas (blue), single skin areas (red) and hollow steel longeron (green) 115
Figure 8-7 Sea trajectory and speed with color mapping for time of the head wave segment 115
Figure 8-8 Sea trajectory and speed with color mapping for time of the following wave segment 115
Figure 8-9 1/3 highest slamming event pressure and strain experienced at the port panel of the head wave segment 116
Figure 8-10 1/3 highest slamming event pressure and strain experienced by the port panel of the following wave segment 116
Figure 8-11: Comparison of CFD and EFD results in calm water 117
Figure 8-12: Free surface and pressure distribution for calm water simulation at Fr = 2.1 and 2.7 117
Figure 8-13: Comparison of motions and resistance against USNA (CFD), USCG (EFD) and Fridsma (EFD) 118
Figure 8-14 Pressure, motions and wave elevation: S1 (left) and S2 (right) 118
Figure 8-15 Pressure distribution for re-entering and emerging slams of S1 119
Figure 8-16 Pressure distribution for re-entering and emerging slams of S2 119
Figure 8-17 Time-step verification: S1 (left) and S2 (right) 120
Figure 8-18 Comparison between CFD and experimental for S1 121
Figure 8-19 Comparison between CFD and experimental for S2 121

Figure 8-20 First three modes of the port panel in vacuum 121
Figure 8-21 First three modes of the port panel in air 122
Figure 8-22 First three modes of the port panel in water 122
Figure 8-23 First three modes of the starboard panel in vacuum 122
Figure 8-24 First three modes of the starboard panel in air 122
Figure 8-25 First three modes of the starboard panel in water 123
Figure 8-26 CFD/FE strains in vacuum and water for S1 123
Figure 8-27 CFD/FE strains in vacuum and water for S2 124
Figure 8-28 Comparison between CFD/FE and experimental strains for S1 124
Figure 8-29 Comparison between CFD/FE and experimental strains for S2 125

1. Abstract

This dissertation consists of four articles on the experimental investigation of slamming in high speed craft. The investigation utilizes data from the purpose-built 9 meter high-speed offshore research boat *Numerette.* The unique hybrid steel/composite construction and high-speed, high channel count instrumentation and data acquisition system have enabled collection of the wealth of experimental data that is analyzed in these articles.

In the first article the role of hull bottom panel stiffness in slamming is investigated. Two panels of differing construction are mounted on starboard and port on the Numerette, which is run at relatively high speeds in the Atlantic Ocean. Displacements of the two different panels are compared. The structural response under slamming loading is then compared with the behavior under static loading. It is shown that the static stiffness relationship is not directly reflected in the experimental slamming data; rather the relative response falls somewhere between the case of a static loading and the dynamic response of a simple mass-spring system.

In the second article, the structural response of bottom panels to slamming loads is investigated further. Experiments are described and results presented for modal and static analysis of the Numerette bottom panels in free air. Strain data is then presented from slamming experiments, investigating the influence of wave encounter conditions and vessel rigid body motions on response in the time and frequency domains.

The third article presents an analysis technique that uses the wavelet transform to provide insight into the behavior of marine structures subjected to slamming loads. Pressure, strain, acceleration and displacement data for an isolated slamming event are presented in the time

domain and in the frequency domain with Fourier transforms and wavelet transforms. Two periods of high acceleration are identified and using the wavelet transform are shown to be vibration at the dry and then wet eigenfrequencies. Mode shapes are identified during these two phases using data from an array of accelerometers. The optimal time-frequency resolution of the wavelet transform makes it a powerful tool in analyzing slamming data, revealing non-stationary behavior that the Fourier transform obscures. Identifying such behavior can be critical, in particular in hull structures with reduced stiffness where strong hydroelastic effects are expected.

The final article presents the validation of a high fidelity CFD/FE FSI code using data from *Numerette*. The CFD code CFDShip-Iowa and finite element solver Ansys are used. Hydrodynamic simulations are performed at a range of Froude numbers and sea conditions. Good agreement is shown with experimental data in calm seas. A one-way fluid structure interaction study is performed and strains show a qualitative agreement between numerical and experimental data.

These articles give insight to the designer of high speed craft by comparing the response of panels of varying, but relevant constructions to slamming loads. Additionally, the time-frequency analysis tool presented enables evaluation of structural response and identification of behavior that can be critical in slamming. Finally the collected data is used to validate a CFD/FE FSI code that could be used early in the design phase to optimize a structure and hull geometry under realistic conditions.

2. Introduction

Slamming or hydrodynamic impact is responsible for the highest loads on the bottoms of high speed craft. Slamming is the impact between a vessel's hull and the water surface that results from the pitching and forward motion of a vessel in rough seas.

This complex phenomenon is a major consideration in operation and design of high speed marine vehicles. Slamming loads are dependent on the sea conditions, vessel speed, wave encounter direction and the geometry and structural characteristics of the hull.

Slamming is characterized by dynamic loading where a large magnitude, high speed pressure peak travels over the hull from the keel to chine. The pressure peak is typically followed by a lower residual pressure over a large area. A simple cross section representation of slamming on a V-bottom is shown in Figure 2-1. Here the hull vertical velocity is v, the deadrise angle is β and the pressure $P(x,t)$ over the bottom is a function of position and time.

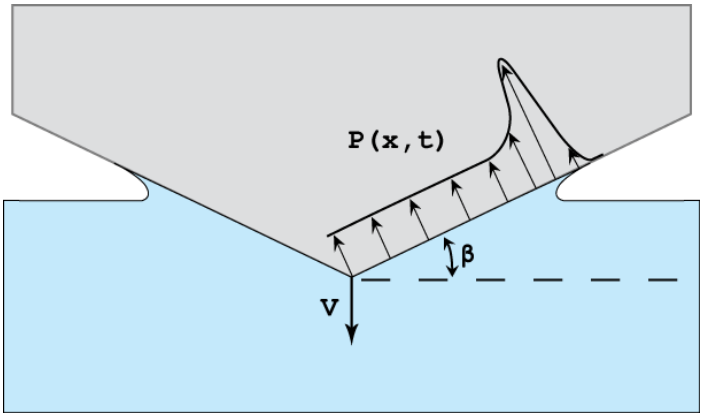

Figure 2-1: Slamming of a V Bottom Hull

In rough seas, the impact velocity can exceed 10 m/s. The resulting pressure on the hull structure can be enormous; up to 8 MPa was measured by Aarsnes [1] in impact testing. This dynamic loading of the bottom of high speed boats is often the factor that limits operation in rough seas. In addition to large vertical accelerations that can cause damage to equipment and payloads and injury to passengers, slamming impacts can often result in serious structural damage.

Designing ships for these loads is a challenging task. If the designer were to simply create a structure that could withstand these peak pressures evenly distributed over a bottom panel, then the ship would be immensely heavy and impractical. In practice, high peak pressures do not necessarily result in large stresses in the structure, e.g. [2]. With the design objectives of guaranteeing safety and durability while minimizing weight and cost a more sensible approach is needed.

Complex phenomena are at work in slamming making a comprehensive analysis difficult. Air cushioning, spray, shape of the water surface, compressibility of the water, cavitation etc. all complicate the event. Additionally, hydroelasticity can be a major factor. In this process, coupling between the elasticity of the structure and hydrodynamic forces result in complex dynamics.

Despite these intricacies, current design codes use semi-empirical formulae that approximate slamming as a static and evenly distributed load. The DNV slamming design pressure [3] is formulated as

$$P_{sl} = 1.3k_l \left(\frac{\Delta}{nA}\right)^{0.3} T_0^{0.7} \frac{50 - \beta_x}{50 - \beta_{cg}} a_{cg} \tag{2-1}$$

Here k_l is a longitudinal slamming pressure distribution factor that varies 0.5 at the transom to 1.0 at the bow, *n* is the number of hulls, *A* is the design load area, Δ is the full load displacement, T_0 is the draught amidships, β_x is the deadrise angle in degrees at the transverse section under consideration, β_{cg} is the deadrise at the longitudinal center of gravity, and a_{cg} is the design vertical acceleration at the center of gravity. The design vertical acceleration can be estimated from the DNV guidelines by

$$a_{cg} = \frac{k_h g_0}{1650} \left(\frac{H_s}{B_{WL/2}} + 0.084\right) (50 - \beta_{cg}) \left(\frac{V}{\sqrt{L}}\right)^2 \frac{LB_{WL/2}^2}{\Delta} \tag{2-2}$$

where H_s is the significant wave height, g_0 is gravitation acceleration, $B_{WL/2}$ is the beam at the waterline amidships, *V* is the speed, *L* the overall length, and k_h is a correction factor for hull type taken as 1.0 for monohulls. The design vertical acceleration is intended to be an extreme case with a 1% probability of being exceeded under the worst operating conditions. This equivalent slamming pressure is based on years of operating experience with a wide variety of craft, beginning with the pioneering work by Allen and Jones [4]. Design codes from ABS [5] and Lloyds [6] make similar approximations.

While these design codes are successful in providing the ship designer with accessible guidelines to develop a structure with acceptable performance, it is quite likely far from optimal [7]. A better understanding of the true nature of slamming loads has the potential to substantially improve the performance and safety of marine structures. Stenius and Kuttenkeuler [8] for example demonstrated fuel efficiency improvements of up to 27% with

the reduced structural mass resulting from a more optimized approach to design. With this goal of an optimized design procedure in mind, analytical models as well as numerical tools and experiments have been developed over the years beginning with Von Karman in 1929.

Analytical Models

Von Karman [9] proposed a momentum based impact theory and compared predictions of peak pressure with experimental data. This theory assumes a symmetric 2-D wedge shaped body making impact with a horizontal water surface. The theory neglects the local uprise of water during impact and assumes a rigid body.

Von Karman expressed the total momentum in terms of the velocity *v* at time *t* as

$$M = \frac{W}{g}v + \frac{1}{2}x^2\rho\pi v \tag{2-3}$$

where *W* is the weight of the body per unit length, *ρ* is the density of water, and *g* acceleration due to gravity. The momentum at the instant of first contact with the water surface is

$$M = \frac{W}{g}v_0 \tag{2-4}$$

where $v_0$is the initial velocity. Setting the velocity $v = \tan\alpha\frac{dx}{dt}$ and solving for the force of impact per unit length gives

$$P = \frac{W}{g}\frac{d^2x}{dt^2}\tan\alpha = \frac{v_0^2\cot\alpha}{\left(1+\frac{\rho g\pi x^2}{2W}\right)^3}\rho\pi x \tag{2-5}$$

The maximum force occurs at the initial moment of contact and results in a maximum pressure of $p = \frac{\rho v_0^2}{2}\pi\cot\alpha$. This pressure scales with the dynamic pressure and an

intensifying factor dependent on the deadrise angle. Note that this approaches infinite pressure at zero deadrise if the fluid is considered incompressible.

Wagner [10] developed a method for slamming analysis based on 2-D potential flow theory. This theory assumes a blunt body and in contrast to Von Karman theory accounts for the local uprise of water.

Hydroelasticity

One of the major shortcomings of the Wagner, Von Karman, and other early slamming theories was the assumption that the structure was perfectly rigid. Flexible structures introduce complications in the analysis due to hydroelasticity. Hydroelastic effects can be characterized as kinematic or inertial [11]. Kinematic effects result when the pressure loads on the hull cause it to deflect, resulting in a change in the geometry and thus a change in the local flow and pressure on the hull. Inertial effects occur as a result of the water changing the effective mass of the structure and in turn affecting the modal frequencies.

Kvalsvold and Faltinsen [12] were among the first to develop an analytical model that accounted for hull flexibility and the effects of hydroelasticity in slamming. They modelled the wet deck of a catamaran as a Timoshenko beam with a simplified flow over it [12], [2]. The hydrodynamic loads were modelled from Wagner theory. Kvalsvold and Faltinsen concluded that the elasticity of the wet deck had a large influence on the total slamming load as well as stresses in the deck. Additionally it was found that the influence of wave shape and the location of the initial wave impact did not have a large effect on the stresses when

impact velocities were large. For this beam model the parameter below was discovered to be nearly constant when velocities were large.

$$\frac{\sigma_{max} L_B}{|V| z_{na}} \sqrt{\frac{I}{\rho L_B^3 E}} \tag{2-6}$$

In this expression, $|V|$ is the impact velocity, σ_{max} is the maximum stress, *I* is the beam area moment of inertia per unit width, ρ is water density, L_B is the beam length, z_{na} is the distance from the neutral axis of the beam to the point of measured stress and *E* is the modulus of elasticity. This indicates that for large impact velocities, the maximum stress is proportional to the impact velocity, rather than the velocity squared. Note that one constraint of this study is that the slamming load consists of a large force impulse with a duration that is short relative to the period of the first wet natural frequency. It should also be noted Faltinsen later concluded that the effects of axial and shear deformations as well as rotary inertia were small and thus an Euler beam model was adequate [13].

Lv and Grenestedt [14], [15] followed the work of Kvalsvold and Faltinsen [12] by characterizing the response of a flexible hull section subjected to a travelling pressure load with an analytical model. In this study, a bottom panel was represented by a transverse Euler-Bernoulli beam. The beam was subject to a moving pressure load modelled as a high intensity pressure peak followed by a lower magnitude residual pressure. The role of various parameters including the speed of propagation of the pressure wave, the magnitude of the pressure peak relative to the residual pressure and the width of the peak were investigated. The response of the dynamically loaded beam was normalized by an equivalent statically loaded beam. It was shown that the travelling speed of the pressure load had a large

influence on the displacement and bending moment. When the travelling speed was slow, the beam behaved like a statically loaded beam with normalized bending moment and deflection near unity. However, when the travelling speed exceeded a critical value the response grew to almost double that of the static case. This occurred when the time for the load to traverse the panel was close to the (wetted) period of vibration of the panel. At higher load travelling speeds the response diminished, approaching zero as speed approached infinity.

Numerical Studies

Numerical methods have been a major component of slamming research for at least 30 years. Both two-dimensional boundary element methods (BEM) and volumetric computational fluid dynamic (CFD) methods have been employed. BEM was first exploited in numerical studies of slamming due to its computational efficiency, e.g. [16]. Large fluid deformations at boundaries and the formation of jets are some of the issues that present challenges in the application of BEM to slamming research.

The use of CFD methods in slamming presumably began with simulation of wedge drop tests in calm water by Arai [17]. The large domains required to simulate realistic ship slamming initially limited the use of CFD in slamming research due to restrictions in computer memory [16]. More modern slamming research has made use of RANS CFD coupled with finite element structural solvers to simulate fluid structure interactions in slamming impacts. Geometry has included simple wedges [18], cylinders [19], and complete ships [20].

Drop Tests

Historically, drop testing has been the most common experimental slamming methodology. This has involved both representative hull sections and full scale vessels. Additionally, tests have been done on effectively rigid and flexible hulls.

Some of the earliest drop tests were performed by Chuang in 1966 [21]. Chuang performed drop tests on V bottom sections with deadrise from 0-15 degrees. Panels were constructed from steel and were effectively rigid. These sections were dropped from a series of heights to control the impact velocity, but the velocity profile during water entry was not controlled. Pressures were recorded and evidence of air entrapment noted. It was found that significant air entrapment only occurred in bottoms with less than 3 degrees of deadrise. For these sections, peak pressure occurred during the air entrapment phase before water contact. At these deadrise angles peak pressures were lower than predicted by Von Karman theory. For steeper deadrise sections peak pressures scaled with dynamic pressure, agreeing well with Von Karman theory.

Later drop tests were performed by Hayman et al. at DNV [22], [23] with both rigid and flexible panels for a variety of deadrise angles and impact speeds. Pressures, accelerations and strains were measured at a multitude of points. As with the earlier tests by Chuang, the water impact velocity was controlled by drop height while the velocity profile was uncontrolled. Peak pressures were found to agree well with theory. However, strains in the foam core of the flexible sandwich panel were significantly higher than those predicted using a static evenly distributed pressure as specified in the DNV guidelines. Numerical simulations

using dynamic and static loads reflected this experimental result. It was concluded that the static approximation did not accurately predict failure of the panel core.

Recently an advanced slamming test apparatus was developed by Battley [24] to address some of the shortcomings of previous experimental drop tests. The main drawback of drop testing is the lack of control of the velocity profile during the water impact. The velocity profile is the result of the drop height and mass of the test specimen and thus not necessarily representative of real vessel slamming. The Servo-Hydraulic Slam Testing System (SSTS) developed by Battley at Industrial Research Limited in Auckland, NZ uses a high speed servo-hydraulic ram with a computer control system to maintain a specified velocity profile during water impact. The system allows for impact speeds up to 10 m/s and deadrise angles of 0 to 40 degrees.

Representative panels have been tested on the SSTS over a wide range of conditions. Varying panel constructions ranging from effectively rigid sandwich panels to flexible single skin composites allow for investigation into the role of hydroelasticity. Data has been acquired from pressure transducers, load cells, displacement sensors, accelerometers and strain gages.

A recent SSTS study by Allen and Battley [25] quantified the role of hydroelasticity on flexible panels. It was discovered that hydroelastic effects were responsible for a reduction in pressure at the center of the flexible panels and an increase in pressure at the chine edge. The reduction in pressure at the panel center correlated well with bending stiffness while the increase in pressure at the chine edge scaled with a combination of bending stiffness and shear stiffness. Deformations resulted in changes of local impact velocity up to 72.6% and

local deadrise changes up to 11 degrees. This had the effect of delaying the time at which the peak impact force occurred and increasing the magnitude.

These laboratory impact tests have demonstrated the potential for significant hydroelastic effects in slamming under specific impact conditions. As indicated by Stenius et al [26] one of the main challenges in slamming research is to identify realistic impact conditions. To do so full scale trials are needed.

Full Scale Trials

In addition to performing drop tests [22], Hayman et al. conducted slamming tests on a real vessel [23]. The glass fiber composite sandwich hull of a 19.6m 33.5 ton coastal rescue craft was instrumented with strain gages and accelerometers. Instruments were concentrated on a panel extending 0.2L to 0.37L from the forward perpendicular. Measurements were taken during operation in rough seas. Poor correlation was found between global accelerations and panel strains. It was concluded that it was necessary to instrument more of the panels subjected to slamming loads and that a larger number of slamming events needed to be recorded under a variety of sea states to build up a statistical basis.

Some of the most thorough full scale testing to date was performed by Rosen et al [27] on the Visby class corvette. The Visby class is a 73m 600 ton displacement high-speed ship with a carbon sandwich panel construction. A ship of the Visby class was equipped with 50 strain gauges, 6 DOF IMU, accelerometers and a 3x3 matrix of pressure transducers. Data were collected during trials in rough seas in the Baltic. Strain measurements were used to verify that structural responses did not exceed the maximum allowable level in operation. The

matrix of pressure sensors was used to develop an estimated pressure distribution on the hull and thus evaluate loads on the structure. The estimated loads were fit to a Weibull distribution and used to predict the extreme values of load expected in service. It was demonstrated that the estimated pressure loads exceeded those predicted by DNV design rules.

To date, efforts in full scale experimental slamming are still sparse. In particular, as numerical methods become more advanced, full scale data are increasingly critical as a validation tool [16]. To this end, a dedicated slamming test vessel was designed by Grenestedt and manufactured at Lehigh University Composites Lab. This vessel is uniquely suited to slamming research in hull geometry, hull construction, and the extent and capability of instrumentation and data acquisition systems.

Numerette Slamming Load Test Facility

The Numerette is a 9 meter long 1.9 meter wide hybrid composite boat. The structure consists of a welded stainless steel frame and composite sandwich panels. The 45 panels including 10 bottom panels, 10 freeboard panels, 5 deck panels, 16 bulkhead panels and 4 hatches were manufactured by vacuum infusion. Glass and carbon fiber reinforcements were used along with PVC foam cores and vinyl ester and epoxy resins. The stainless steel structure consists of 2mm thick TIG-welded and boxed AL-6XN.

To investigate the role of stiffness and mass effects in slamming, a variety of composite layups were used in the hull. At every lengthwise location in the boat, the left and right

panels differ in material and/or fiber orientation. This results in a considerable disparity in stiffness.

To characterize the loads on Numerette as well as the structural response, the boat was heavily instrumented and fitted with a high performance ruggedized data acquisition system. Instrumentation includes 123 strain gages, 101 pressure transducers, 23 accelerometers, 6 displacement transducers, cameras and 2 GPS aided 6DOF inertial navigation systems. Instruments are synchronized and data is recorded to onboard solid state disks.

Outline of Articles

The first article in this dissertation addresses the fundamental question of the role of panel stiffness in slamming directly. An experiment is defined in which the Numerette is operated at constant speed and a range of headings. Panel displacements are measured for two panels on either side of the boat. The statistical relative panel displacements are compared against static loading experimental data.

The second article investigates the statistical variation in structural response to slamming loads in more detail. This involves first describing the construction of Numerette and the onboard data acquisition system. Secondly, the structure is characterized by measuring displacements of the bottom panels when subjected to static loads in a free air environment. Next the dynamics of the dry structure are measured with experimental modal analysis. Finally, sea trials are detailed and experimental strains for different panels are compared.

The third article makes use of wavelet analysis techniques to characterize the dynamics of slamming. It is proposed that coupled wet vibrations of marine structures can be a critical

load case, resulting in extreme displacements and strain. Experimental slamming data is initially reviewed in the time domain, demonstrating a progression of the impact along the hull as evidenced by strain data. Traditional Fourier techniques are used to describe the data in the frequency domain, but this method is shown to be inappropriate for non-stationary slamming data. In contrast wavelet analysis reveals a wealth of information about the structural response during the impact. In an initial phase, high frequency vibration is present and is followed by a second period of lower frequency vibration. An array of accelerometers is used to demonstrate that the higher frequency vibrations correspond to dry modes of the structures and the lower frequency vibrations are wet structural modes.

The final article uses experimental test data gathered with Numerette to validate a high fidelity computation fluid dynamic finite element fluid structure interaction (CFD/FE FSI) code. The code CFDShip-Iowa is used to provide hydrodynamic simulation while Ansys is used as a finite element solver. Hydrodynamic simulations are performed at a range of Froude numbers in calm water and regular waves. These simulations agree with experimental data for drag and rigid body motions. In regular waves, one way fluid structure interaction simulations show good correlation with experimental pressure and strain data.

3. Conclusions

Slamming is critical for the structural design and operation of high-speed craft. Despite almost 100 years of research in the area, current ship design codes still use a much simplified static load approximation that very likely results in suboptimal designs. Analytical theories, numerical simulations and laboratory scale experiments have demonstrated the potential of

a more refined approach but full scale experimental studies to validate this have been sparse.

In this dissertation bottom slamming of high speed craft has been investigated experimentally at full scale to address this gap in the body of research. A heavily instrumented, dedicated slamming research high-speed boat was developed. The response of hull bottom panels to slamming loads was found to deviate from the behavior that current slamming design codes predict. For example, a panel 1.6 times more compliant when subjected to quasi static loads deflected only 1.4 times more under slamming loads.

A linear relationship was observed between water impact speeds and peak strains. This is in contrast to the quadratic relationship predicted by momentum theory, but is consistent with some slamming models that account for hydroelasticity, e.g. Kvalsvold and Faltinsen [2]. This occurred despite impact speeds below the range where hydroelastic effects are expected to be significant. Direct measurement of the water surface is needed to better estimate the impact speed and validity of this relationship.

The wavelet transform was shown to be useful in resolving the time-frequency behavior of ship structures during slamming. A single event was studied in detail and wavelet analysis indicated how an initial impact excited a global dry response of the structure, followed by local wetting and a change in the frequency spectrum. Mode shapes were resolved from an array of accelerometers, showing the onset of “wet vibrations”. The magnitude of vibration was small in this case, but at higher impact speeds, lower deadrise angles or with more compliant structures these oscillations are predicted to be severe.

The experiments performed have resulted in an extensive full scale slamming dataset. Experimental validation will be increasingly important to the marine industry as future high-speed craft development will rely more on CFD design tools. One such tool, CFDship IOWA shows good agreement for resistance, rigid body motions and pressures with the collected experimental data. Strains had good qualitative agreement with experimental data but a relatively large error. As numerical tools are refined to include phenomena like two-way fluid structure interaction this experimental dataset can continue to serve as a benchmark.

4. Future Work

The comprehensive instrumentation of the Numerette slamming test boat enables characterization of structural response and validation of simulations in a statistical sense. However, without a precise description of the sea surface it is difficult to directly connect experimental data to simulations and laboratory experiments on the basis of individual slamming events. Recent improvements to the speed and fidelity of LIDAR and stereo vision systems may make them suitable for experimental wave measurement. Initial trials of these technologies on Numerette showed they hold promise but further work is needed to tune the algorithms to consistently detect the water surface. The inclusion of improved sea state characterization will make the experimental dataset an even more valuable validation tool.

5. On Stiff Versus Compliant Bottom Panels of High Speed Craft

J L Grenestedt and **R S Thodal,** Lehigh University, USA

Summary

An 8.8 m high-speed V-bottom hull was designed, manufactured, instrumented with a large number of strain gages, displacement transducers, accelerometers, etc., and operated in the Atlantic Ocean. The bottom was made of ten discrete panels, each with different construction. At one longitudinal location the starboard and port panels had the same fibers and the same sandwich core, but the orientation of the fibers differed. Due to the aspect ratio of the bottom panels (long and narrow), the effective stiffness of the starboard panel was approximately 1.6 times that of the port panel. The scope of this note is to present some of the differences in slamming response between these two bottom panels with different stiffness.

Introduction

Design codes of high speed light craft, such as those of ABS [5] and DNV [3], suggest that bottoms should be designed using "equivalent" uniformly distributed static pressures to simulate slamming loads. However, measurements of bottom slamming in high speed craft show that the pressures are very dynamic and far from uniform.

Under static loads a panel would deform in inverse proportion to its stiffness. For example, compare a stiff panel with 1.6 times the stiffness of a compliant panel. If the load were static then the compliant panel would deform 1.6 times as much as the stiff panel. On the other hand, if the load were so dynamic that the panel hardly had time to move during the time

the load was applied, then the load could be modelled as an impulse of infinitesimal duration e.g., [13]. The panel would then obtain an instant displacement rate, which would only scale with the mass of the panel. If the compliant and stiff panels had the same mass, then their initial displacement rates would be the same. If the subsequent displacement could be modelled as a simple mass-spring system, then the maximum deflection would scale with the square root of the stiffness, i.e., the compliant panel would deform $\sqrt{1.6}$ times that of the stiff panel. The maximum acceleration after the initial impulse would occur simultaneously with the maximum deflection, and it would scale with the square root of the stiffness, i.e., the stiff panel would have $\sqrt{1.6}$ times higher acceleration than the compliant panel. A third and highly simplified way to look at slamming is to think of it as a "packet" of water thrown onto a panel, where the panel has to absorb all energy of the packet. If the panel were modelled as a mass-less spring then the compliant panel would deform $\sqrt{1.6}$ times that of the stiff panel. Using a simple dynamic load on a one-dimensional representation of a bottom panel, Lv and Grenestedt [15] [14] analytically showed that there are multiple resonance phenomena which complicate the estimation of how much a compliant panel deforms compared to a stiff one. Fluid-structure interaction naturally further complicates the issue (e.g., [28]). The present note presents some experimental results from slamming tests using a two-seat manned boat with a quite special bottom, Figure 5-1, where starboard and port panels differ (have different stiffnesses). The results are not conclusive, but surprisingly consistent.

Figure 5-1: The Numerette slamming boat. The section behind the colored bow is the one presently studied

The ONR / Lehigh University Slamming Test Boat, The Numerette

The Numerette boat is 8.8 m long, has 24.7 degrees deadrise in the stern, and is powered by a 317 kW inboard/outboard engine and a submerged propeller. The hull consists of a stainless steel skeleton closed out with vacuum infused composite sandwich panels. The bottom, partially shown in Figure 5-1 and Figure 5-2, consists of ten separate panels. The panels presently studied are 5.5-6.9 m forward of the transom, well ahead of LCG. They are subjected to substantial slamming pressures in sea state 3 and higher. The starboard and port panels are both constructed with 18 mm thick Divinycell H250 foam core, an inner skin of 2 plies 620g/m^2 Devold DBL700 (0°, ±45) carbon, and an outer skin of 3 plies DBL700 (0°, ±45°) and 1 ply 443g/m^2 Devold L(X) 440-C10 (0°) carbon. The panels differ in the orientation of the DBL700 reinforcement; the 0° fibers are oriented transverse to the keel in the starboard panel and parallel to the keel in the port panel. The panels presently studied are located between the keel and the longeron and have an aspect ratio slightly under 4. This results in the two panels having the same mass, but different effective stiffness. A preliminary test was performed to characterize the displacement of these bottom panels

under static loads. In this experiment a 21 point test grid was laid out on the panel and six LVDT's were installed to measure displacements. A fixture with a load cell was used to introduce a known load at each grid point one at a time, while displacements were measured. Superposing the displacements from the 21 load cases gave an estimated deflection under uniform load. It was found that the displacement at the center of the port panel was 1.6 times greater than that of the starboard panel when subjected to the same simulated evenly distributed load. Modal analyses were also performed on both panels. The lowest eigenfrequency of the two panels was similar due to a "global" vibration mode strongly influenced by the stainless steel longerons. As expected local modes had quite different eigenfrequencies.

Figure 5-2: Port and starboard bottom panels, stainless steel longerons, bulkhead, and bottom sensors (pressure sensors, accelerometers, strain gages, LVDT's).

Slamming Tests in the Atlantic Ocean

Experiments were conducted in the Atlantic Ocean near Barnegat Light, New Jersey, USA, within 10km of the Barnegat inlet. The closest wave buoy, NOAA 44091 indicated sea state 3 conditions with a significant wave height of 0.8 meters and dominant wave period of 11 seconds with 104 degree direction.

The tests consisted of many short, constant track, constant speed segments. A transom mounted trim tab was used to maintain neutral roll during the test period (slamming is highly affected by roll angle). The target speed was 70 km/h (19.4 m/s). Segments were logged at 30 degree track increments. The distributions of speed and heading during the test session are indicated in Figure 5-3. Displacements, accelerations and strains were measured at the locations shown in Figure 5-4. Each sensor was logged at 25kHz; the data acquisition system can log data considerably faster but 25kHz resolves strain peaks etc very well. The results are presented in the next section.

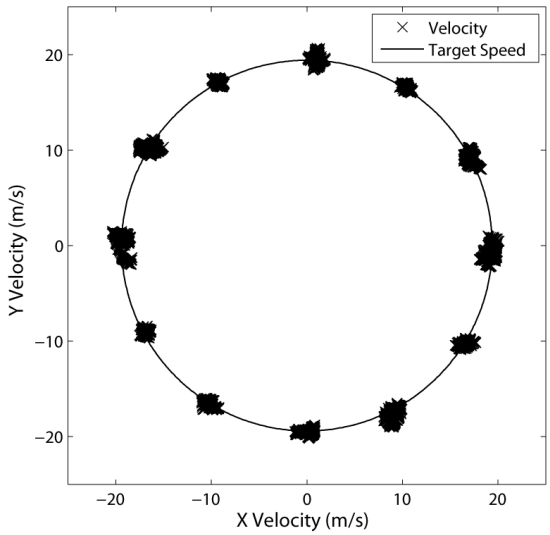

Figure 5-3:Speed and heading during recent tests in the Atlantic.

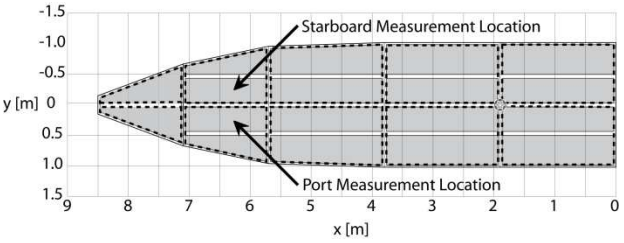

Figure 5-4:Sketch of where the measurements presented where taken.

Results

Three measures were used to indicate the relative response of the port and starboard panels. The first is the RMS value, the second is the mean of 1/3 highest peaks (maximum value at each slamming event), and the third is the 99th percentile of all values (not only peaks) in the records. These results are presented in Table 5-1.

Table 5-1: Results from slamming tests in the Atlantic

	Port	Starboard	Ratio
Displacement RMS (mm)	0.0391	0.0271	1.44
Mean 1/3 Peak Displacement (mm)	0.435	0.298	1.46
Displacement 99th Percentile (mm)	0.201	0.143	1.40
Strain RMS	5.28e-05	3.40e-05	1.55
Mean 1/3 Peak Strain	0.000528	0.000338	1.56
Strain 99th Percentile	0.000282	0.000191	1.48

The results indicate that the dynamic panel displacement ratio is consistently lower than the static ratio. The values appear to fall between those of the static stiffness ratio (i.e., 1.6) and the square root of the ratio ($\sqrt{1.6} = 1.26$).

The strains presented are inner skin transverse strain minus outer skin transverse strain, which is a measure of transverse curvature of a bottom panel. The strains show a larger ratio between starboard and port panels than displacements.

It may be worth mentioning that FFTs of displacements (Figure 5-6) show a similar trend to the statistical measures. In the range of 1-10Hz the ratio between the port and starboard displacements is approximately 1.4. At higher frequencies the trend is that the ratio is

decreasing, but it is not as clear. The behaviour in the frequency domain is investigated in more detail in [29].

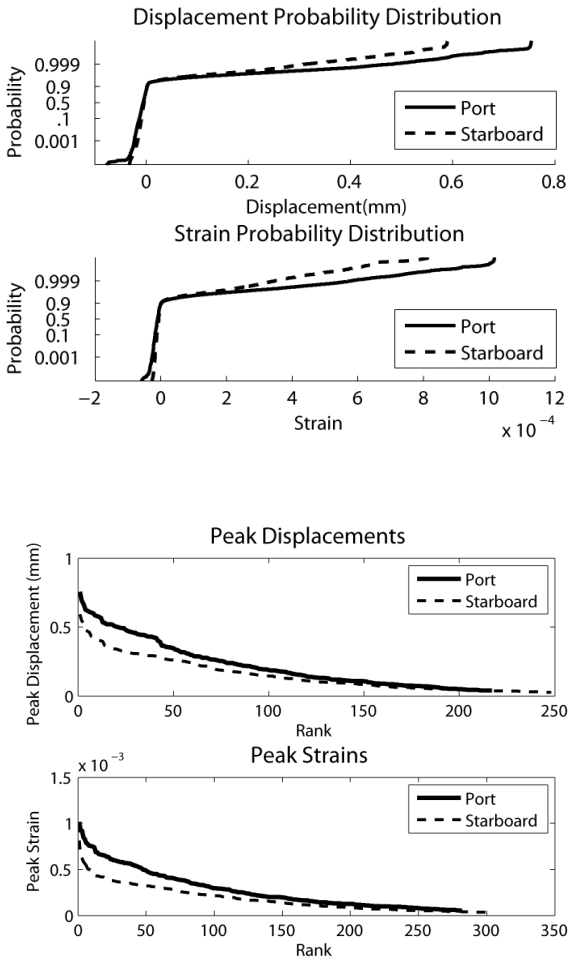

Figure 5-5 Top: normal probability distributions of displacements and strains. Bottom: peak displacements and strains, ordered from largest to smallest.

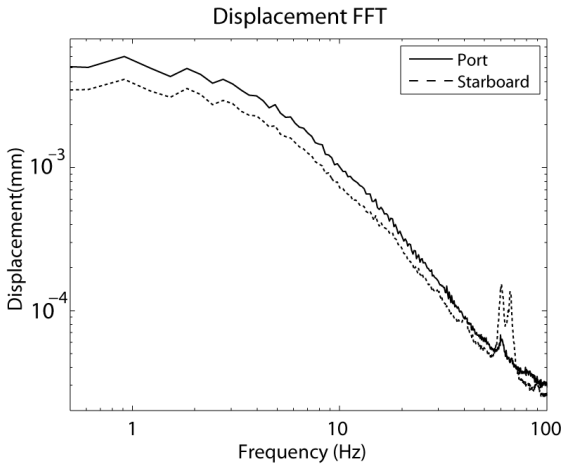

Figure 5-6: FFT of port and starboard displacements.

Conclusions and Discussion

Experiments performed with the Numerette slamming craft in the Atlantic indicate that the port panel, which was 1.6 times more compliant than the starboard panel, had approximately 1.4 times higher displacements and 1.5 times higher strains than the starboard panel when operating at 70 km/h in sea state 3.

No simple relation between starboard and port bottom panel accelerations was found. The peak accelerations measured on the port and starboard panels were quite similar. The peaks would sometimes occur well before the maximum panel deflection was reached, sometimes simultaneously, and sometimes well after. However, when the signals were lowpass filtered to remove vibration at high frequencies, accelerations were slightly higher on the stiffer starboard panel.

In closing it should be mentioned that a larger difference in stiffness between the bottom panels would be desirable for a better understanding of the behavior of stiff versus compliant panels.

6. Experimental Study of Slamming on High-Speed Craft Operating in the Atlantic

Robert Thodal* rst204@lehigh.edu, Joachim L. Grenestedt*, Jian Lv

*Mechanical Engineering and Mechanics, P.C. Rossin College of Engineering and Applied Science, Lehigh University, Bethlehem, PA 18015, USA

Keywords: slamming; high-speed craft; hydroelasticity; vibration; fluid-structure interaction; experimental

Abstract

The highest loads on bottoms of fast craft are due to slamming, or hydrodynamic impact. Slamming pressures and associated deformations are not only affected by bottom stiffness and geometry, speeds, and wave shapes, but also by fluid-structure interactions. In order to study slamming an instrumented slamming load test facility was designed and built. The facility loosely resembles a high-speed offshore boat, but it has a faceted hull consisting of ten separate bottom panels, each with a unique construction. At the same lengthwise location, bottom panels on starboard and port have different layups, thicknesses, fibers, etc. After over 30 hours running in calm water and rough water, the strain data recorded from panel embedded strain gauges was collected and analyzed. The results indicate that subject to moderate slamming loads, the strains of composite bottom panels essentially scale with their static stiffness. However, the most severe slamming events resulted in a deviation from the static stiffness relationship. Estimates of water impact velocity suggest that impact speeds for these slamming events approach a critical value at which hydrodynamic and inertial effects become significant.

Introduction

Slamming impact is an important phenomenon in high-speed ships and ocean engineering. Slamming can result in large transient hydrodynamic impact loads on the hull, leading to violent motions, onboard equipment damage, and even structural damage. Hence, slamming loads are very important in the structural design of all high-speed vessels and need to be investigated.

Pioneering research on panel-water impacts was started with the work of von Karman [9]. The research that followed can be categorized as theoretical, numerical or experimental studies. Many effective theoretical methods based on a solid background of experimental data were developed decades ago, e.g. [30, 31] and [4]. Recent fundamental theoretical and experimental work [32, 33, 34] has investigated wave impact on horizontal or nearly horizontal one-beam and three-beam models. A review of some of the major developments can be found in [13]. Numerical modeling research presented recently has utilized non-linear boundary element methods [35], computational fluid dynamics [36] and explicit finite element analysis [37, 38, 39]

Experimental research is also well-reported in the literature [40, 21, 22, 41, 42, 43, 44, 45, 46, 47]. Many of these experiments involve drop tests [21, 13, 22, 47]. Drop test experiments have used both essentially rigid models and elastic models to investigate slamming pressure distributions. The water entry velocity of the hull in vessel experiments has been primarily controlled by the drop height and the mass of the specimen. However when a drop test specimen hits the water, it is difficult to control the hull motion in a way that accurately simulates real vessel slamming. Considering that the velocity, pressure, and strain profiles

depend on the overall behavior of the vessel and the position of the panel, the real vessel test is regarded as an integral part of hydrodynamic slamming studies. Some efforts at tests with real vessels have been presented during the past decades [40, 42, 43, 44], but this type of testing has not been overly comprehensive and remains an open area today.

Experiments performed by Battley [48, 49, 50, 51, 26] have made use of a Servo-hydraulic Slamming Testing System (SSTS) to allow for tests with control of panel velocity profiles. Experiments have been conducted for a variety of deadrise angles, velocity profiles, and panel construction. Panels have been tested that range from extremely soft to effectively rigid.

Stenius [39] identified a dynamic hydroelastic parameter to characterize the relation between the loading rate and wetted natural frequency of a panel. Impacts with a loading rate lower than the wetted natural frequency are expected to result in a quasi-static response while impacts with a greater loading rate show hydroelastic effects. Simulations [26, 52] and experiments on the SSTS have demonstrated the increasing role of these hydroelastic effects at high loading rates. These efforts have been successful in characterizing the behavior of panels subjected to simulated slamming loads but it is unclear if these loads provide a complete and representative spectrum of real vessel slamming.

Lv and Grenestedt [14, 15] recently completed an analytical study of the response of hull bottom panels to slamming loads. Slamming loads were modelled as a high intensity peak followed by a lower intensity residual pressure moving across the panel at a constant speed. Hydroelastic effects were ignored, or included only as a constant added mass term. The structural response during the initial loading phase and a later vibration phase were

investigated for a variety of loads and panel properties. Lv and Grenestedt identify a critical range of non-dimension loading rates where the structural response is greatest.

In order to accumulate valuable test data to describe the characteristics of vessel water slamming and investigate this phenomenon more comprehensively, an instrumented slamming load test facility was designed, built and tested in a variety of sea states. Strain data from strain gages embedded in bottom composite sandwich panels and on the ship's steel frame were collected by an onboard data acquisition system. Together with video and acceleration data recorded during testing, the strain data is analyzed in this paper.

The Numerette, an Instrumented Slamming Load Test Facility

The Numerette is a 9 meter long, 1.9 meter wide hybrid slamming load test facility boat which was designed by Grenestedt and manufactured at the Lehigh University Composites Lab, Figure 6-1. This hybrid boat was made with a welded non-magnetic AL-6XN stainless steel frame and composite sandwich panels. The stainless steel used is 2 mm thick. The composite panels including 10 bottom panels, 10 side panels, 5 deck panels, 16 bulkhead panels and 4 hatches were manufactured with the vacuum infusion method. Carbon fiber, glass fiber, PVC foam core, epoxy and vinyl ester resin were used during the panel manufacturing process.

Figure 6-1: Slamming load test facility boat

All side panels share a common layup. The outer skin consists of one layer of TC-18-N carbon fiber (0°, 90°) by JB Martin and one layer of Hexcel 7725 glass fiber (±45°). The foam core is Divinycell H80 with a thickness of 12.7mm. The inner skin of these panels was made from one layer of DB240 glass fiber (±45°). The 0° is here defined as parallel with the keel of the boat. On the top of the inner skin, two layers of DB240 reinforcement strips were laid along the edges of the foam. The layup of every bottom panel was different to allow for comparison and better understanding of stiffness and mass effects on slamming. More details are presented in the following section. All composite panels were bonded to the steel frame with Proset 176/276 epoxy. The bonding area on the outside steel frame is approximately 40mm wide. Bonded specimen tensile tests showed that the bonding shear strength completely fulfilled the design requirements. Six years of operation has also proven this.

This test boat can accommodate two passengers and has a full load displacement of 2450kg. The top speed achieved during the tests with the installed 425 HP Mercury V8 engine was 27 m/s. After well over 30 hours of running in a variety of sea conditions (up to sea state 4), the

structural integrity was maintained. The data acquisition system functioned faultlessly and large amounts of test data were acquired.

Bottom Construction

The bottom panels of Numerette are fiber reinforced plastic (FRP) sandwich panels manufactured by vacuum infusing Ashland 8084 vinyl ester resin into thin glass fiber or carbon fiber skins on each side of a polymer foam core. All foam cores of the bottom panels are 18-mm-thick Divinycell H250 foam with infusion grooves on both sides. The foam cores were routed slightly smaller than the opening in the steel frame and the edges were beveled 30°. The skins come together at the end of the foam core where the panel was bonded to the steel frame.

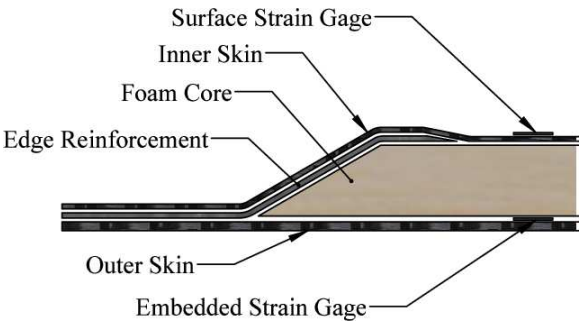

Figure 6-2: Composite sandwich panel with strain gages

In the present research, the strains of the inner and outer skins of the bottom panels were measured. The strain gages could not be attached to the outer skin using traditional methods due to the harsh environment and the requirement that the hull be hydrodynamic smooth, so foil strain gages were embedded in the bottom panels, Figure 6-2. The strain gages were bonded to flat thin fiberglass plates. The plates were made of a single layer of

Hexcel 7725 glass fiber fabric infused with vinyl ester, and waterjet cut into paddle-like shapes. Figure 6-3 shows such a paddle bonded to the foam core. The leads of the strain gages were set in a zigzag pattern to protect them from potential damage under high strains. The paddles were aligned and bonded in place using 3M's DP 125 two part epoxy. Signal wires connecting the strain gages with the data acquisition system were run through 6.4 mm wide channels machined in the foam core from the strain gages to the edge of the panel. The wires exited the foam core through protective silicone tubing. The channels were routed at a depth near the neutral axis of the sandwich panel to reduce strain in the wires during panel bending. Once the wires were positioned, all channels were covered with filler pieces routed out of the same H250 foam. The wires, filler pieces and tubing were bonded to the core with the wires running out of the corner of the foam core.

Figure 6-3:Strain gage paddles bonded to PVC foam core

All bottom sandwich panels were manufactured on curved-surface molds, which were very accurate, lightweight, inexpensive and compatible with vinyl ester. These molds were

manufactured using a CNC router to cut Styrofoam billets undersized, which were then coated with epoxy tooling paste, and CNC routed when cured to the final shape. The finished surfaces of tooling paste on the mold were sealed with a very thin coat of epoxy.

To allow for study of how bottom panel properties interact with slamming, a variety of layups were used on the 10 bottom panels, Table 6-1. These panels differed in material, layer count and fiber orientation. For example the port bottom panel in Bay 1 was manufactured as follows. Three layers of DB240 glass fiber reinforcement for the outer (flat) sandwich skin were placed on the mold. All fibers were laid at ±45°, where the 0° direction was parallel with the keel of the boat. The foam core was placed on the fiber reinforcements with the beveled side up. Two layers of DB240 were laid on top of the foam with the same layup orientation as the first three layers. Two layers of DB240 reinforcement strips were laid along the four edges of the foam, also with the fibers at ±45°. All panels were vacuum infused with vinyl ester resin and left under vacuum to cure at room temperature for 24 hours before demolding.

Table 6-1:Bottom panel layup details (top to bottom, 0° parallel to keel). The materials used in the bottom were Owens Corning double bias glass fiber fabric DB240 (840 g/m2), Devold AMT carbon fiber fabrics DBL 700 (620 g/m2) and L(X) 440 (434 g/m2), and Divinycell H250 foam core (250 kg/m^3).

	Bay 1	Bay 2	Bay 3	Bay 4	Bay 5
Port	2 DB240 (±45°) H250 Foam core 3 DB240 (±45°)	2 DBL700(90°, ±45°) H250 Foam core 3 DBL700(90°, ±45°) 1 L(X) 440-C10 (0°)	2 DBL700 (90°, ±45°) H250 Foam core 3 DBL700 (90°, ±45°) 1 L(X) 440-C10 (0°)	2 DBL700(0°, ±45°) H250 Foam core 3 DBL700(0°, ±45°) 1 L(X) 440-C10 (0°)	2 DBL700(90°, ±45°) H250 Foam core 3 DBL700(90°, ±45°)
Starboard	2 DB240 (±45°) H250 Foam core 3 DB240 (±45°)	2 DBL700(0°, ±45°) H250 Foam core 3 DBL700(0°, ±45°) 1 L(X) 440-C10 (0°)	2 DB240 (±45°) H250 Foam core 3 DB240 (±45°) 1 L(X) 440-C10 (0°)	2 DBL700(90°, ±45°) H250 Foam core 3 DBL700(90°, ±45°) 1 L(X) 440-C10 (0°)	2 DBL700(0°, ±45°) H250 Foam core 3 DBL700(0°, ±45°)

Instrumentation and Data Acquisition

The composite bottom panels and stainless steel structure in bays 2, 3 and 4 of the slamming load test facility were instrumented with a total of 123 strain gages. The gages used were Vishay C2A-13-250LW-350, CEA-06-250UT-350/P2 and CEA-06-250UN-350/P2. On the bottom panels gages were installed on both the inner skins and embedded on the outer skins. On bay 2 bottom panels all gages were linear (single axis) oriented in the transverse direction. On bay 3 and 4 bottom panels a combination of linear and t-rosette gages were used where all linear gages were oriented transverse and t-rosettes oriented to give transverse and longitudinal strains. The gages on the steel structure in bays 2, 3, and 4 were all linear oriented longitudinally (parallel to the keel). These gages were installed on the keel, chine longerons, deck longerons and the top and bottom flanges of the main longerons. Figure 6-4 shows the locations and orientations of gages on the bottom panels. Figure 6-5 shows the locations of gages on the steel structure.

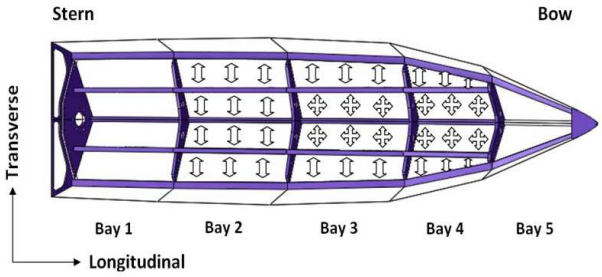

Figure 6-4:Bottom panel strain gage locations and orientation

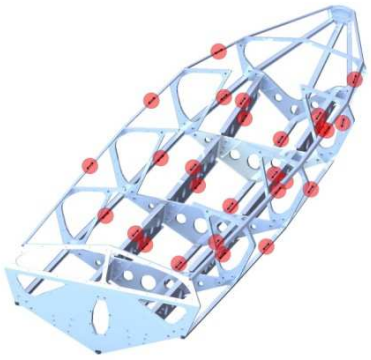

Figure 6-5 Steel structure strain gage locations

Strain gage signal conditioning was implemented with National Instruments 9237 4-channel compact DAQ modules. A total of 39 modules were installed in five compact DAQ chassis. This allows for up to 156 strain channels to be simultaneously sampled at up to 50 kHz per channel with 24 bit precision. Accelerometer signal conditioning includes three National Instruments PXI-4472B modules to simultaneously measure up to 24 channels of IEPE type accelerometers at up to 102.4 kHz per channel with 24 bit resolution.

A Compact DAQ 9401 digital I/O module was used as a master timing controller to synchronize the five Compact DAQ chassis and the PXI chassis. A National Instruments PXI-8110 controller running a custom LabView program was used to record the data onto solid state disks. Inertial data from a VectorNav VN-200 inertial navigation system synchronized to the PXI and compact DAQ system were also recorded. Figure 6-6 shows the enclosure housing the PXI instruments, and Figure 6-7 the enclosure housing the compact DAQ instruments.

Figure 6-6: PXI Instrumentation

Figure 6-7: Compact DAQ Instrumentation

Experimental Methodology

Static Panel Stiffness Testing

Tests were performed in the lab to determine the displacement of the various bottom panels to known static loads. A fixture was created consisting of an aluminum beam with a sliding carriage mounted to a Transducer Techniques LPU-1k load cell. The fixture is shown in Figure 6-8. The load cell is mounted on a spherical bearing and has a 76 mm diameter pad attached to the load button. Load was introduced to the bottom panel through the pad by applying a force to the aluminum beam. Displacement at the inner skin of the panel was measured with six Omega LD320-15 LVDTs mounted to a frame between the keel and main longeron as shown in Figure 6-9. Load was introduced at 21 points on the bottom panels as defined by the grid shown in Figure 6-10. Load was applied gradually until a maximum of approximately 1000 Newtons was reached, then slowly released. Data was sampled at 1667 Hz, the minimum supported by the NI-9237 module used for load cell data acquisition.

Linear regression was performed between each displacement and the load to produce a function expressing the displacement at a given location per unit load applied at each of the 21 grid points. Linear combinations of the resulting functions can be used to estimate the displacement due to a distributed load over the panel. The linear combination of all 21 grid points was taken to approximate a hydrostatic pressure on the panel. The result of this data reduction is a value for displacement at each of the 6 LVDT locations for an evenly distributed pressure on the panel. By taking the ratio of these displacements between a starboard and port panel, the relative stiffness of the panels was estimated. Establishing a stiffness ratio from measured strains was not possible, as local effects from the load application site significantly affected results.

Figure 6-8 Static load test fixture

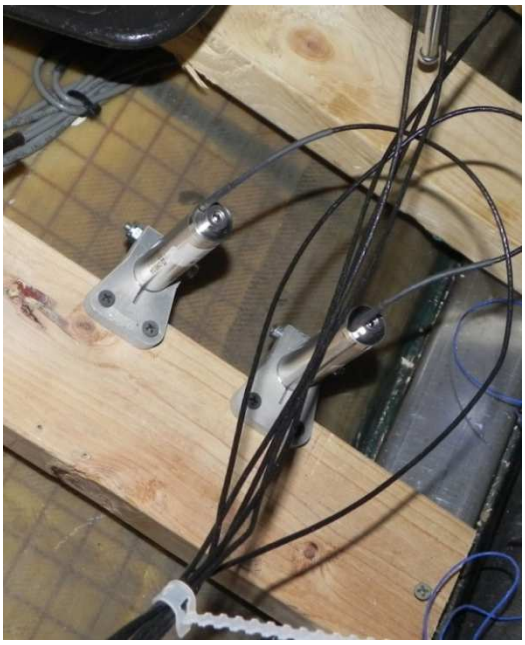

Figure 6-9 Static Load Test LVDTs

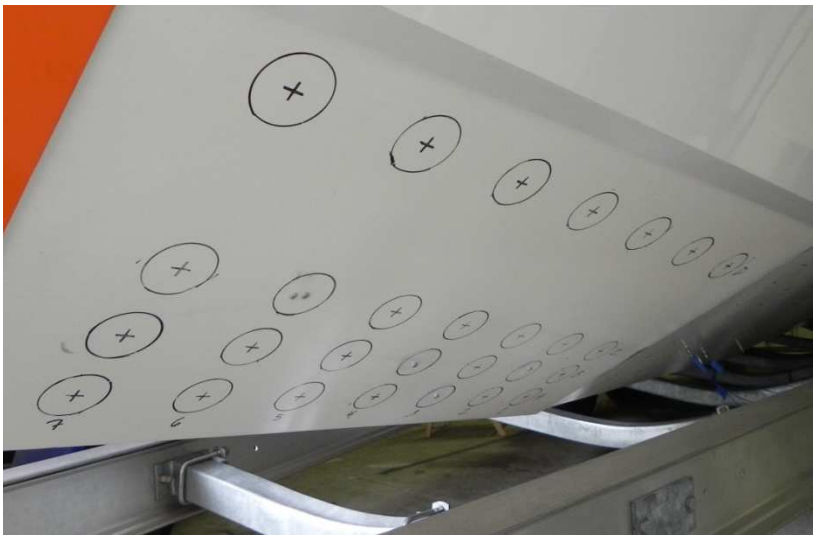

Figure 6-10 Static load test grid

Dry Modal Testing

In order to determine the resonance frequencies of the bottom panels, a modal test was devised to excite the panels and measure their response. The panel of interest was instrumented on the inner skin with a PCB Piezotronics model 352c04 +/-500g accelerometer with a -3 dB frequency range of 0.5 Hz to 10 kHz. The accelerometer was screw mounted to an aluminum base bonded to the inner surface of the panel with a cyanoacrylate adhesive. A PCB piezotronics 086D05 22kN (5klbf) peak force impact hammer equipped with a medium stiffness impact cap (white) and vinyl cover was used to excite the structure and measure the force. Accelerations and load were recorded at 5 kHz per channel with a National Instruments PXI-4472B module signal conditioner.

The least squares complex exponential modal analysis method was used to identify the panel modes from experimental data. Each panel was excited in a grid of 75 locations with the impact hammer and the response recorded by an accelerometer at a fixed location.

Wetted Eigenfrequencies

The non-dimensional dynamic hydroelastic characterization factor [50, 39] for a beam approximation of a bottom panel is given as

$$R = 4\left(\frac{\mu_{np}}{\pi}\right)^2 \frac{\tan\beta}{V}\sqrt{\frac{D}{\pi\rho_w b^3}} \qquad (6\text{-}1)$$

where β is the deadrise, *D* is bending stiffness per unit width of the beam, ρ_w is water density, *V* is impact velocity, *b* is panel width (or length of the beam approximating the bottom panel), and μ_{np} is a parameter related to the boundary conditions given as $\mu_{np} = \pi$ for simply supported boundaries and $\mu_{np} = 4.73$ for clamped boundaries. Further, the first wetted natural period is

$$T_{NP} = \frac{2\pi}{\mu_{np}^2}\sqrt{\frac{(\overline{m} + \overline{m_a})b^3}{D}} \quad (6\text{-}2)$$

Here $\overline{m}$ is the structural mass per unit length of the beam and $\overline{m_a}$ is added mass due to coupling of water. $\overline{m_a}$ is

$$\overline{m_a} = \frac{1}{2}k_a\frac{\pi}{2}\rho_w(b\cos\beta)^2 \quad (6\text{-}3)$$

The factor k_a is an added mass scaling factor, $k_a = 1$ is used.

An alternative beam approximation of the wetted natural frequencies for a bottom panel [14] is given as

$$\omega_i = \frac{\pi^2 i^2}{L^2}\sqrt{\frac{EI}{\mu^*}}, (i = 1,2,3) \quad (6\text{-}4)$$

where *L* is panel width (or length of the beam approximating the bottom panel), *EI* is the bending stiffness, and μ^* is mass per unit length of the panel including added water mass.

$$\mu^* = \mu + k\rho_w\pi Ld/8 \quad (6\text{-}5)$$

Here μ is the mass per unit length of just the panel, d is panel length (or width of the beam approximating the bottom panel) and *k* is a factor describing the degree of wetting of the panel ranging from *k*=0 (dry) to *k*=1 (fully submerged).

In both cases, the panel bending stiffness *EI* and *D* were chosen such that with no added water mass the modal frequency matched the result for a single transverse half sine mode shape from the dry modal test experiments (vibration mode 2).

A non-dimensional characteristic velocity $\bar{c}$ was introduced in [14] to describe the ratio of the loading rate to the first natural period of the wetted panel. This parameter is used to characterize the impact velocity at which inertial effects become significant.

$$\bar{c} = \frac{V\pi}{2sin(\beta)}\sqrt{\frac{\mu^* L^2}{EI}} \qquad (6\text{-}6)$$

Note the characteristic velocity $\bar{c}$ and hydroelastic characterization factor *R* are related by $\bar{c} = \pi/(R\sqrt{2}cos(\beta))$ assuming simply supported boundary conditions.

Sea Trials

The data presented here was collected on October 10, 2014 off the coast of Barnegat Light, NJ. The closest wave buoy was the National Oceanic and Atmospheric Administration's NDBC Station 44066.

Figure 6-11 Image from cockpit mounted camera taken during Atlantic testing

The test procedure involved performing 1-2 minute long sustained data logging sessions at speeds of 15-20m/s under constant heading. Data from 110 strain channels and 22 acceleration channels were recorded at 25 kHz per channel, while inertial navigation solutions were recorded at 200 Hz. Strain gages were located on the steel frame structure and the composite bottom panels. PCB 354C03 +/-50g triaxial accelerometers were fixed to the steel structure at bulkhead 2 and 5 to capture rigid body motion. PCB 352C04 +/-500g single axis accelerometers were mounted on composite bottom panels. At the start of each test, the strain signals were zeroed while the boat was stopped. After logging was started the boat accelerated to the maximum safe speed. Neutral roll was maintained by use of a single trim tab.

A variety of methods were used to reduce the data from the sea trials. The first efforts made were to characterize the slamming events from strain response in the time domain. The slamming rise time was determined by calculating the time between zero strain and maximum strain during a slamming event.

A peak detection algorithm was used to identify slamming events and assess parameters such as the peak accelerations and strain magnitude, as well as corresponding operating conditions such as roll angle and forward speed. The peak threshold for the algorithm was chosen as the mean value of the signal plus the standard deviation. A minimum peak separation of 0.5 seconds was also imposed. The peak detection algorithm results in peaks being detected at approximately the wave encounter frequency as determined by FFT. The detected peak data was further reduced by identifying the largest 1/3 magnitude slamming events, and calculating the mean of these. This method is consistent with statistical sea state evaluation methods.

Results and Discussions

The results presented here are limited to data collected from the bottom panels in bay 4. The starboard and port panels in bay 4 are identical with exception of the orientation of the DBL700 carbon fiber reinforcement; see Table 6-1.

Static Panel Stiffness Tests

The ratios of displacements to static load between the port and starboard panels in bay 4 are shown in Figure 6-12. This figure shows the shape of the bay 4 panels and the location of relevant structure including the keel, chine, main longeron and bulkheads. The locations where displacements were measured and the displacement ratios between port and starboard are indicated by the arrows. The static displacement testing shows a consistent trend between the port and starboard panels in bay 4. The measurements from the six

LVDT's at different locations indicate that the port panel displacement to a given load is on average 1.6 times that of the starboard panel. The lower stiffness in the port panel is anticipated due to the fiber orientation and panel shape. The section of the bay 4 panel between the keel and longeron is long and narrow, approximately 1400mm in length and 400mm wide. The 0 degree fibers are parallel to the keel in the port panel and perpendicular to the keel in the starboard panel. The fiber spanning the narrow width of the starboard panel results in high stiffness.

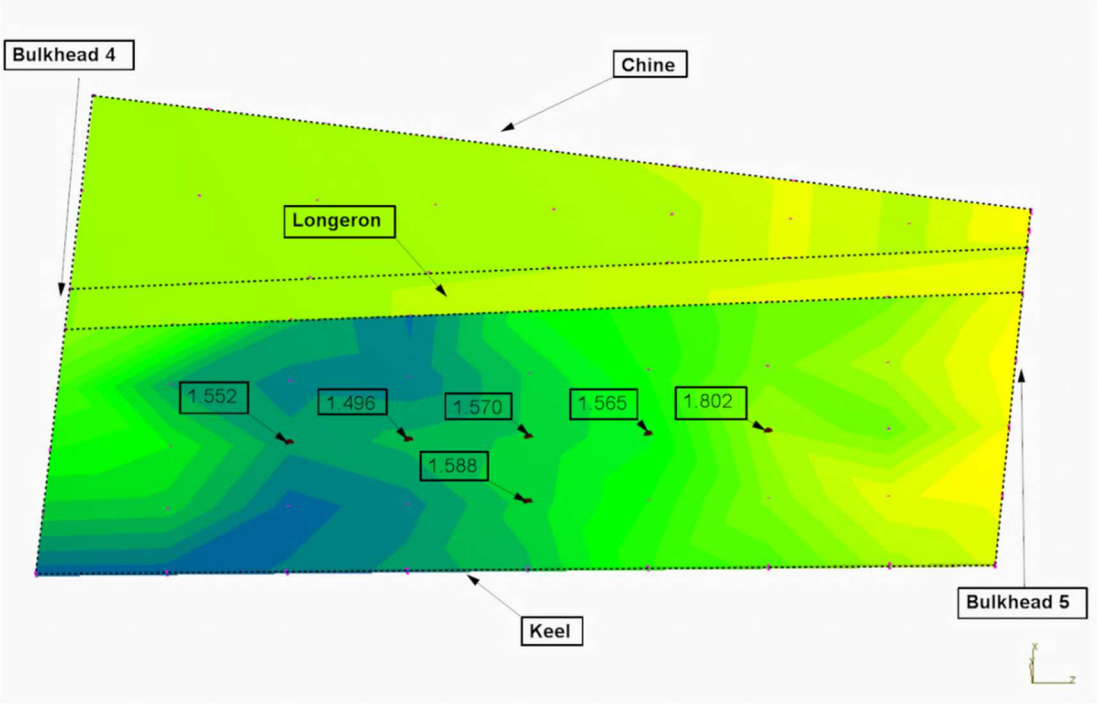

Figure 6-12 Bay 4 panel static stiffness ratios port/starboard

Dry Eigenfrequency Identification

Typical "accelerance" frequency response functions from experimental modal analysis for the port and starboard bay 4 panels are shown in Figure 6-13 and Figure 6-14. Synthesized FRFs from identified modes are also plotted.

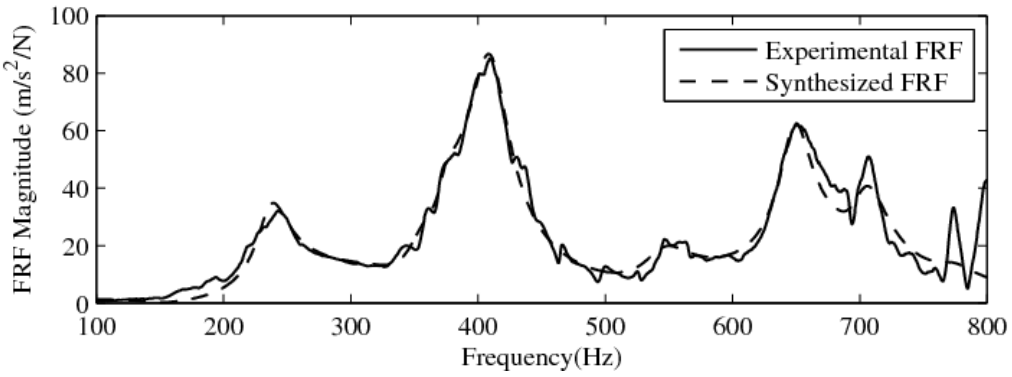

Figure 6-13 Bay 4 port accelerance FRF

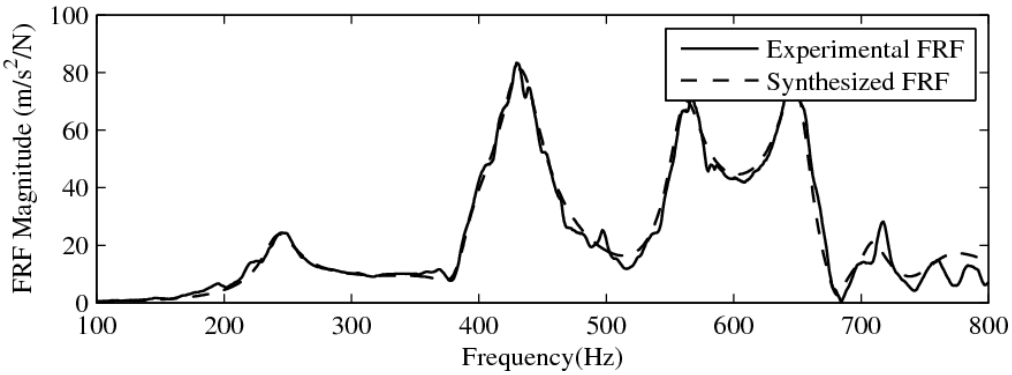

Figure 6-14 Bay 4 Starboard accelerance FRF

The first mode of vibration is a longitudinal half sine wave deflection of the panel and longeron, Figure 6-15. The next three modes are pure panel modes with essentially no deflection of the main longeron. These modes have a single transverse half sine bending wave and one, two and three longitudinal bending half-waves, respectively. Mode 5 consists of two transverse half sine waves and a single longitudinal bending wave.

Table 6-2 summarizes the frequencies of these modes for the bay 4 panels.

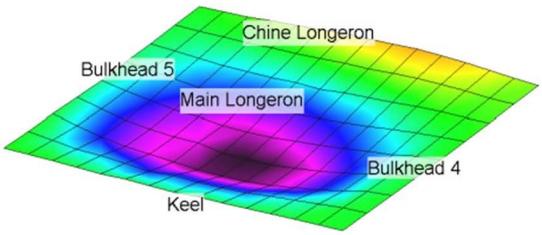

Figure 6-15 Bay 4 port panel mode 1

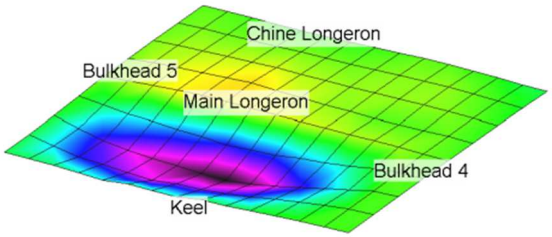

Figure 6-16 Bay 4 port panel mode 2

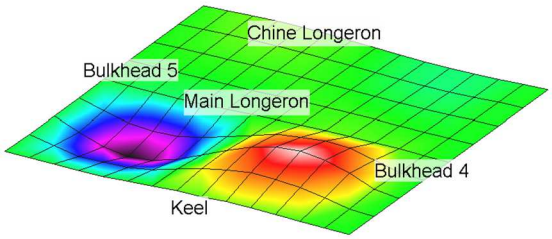

Figure 6-17 Bay 4 port panel mode 3

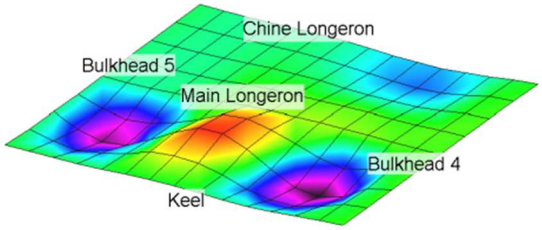

Figure 6-18 Bay 4 port panel mode 4

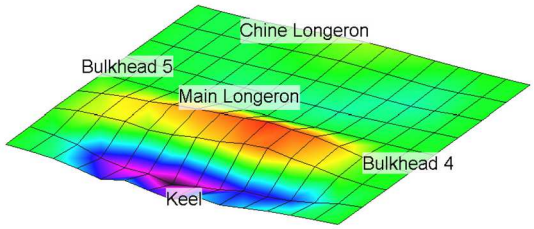

Figure 6-19 Bay 4 port panel mode 5

Table 6-2 Bay 4 panel eigenfrequencies

	Bay 4 Port Panel	Bay 4 Starboard Panel
Mode 1 Frequency (Hz)	238	246
Mode 2 Frequency (Hz)	373	394
Mode 3 Frequency (Hz)	411	437
Mode 4 Frequency (Hz)	555	561
Mode 5 Frequency (Hz)	647	650

Sea Trial Testing Slamming Characterization

A typical strain gage time history from sea trials is shown in Figure 6-20. The peaks seen in the time history are individual slamming events. The time between these events is typically 0.5 to 2.0 seconds.

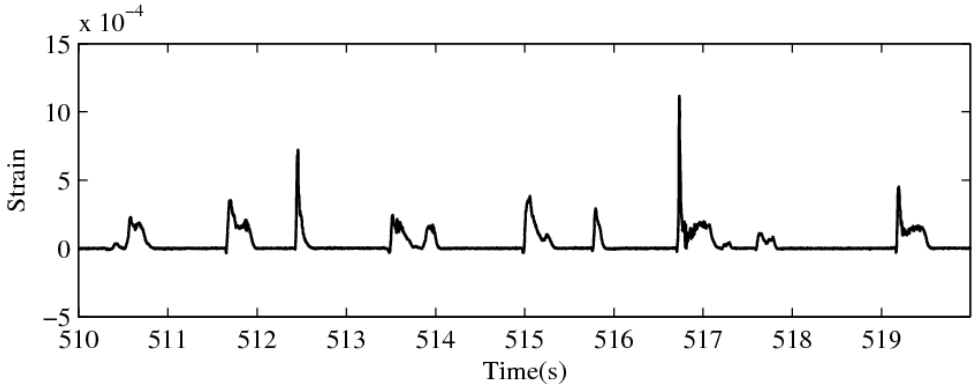

Figure 6-20 Typical strain gage time history for sea testing

An isolated slamming event is shown in Figure 6-21. The top plot shows 90 (transverse) and 0 degree (longitudinal) strain signals for the inner and outer skins on the port panel, while the bottom shows the response for the starboard panel. The strains on the inner skin are in tension, while the outer skin is in compression. The largest magnitude strains are seen on the

inner skin in the 90 degree direction, followed by the outer skin 90 degree. The strains in the 0 degree direction are small compared to 90 degree strains and many of these results presented will focus on the behavior of the gages oriented in the 90 degree (transverse) direction. This gives some support to the simplifying approach of modeling slamming using a beam in the transverse direction, as done by for example in [14, 15], rather than using a complete bottom panel.

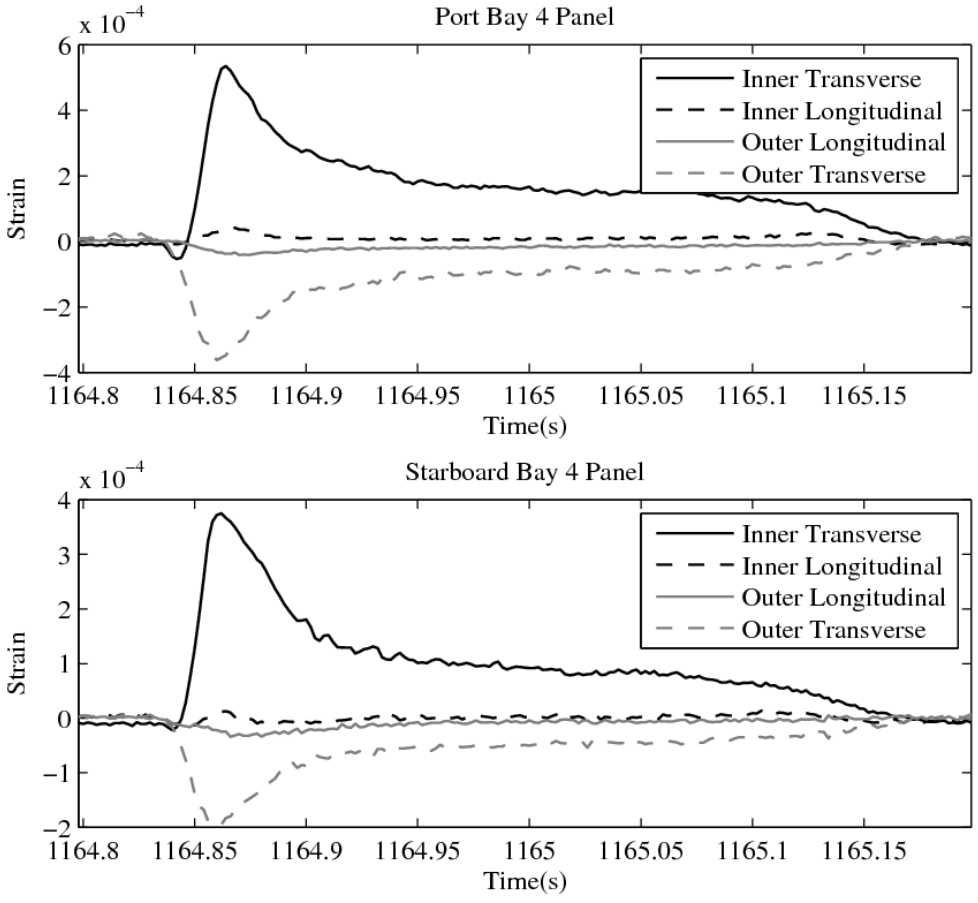

Figure 6-21 Strain response, single slamming event

These slamming events are characterized by a sharp rise to peak strain, after which the strain quickly drops off to a fairly constant residual level, and eventually decays to zero. In this case the initial rise time for the response is 20ms, initial drop off occurs 50ms after peak strain, and the duration of the decay to zero strain is an additional 200ms.

Test conditions

Figure 6-22 shows the vessel trajectories during a 30 minute test. A characterization of the sea state from NOAA buoy 44066 during the test period is given in Table 6-3. From this data an average wave direction of 191 degrees and high sea state 3 is inferred.

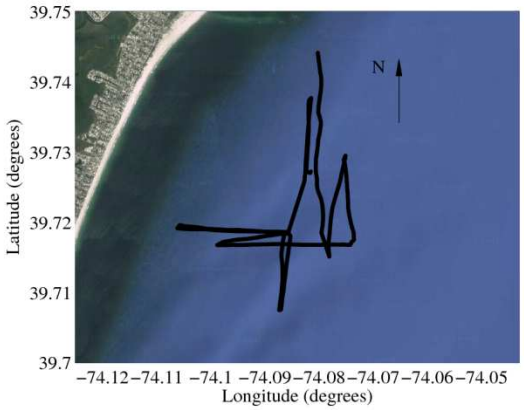

Figure 6-22 Test tracks

Table 6-3 NOAA wave buoy 44066 data, WVHT=Significant wave height, MWD= Mean wave direction of waves at dominant period, DPD= dominant wave period

Time	WVHT(m)	MWD(deg)	DPD(s)
1250	1.13	187	5.56
1350	1.18	185	5.88
1450	1.22	202	5.88

The distribution of heading and speed during the test is displayed in Figure 6-23. In this plot, the radial position indicates the speed, while the angular position indicates heading relative to north. This plot shows the maximum speed achieved in head seas (heading south) was approximately 15 m/s, while under following and quartering seas a maximum speed of 20 m/s was reached.

In order to isolate the role of heading, the data is filtered to select segments of head and following seas. The heading polar plot in Figure 6-24 shows the filtered test data. Only tracks with headings +/- 30 degrees from the mean wave direction during the test period were considered.

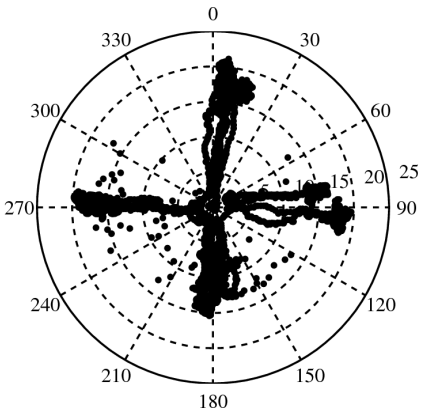

Figure 6-23 Distribution of heading and speed

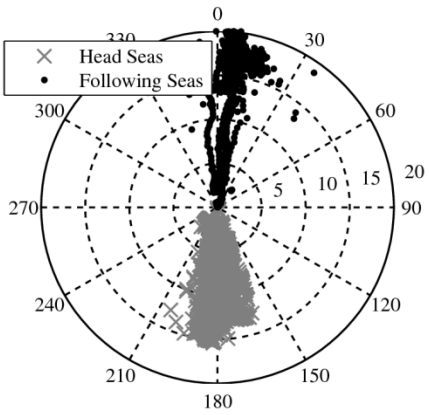

Figure 6-24 Test segments identified as head and following seas

Strain data for the 30 minute duration test were analyzed using a peak detection algorithm. The waveforms for the highest third slamming peaks for port and starboard bay 4 panel transverse strains are plotted In

Figure 6-25, Figure 6-26, Figure 6-27, and Figure 6-28, for head and following seas. In these plots the average slam waveform is denoted by the bold line. Further, the expected value and standard deviation are indicated by error bars. These plots indicate that on average higher strains resulted during head sea conditions, however this does not take into account the role of speed or factors like roll angle.

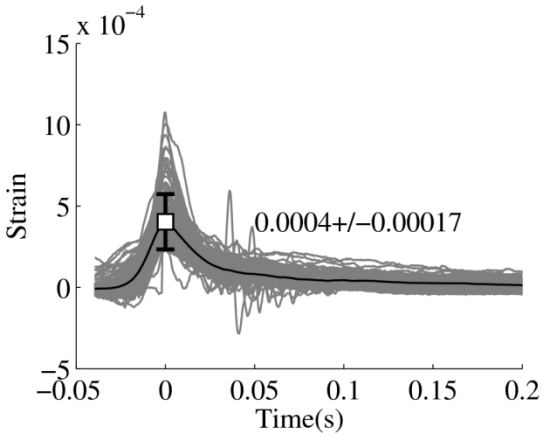

Figure 6-25: Largest 3rd Peak Strain Waveforms and mean bay 4 port transverse strain in head seas

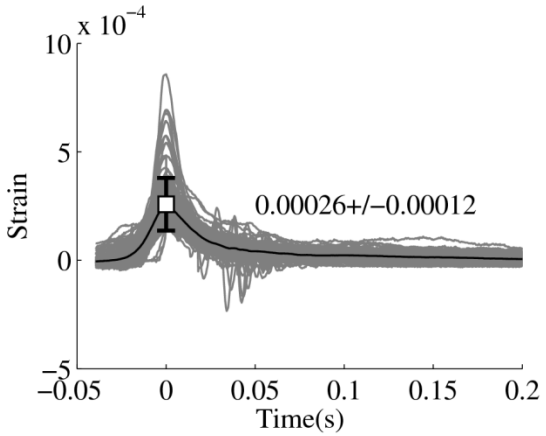

Figure 6-26: Largest 3rd Peak Strain Waveforms and mean bay 4 starboard transverse strain in head seas

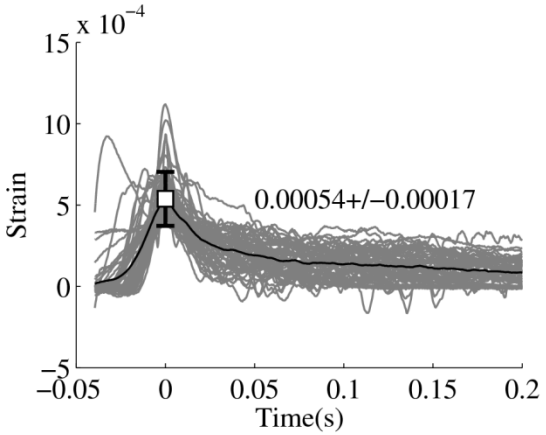

Figure 6-27: Largest 3rd Peak Strain Waveforms and mean bay 4 port transverse strain in following seas

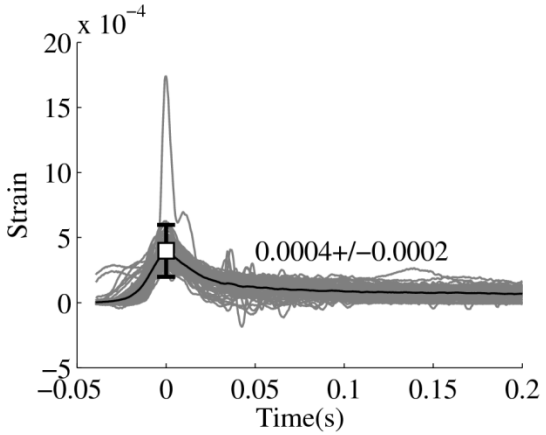

Figure 6-28: Largest 3rd Peak Strain Waveforms and mean bay 4 starboard transverse strain in following seas

The following figures show relationships between strain peaks and forward speed. This data shows that for a given speed, the mean strains are nearly twice as high under head seas as following seas. Pure quadratic functions were fit to the two data sets of each figure. As seen a quadratic relationship between peak strain and speed does not provide a good fit, in particular in head seas.

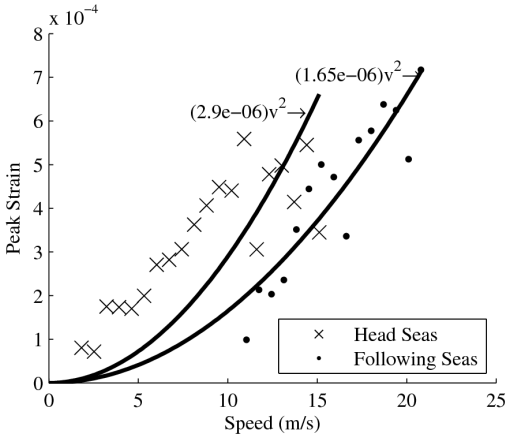

Figure 6-29: Forward speed vs bay 4 port mean peak 3rd transverse strain in head and following seas

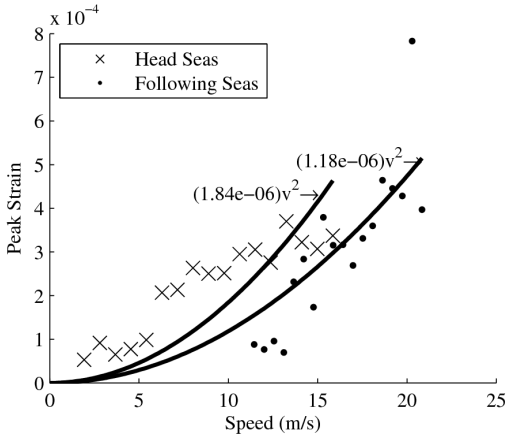

Figure 6-30: Forward speed vs bay 4 starboard mean peak 3rd transverse strain in head and following seas

Another parameter investigated is roll angle. In Figure 6-31 and Figure 6-32, roll angle is plotted against the mean highest third peak strains. There is some correlation between roll excursions and peak strains. Roll to the port side (negative roll) reduces effective deadrise angle and results in higher port panel peak strains, while the opposite is true of the starboard panel.

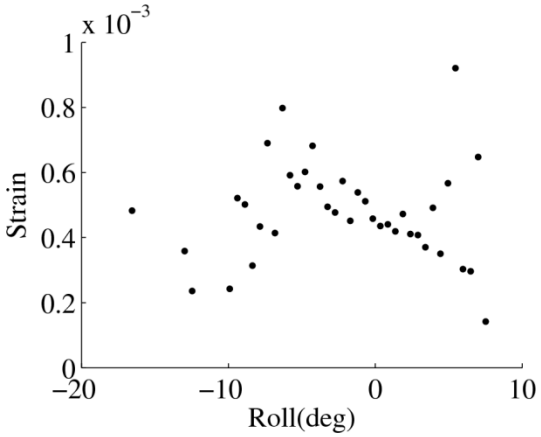

Figure 6-31 Roll angle vs bay 4 port transverse strain

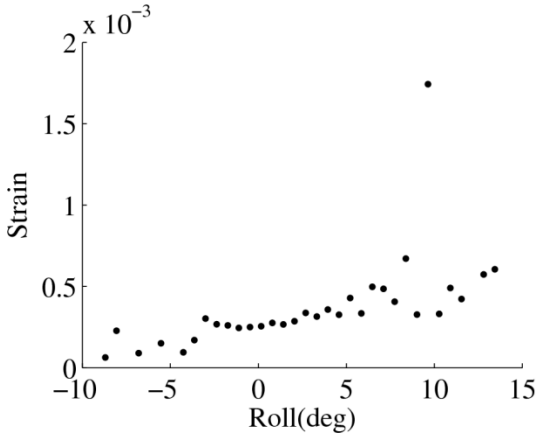

Figure 6-32 Roll angle vs bay 4 starboard transverse strain

Peak strains are plotted versus peak vertical accelerations at the longitudinal center of gravity in Figure 6-33 and Figure 6-34. These plots indicate a fairly linear relationship up to vertical accelerations of approximately 30 m/s^2. LCG accelerations above 30 m/s^2 show significant scatter with respect to strain. This may be due to the small sample size of slamming events at these high accelerations or the onset of hydroelastic effects.

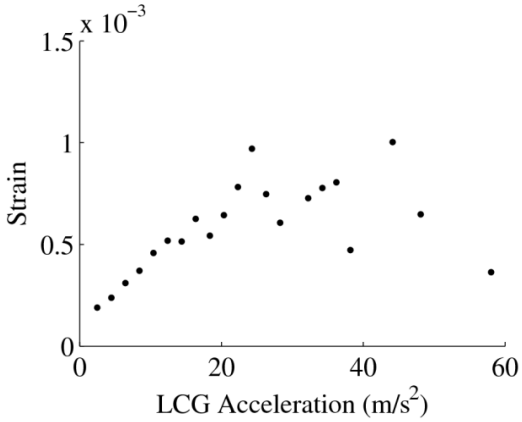

Figure 6-33 LCG vertical acceleration vs bay 4 port transverse strain

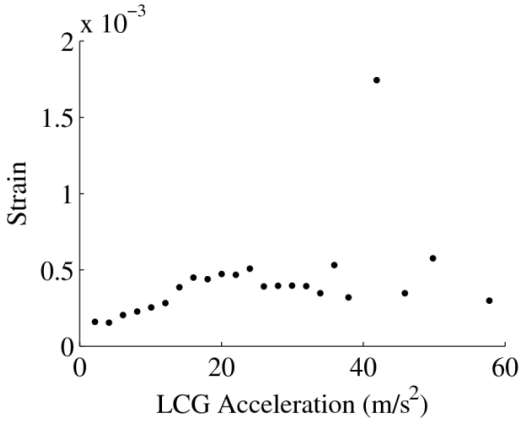

Figure 6-34 LCG Vertical acceleration vs bay 4 starboard panel transverse strain

Figure 6-35 and Figure 6-36 show peak transverse strains vs vertical velocity for the port and starboard panels. Here the vertical velocity is the greatest negative velocity measured in the vicinity of the panel in the 0.5 second period preceding a slamming event. This shows a linear trend to -3 m/s. As may be implied by the non-zero intercept, these plots do not account for local wave geometry and motion, the forward speed of the craft, roll behavior or deadrise angle.

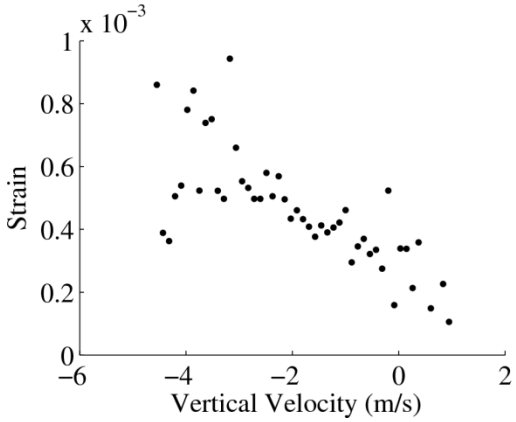

Figure 6-35 Vertical velocity vs peak bay 4 port transverse strain

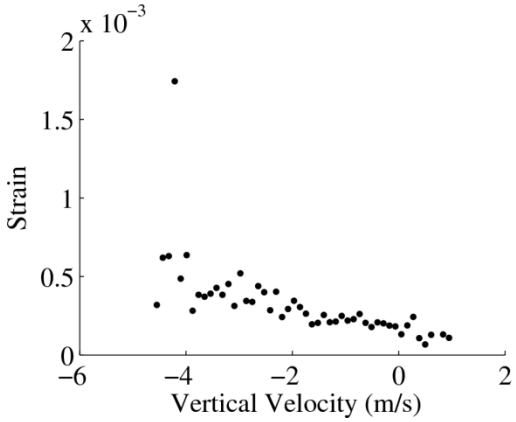

Figure 6-36 Vertical velocity vs peak bay 4 starboard panel transverse strain

Relative panel response

Figure 6-37 and Figure 6-38 show strain peaks sorted from smallest to largest for port and starboard transverse strains in bay 4 for head and following sea conditions. The secondary plots indicate the ratio between the sorted peak values. The ratio is 1.5 for the lower magnitude slamming events which correlates reasonably well with the static tests. There is a deviation from the static ratio at the highest strain level, again possibly due to hydroelastic effects or the small sample size.

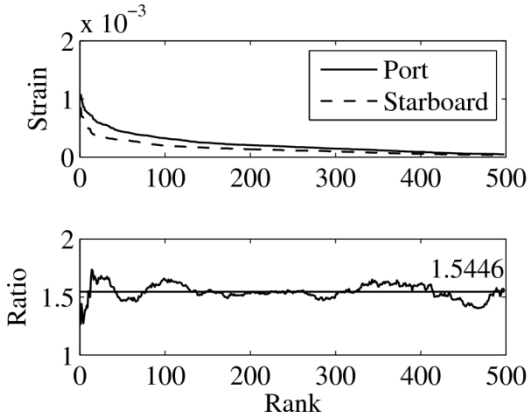

Figure 6-37 Peak transverse strains in bay 4 port and starboard panels in head seas

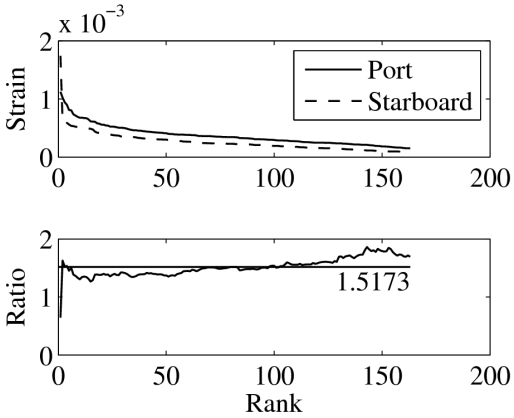

Figure 6-38 Peak transverse strains in bay 4 port and starboard panels in following seas

Histograms demonstrating the strain ratio between the left and right panels at every point in time are shown in Figure 6-39 and Figure 6-40. These plots express the number of times a specific ratio of port and starboard strain occurred at any point during the test. The histograms indicate that the strain ratio is centered at 1.434 in head seas and 1.6245 in following seas.

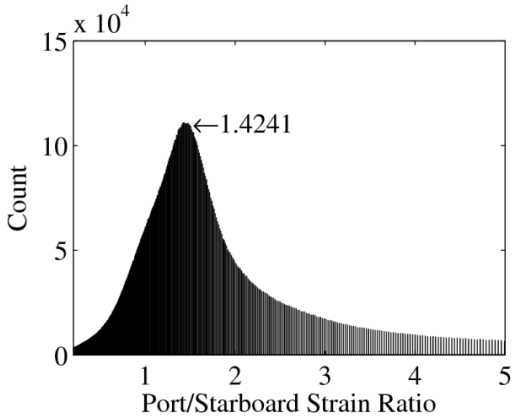

Figure 6-39 Bay 4 transverse strain head sea histogram

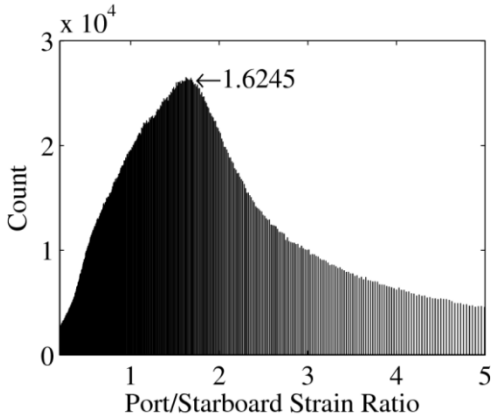

Figure 6-40 Bay 4 transverse strain following sea histogram

The averaged strain waveform plots under head seas,

Figure 6-25 and Figure 6-26 also demonstrate a similar relative strain level.

Panel Response in frequency domain

Fast Fourier transforms (FFT) of bay 4 bottom panel accelerations from sea trials are given in Figure 6-41. These are 10 second FFTs averaged over the duration of the 30 minute test for the accelerometers mounted on the port and starboard panels. The low frequency peak in the plots at 0.86 Hz is indicative of the wave encounter frequency. There are also peaks that correlate well with the first five dry eigenfrequencies of the panels. The FFTs of the bay 4 transverse panel strains are shown in Figure 6-42. The strain Fourier plots also demonstrate the wave encounter frequency, but dry panel modal frequencies are not as clear.

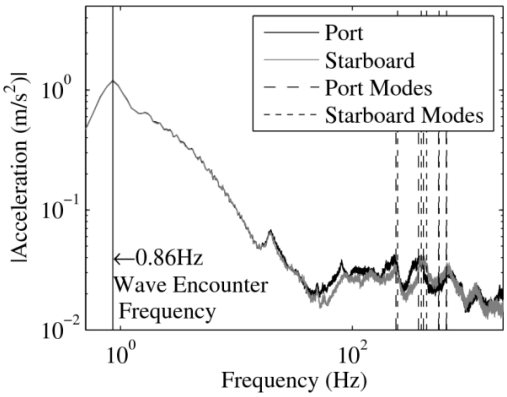

Figure 6-41 Bay 4 Panel Acceleration FFT

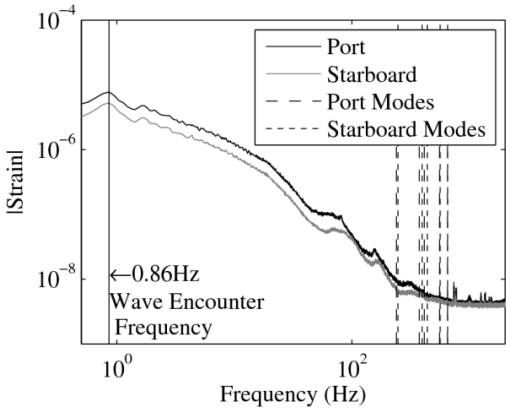

Figure 6-42 Bay 4 Panel Transverse Strain FFT

Both the acceleration and strain FFT plots show subtle peaks in the vicinity of 50-100 Hz. Efforts to better resolve this frequency content using conventional and short time Fourier analysis methods were unsuccessful for these dynamic and non-stationary slamming events. The demands of both precise time localization and frequency resolution are at odds in Fourier analysis and a different method is needed to analyze the evolution of frequency content in slamming. The use of wavelet analysis is being investigated.

However, vibratory behavior in this frequency range can be observed in the time domain in some cases. The waveforms from slams with the highest 1% magnitudes are shown in Figure 6-43 and Figure 6-44. Following the initial slamming peak, these plots show a short duration vibration. The frequency is on average 73 Hz in the port panel and 92 Hz in the starboard panel.

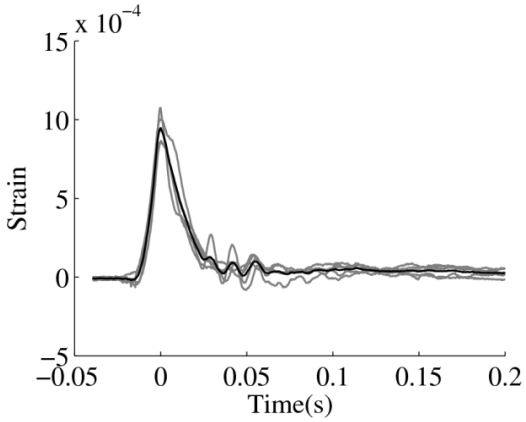

Figure 6-43 Transverse strain waveforms from highest 1% of slams in bay 4 port panel in head seas

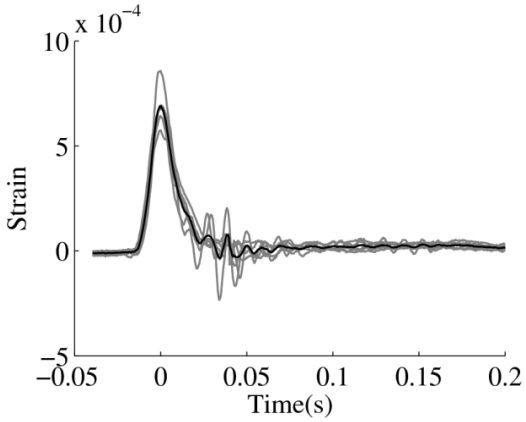

Figure 6-44 Transverse strain waveforms from highest 1% of slams in bay 4 starboard panel in head seas

This vibration may be due to coupling of water mass to the panel resulting in "wet eigenfrequencies". Table 6-4 gives a comparison of the vibration frequencies observed in the port and starboard bay 4 panels and the wet eigenfrequencies predicted by the methods from [39] and [14]. The panel was assumed to be fully wetted for the latter estimate (k=1). The deadrise of the bay 4 bottom panels vary from $28°$ at the rear bulkhead to $38°$ at the fore bulkhead. The local deadrise angle at the panel center $\beta = 32°$ was used for the Stenius wet eigenfrequency estimate. These estimates correspond to dry mode 2, excitation of the panel region extending from the keel to the main longeron.

Table 6-4 Comparison of Observed and Calculated Panel Vibration Frequencies for Bay 4 Panels (Mode 2)

	Port Frequency (Hz)	Starboard Frequency (Hz)
Observed Wet Eigenfrequency	73	92
Lv Wet Frequency (k=1)	91	96
Stenius Wet Frequency ($\beta = 32°$)	76	81

Panel Response and Water Impact Velocity

The critical vertical velocity at which the hydroelastic parameter R=1, equation (6-1) is 21 m/s for the port panel and 22 m/s for the starboard panel assuming the local deadrise is a constant 32 degrees. At vertical speeds above this, or when effective deadrise is reduced by roll excursions, hydroelastic effects are expected to play a role. As the forward velocity of the vessel was up to 20 m/s and roll angle up to 20 degrees during the test period, certain wave geometry or vessel motion may have resulted in supercritical impact velocity and a response dominated by hydroelastic, rather than static, behavior.

Figure 6-45 and Figure 6-46 show peak strain values plotted against an approximation of the hydroelastic parameter R. This approximation of R takes into account roll angle at the time of the slam in correcting local deadrise. For both port and starboard panels, the minimum value of R encountered during the sea trials is approximately 1.4.

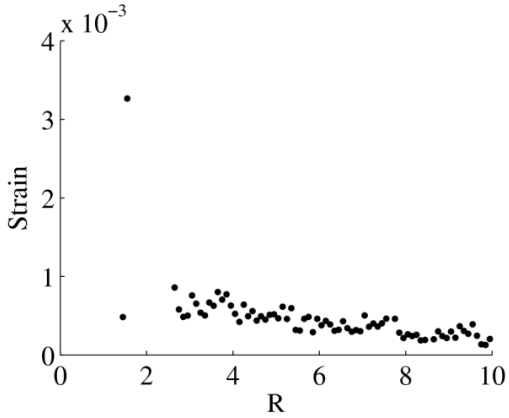

Figure 6-45 Peak transverse strains vs hydroelastic parameter R in bay 4 port bottom panel

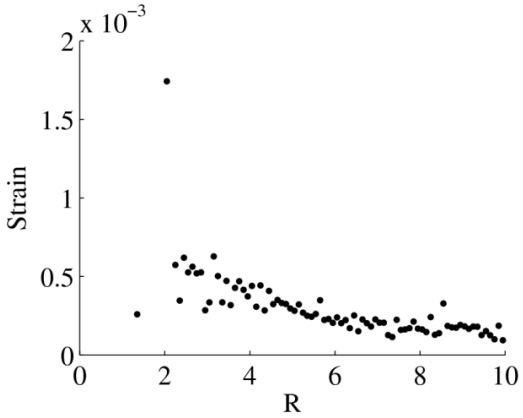

Figure 6-46 Peak transverse strains vs hydroelastic parameter R in bay 4 starboard bottom panel

The non-dimensional characteristic velocity parameter $\bar{c}$ of [14] is plotted against strain in Figure 6-47 and Figure 6-48. Port and starboard panels have maximum characteristic velocities of 1.6 and 1.7 respectively. At values above 1, inertial effects are expected to become significant [15]. In the present data, the relationship with strain is nearly linear with two outliers at the highest strain and loading rates. The ratio of the linear fits, 1.6 is close to the static stiffness ratio for the port and starboard panels.

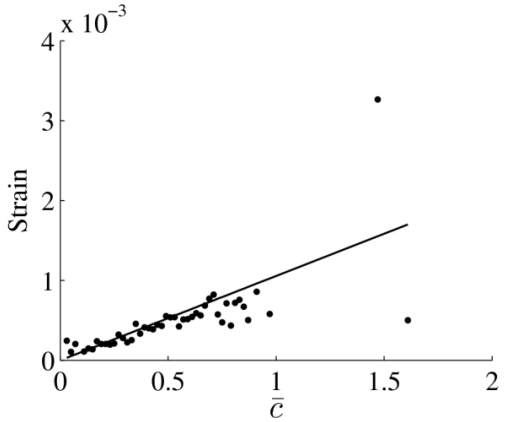

Figure 6-47 Characteristic velocity $\bar{C}$ vs peak transverse strains in bay 4 port bottom panel

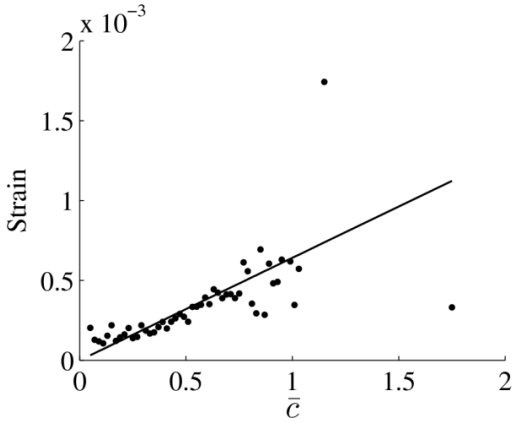

Figure 6-48 Characteristic velocity $\bar{C}$ vs peak transverse strains in bay 4 starboard bottom panel

The outliers at the highest impact speed and strain may be due to general error in estimating water impact speed or it may be indicative of hydroelastic or inertial effects.

At the end of the initial slamming phase it has been proposed that the velocity difference between the water and panel surface is zero [13], thus a velocity differential between the panel and rigid body will occur. In order to further investigate this behavior, the velocity differential was estimated by integrating accelerations measured at the panel center and at bulkheads assumed to be rigid.

Plots indicating peak strains vs panel velocity difference are given in Figure 6-49 and Figure 6-50. The plots demonstrate a linear scaling in the panel-rigid body velocity differential and peak strain. Once again the ratio between port and starboard slopes of 1.5 appears to mirror the static stiffness of the panels.

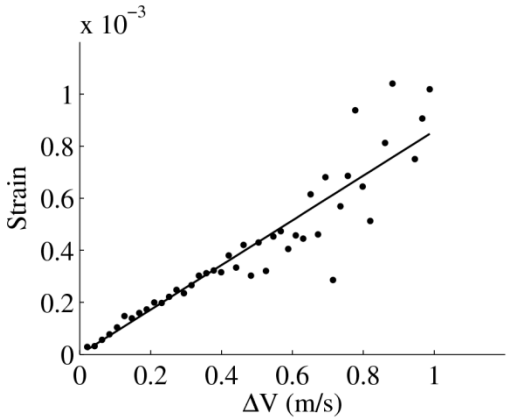

Figure 6-49 Rigid body-panel velocity differential vs peak transverse strains in bay 4 port bottom panel

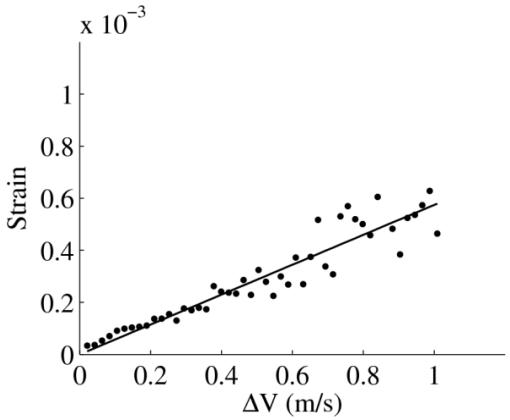

Figure 6-50 Rigid body-panel velocity differential vs peak transverse strains in bay 4 starboard bottom panel

Summary and Conclusion

Operation of the "Numerette" Slamming Load Test Facility has resulted in the collection of a wealth of slamming data. Subject to low to moderate slamming loads the strain response in the bottom panels differed somewhat from the relationship observed in static testing. A panel that was 1.6 times more compliant under static loading had roughly 1.5 times higher strains subject to slamming loads. Further, a linear relationship was observed between the water impact speed and strain. Future tests will see the addition of displacement and pressure transducers that will make it possible to better correlate the slamming loads and the structural response.

Estimates of the loading rates during testing suggest impact speeds observed during testing are mostly below that at which hydrodynamic effects or inertial effects are to be expected. Regardless, the highest strain slamming events show a vibratory frequency similar to the wetted natural frequencies predicted in [39] and [14]. Additionally, deviation from the linear relationship between impact velocity and strain was observed during the highest intensity slamming events. This may be a result of error in estimating the water impact speed as a direct measurement of the water surface was not made. Future work may include installation of proximity sensors for better estimation of water impact velocity and modification of panels to reduce stiffness.

In order to analyze non-stationary fluid structure interactions expected at critical impact speeds an alternative to Fourier analysis is needed. The simultaneous requirements of localization in time and frequency demanded are at odds in Fourier analysis. Future work will investigate the use of wavelet analysis methods to more precisely characterize the

evolution of the strain and acceleration frequency spectra during highly dynamic slamming events.

Acknowledgements

Funding for developing and testing the slamming load facility was provided by ONR (awards N00014-08-1-0203, N00014-08-1-0227, N00014-08-1-0228, N000141-01-07-6-7). The program monitor, Dr. Roshdy Barsoum, is gratefully acknowledged for his support.

7. Analysis of Bottom Panel Slamming Using the Wavelet Transform

Thodal, R.S., Grenestedt, J.L.

Abstract

In the present research, bottom slamming data including accelerations, strains and deflections were recorded during tests of a 9 meter high-speed boat in the Atlantic Ocean. The data were analyzed using wavelet transforms. Wavelets have the advantage that frequency content at different times can be obtained with high resolution in both domains. One particular slamming event was extracted and analyzed in more detail. This particular event showed rather high accelerations at two times, separated by 0.1 s. Wavelet analyses indicated that the initial peak was associated with vibrations with dry panel frequencies, whereas the second peak vibrated with wet panel eigenfrequencies. In other words, the former peak was due to excitation away from the panel where the accelerometer was mounted whereas the latter peak was due to water slamming on this panel. The frequencies and modes of vibrations observed during these transients show good agreement with prior experiments and theory. The ability to identify dry and wet vibration modes has important implications for the slamming response when impact speeds approach the critical range where hydroelastic inertial effects become dominant.

Introduction

Bottom slamming is a critical consideration in the design and operation of high speed ships and marine structures. Slamming impact loads can result in extreme motions, injury to personnel and damage to equipment and structures. This process is characterized by a high intensity pressure peak moving rapidly over the hull, followed by a lower magnitude residual pressure. The pressures largely depend on the impact speed and the deadrise angle of the hull.

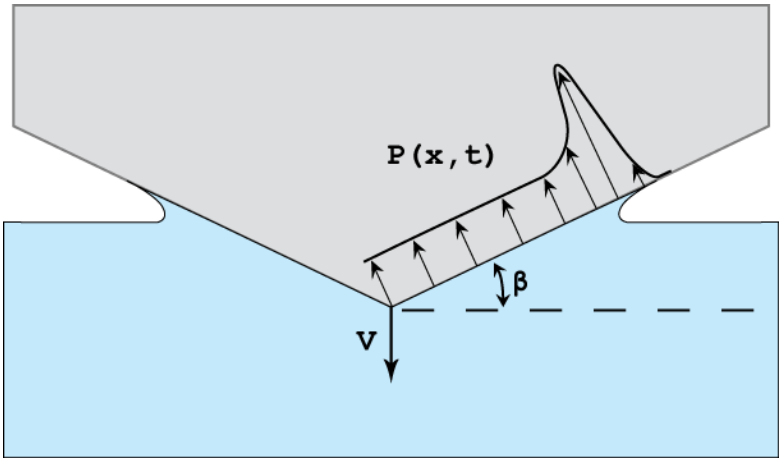

Figure 7-1:Slamming of a wedge shaped body

Currently, consideration for slamming in high speed ship design is largely driven by semi-empirical design methods from classification societies such as DNV [3] and ABS [5]. These methods use the ship geometry and expected operating conditions to define an equivalent slamming pressure. This static, evenly distributed pressure load does not accurately represent the physical mechanisms of slamming, but is intended to serve as a conservative load case that is simple to use in the design phase. This approximation results in compromises to performance, safety, and structural efficiency. The development of design

methods that more accurately account for the true loads and responses in slamming has the potential to substantially improve the design of high speed craft.

Von Karmann made some of the first major contributions toward this goal of a comprehensive slamming model. Von Karmann [9] developed a simple momentum based theory for estimating pressure loads on a rigid wedge shaped body impacting a calm water surface. This early analytical work was subsequently refined by many others including Wagner [10]. Wagner introduced a potential flow theory that included the effects of the local uprise of water. Peak pressures predicted by these early theories proved to agree well with drop test experiments [21]. However most early experiments were conducted with wedges constructed from steel panels that were effectively rigid. This was consistent with the theories available but not necessarily relevant to real ship structures.

Flexible hull structures introduce additional complexity to the analysis of slamming, as kinematic and inertial hydroelastic effects can occur, e.g., Stenius et al [11]. Kinematic effects occur when pressure loads lead to deformation of bottom panels. This deformation results in changes in the kinematic boundary conditions, affecting the pressure distribution. Inertial effects result from the mass of the structure as well as coupling of water mass to the panel, the additional mass reduces the natural frequencies of the structure.

Research in slamming over the last 30 years has extended the field to flexible structures and the effects of hydroelasticity. Kvalsvold and Faltinsen [12], [2] were some of the first to address the phenomenon in depth. Early efforts modelled the wet deck of catamaran as a Timoshenko beam with a simplified flow over it. This model demonstrated that there was a potential for large deviations in the net force on a flexible wet deck relative to a rigid

representation. It was found that a key parameter in the role of hydroelasticity in the structural response is the non-dimensional impact velocity or the wetting period during impact relative to the first natural frequency of the structure. At high impact velocities and low deadrise angles, the wetting time is reduced and for a typical boat bottom the hydroelastic effects become more pronounced. However, for more compliant bottoms the structural response may be reduced as wetting times get shorter (Lv and Grenestedt [14], [15]).

Faltinsen compared strains of an orthotropic plate loaded in a quasi-static manner to the hydroelastic beam model at a range of non-dimensional impact velocities [53]. It was shown that at low impact velocities, the two behaved very similarly and strain scaled with velocity squared. At high impact velocities, the hydroelastic model diverged from quasi static behavior, resulting in lower strains that scaled with velocity to the first power. At velocities between these extremes was a critical region where the wetting period was similar to the lowest wetted natural frequency. In this case the response actually exceeded that of the quasi-static case.

This result agrees with other analytical, numerical and experimental studies of slamming on flexible structures. Lv and Grenestedt [14], [15] recently completed a study wherein the bottom panel of a boat was treated as an Euler-Bernoulli beam subjected to a pressure load modelled as a high intensity peak travelling over the beam followed by a lower residual pressure. A wide range of stiffness, pressure ratios and speeds were investigated. The response in terms of bending moment and deflection was almost double the quasi static case when the wetting period was close to the first natural frequency. When the pressure load

moved slowly the response was equal to the quasi static case; however, at very high speeds the response was less than in the quasi static case.

Stenius investigated hydroelasticity numerically using the commercial finite element code LS-DYNA [11]. One result of the study was a comparison of maximum deflections for the hydroelastic solution relative to the rigid quasi static solution for a range of non-dimensional impact velocities. The result showed the hydroelastic response was up to 40% greater than the quasi static response in the region of the critical impact velocity.

Experimental studies of flexible panels in slamming include, among others, Hayman [23], Samuelides and Katsaounis [54], Battley and Lake [49], Stenius et al. [52] . The earlier tests by Hayman and Katsaounis were drop tests wherein the impact velocity profile was controlled by the mass and drop height of the specimen. This was a major limitation of early tests, limiting the applicability to real slamming [24]. Later experiments performed with the Servo Hydraulic Slamming Test System (SSTS) developed by Battley at Industrial Research Limited allowed for controlled velocity profiles. In one recent study by Stenius et al [52] impact tests were performed with the SSTS on panels with a wide range of stiffness. These panels were instrumented with transducers to measure strain, displacement and pressures. The influence of hydroelastic effects was identified by comparing experimental data with a semi empirical rigid quasi static reference solution from a finite element analysis. It was shown that inclusion of hydroelastic effects resulted in a change in magnitude of strains and displacements as well as a lag in the time at which the peak response occurred. Differences in response magnitude of up to 50% were observed. However, it was also noted that in the

range of impact speeds expected in a high speed ship design, the hydroelastic effects are limited.

In the present research, data from full scale slamming experiments with a purpose built high speed boat is analyzed to assess the structural response during a slamming impact, including evidence, if any of hydroelasticity. It is expected that if hydroelastic effects are significant, the response will be dominated by vibration at the wet eigenfrequencies. Conversely if the response is quasi static in nature, the spectral content will be concentrated at the excitation frequency. Wavelet analysis techniques are used to simultaneously localize the response in the time and frequency domains. This makes it possible to identify the transition from vibration at dry eigenfrequencies preceding water impact into vibration at wet eigenfrequencies as the panel surface is wetted. Further, an array of accelerometers is used so the vibratory modes can be directly identified.

Wavelet analysis methods have seen some limited use in analysis of experimental slamming data recently. Dessi [55] and Kim et al. [56] used the wavelet transform in detection algorithms for slamming. The method was used to detect high frequency global vibrations by analyzing experimental vertical bending moment data from strain gages on a scale model in a tow tank. The severity of vibration at the ship's vertical bending mode frequency was correlated with other parameters such as impact velocity.

Amin et al. [57] also used the continuous wavelet transform of strain data to investigate hull vibrations in slamming. The high frequency structural response and fatigue effects as well as the non-stationary, random nature of slamming were cited as motivations for use of the wavelet transform. The wavelet transform was applied to experimental data from a strain

gage located on the keel of a catamaran in order to assess the response during slamming impacts. This approach proved useful in identifying critical frequencies as well as damping ratios for global modes in slamming.

Hydroelastic Characterization

Many slamming theories have attempted to predict the degree of influence hydroelastic inertial effects have on structural response. The element that is common to many of these is characterization by the ratio of the loading period to the period of the lowest (wetted) natural frequency [53], [39], [14]. If the loading period is long relative to the first wetted natural frequency, the structure is expected to behave in a quasi-static manner, whereas for higher loading rates hydroelastic effects are expected.

The non-dimensional dynamic hydroelastic characterization factor for a beam approximation of a bottom panel [39] is given as

$$R = 4\left(\frac{\mu_{np}}{\pi}\right)^2 \frac{\tan\beta}{V}\sqrt{\frac{D}{\pi\rho_w b^3}} \qquad (7\text{-}1)$$

where β is the deadrise, D is bending stiffness per unit width of the beam, ρ_w is water density, V is impact velocity, b is panel width (or length of the beam approximating the bottom panel), and μ_{np} is a parameter related to the boundary conditions given as $\mu_{np} = \pi$ for simply supported boundaries and $\mu_{np} = 4.73$ for clamped boundaries. Further, the first wetted natural period is

$$T_{NP} = \frac{2\pi}{\mu_{np}^2}\sqrt{\frac{(\overline{m} + \overline{m_a})b^3}{D}} \quad (7\text{-}2)$$

Here $\overline{m}$ is the structural mass per unit length of the beam and $\overline{m_a}$ is added mass due to coupling of water. $\overline{m_a}$ is

$$\overline{m_a} = \frac{1}{2}k_a\frac{\pi}{2}\rho_w(b\cos\beta)^2 \quad (7\text{-}3)$$

The factor k_a is an added mass scaling factor.

A similar non-dimensional characteristic velocity $\bar{c}$ was introduced in [14] to describe the ratio of the loading rate to the first natural period of the wetted panel.

$$\bar{c} = \frac{V\pi}{2sin(\beta)}\sqrt{\frac{\mu^* L^2}{EI}} \quad (7\text{-}4)$$

Here, *L* is panel width (or length of the beam approximating the bottom panel), *EI* is the bending stiffness, and μ^* is mass per unit length of the panel including added water mass given as

$$\mu^* = \mu + k\rho_w\pi Ld/8 \quad (7\text{-}5)$$

Here μ is the mass per unit length of just the panel, *d* is panel length (or width of the beam approximating the bottom panel) and *k* is a factor describing the degree of wetting of the panel ranging from *k*=0 (dry) to *k*=1 (fully submerged).

Note the characteristic velocity $\bar{c}$ and hydroelastic characterization factor *R* are related by $\bar{c} = \pi/(R\sqrt{2}cos\beta)$ assuming simply supported boundary conditions.

Frequency Domain Methods

In order to experimentally analyze some of these phenomena in slamming, a method is needed that can identify the behavior of the structure in the frequency domain. This represents a challenge as the relevant signals are highly non-stationary, the excitation of the structure is very short in duration and the response is coupled to the time dependent wetting of the hull.

Traditional Fourier analysis of quantities relevant to slamming such as pressure, strain and acceleration results in a loss of time localization and obfuscation of frequency content. The short time Fast Fourier Transform (STFFT) requires an undesired tradeoff in terms of time and frequency localization. Wavelet techniques have recently been developed to provide a better compromise in this area. The wavelet transform differs from the fourier transform in that it uses a windowing scheme wherein low frequency components have long time windows and high frequencies have short time windows. The result is a more optimal time-frequency resolution.

The wavelet transform $W_\psi(a,b)$ of a signal $x(t)$ can be expressed as the convolution of $x(t)$ and a family of wavelets $\psi_{a,b}(t)$ [58].

$$W_\psi(a,b) = \int_{-\infty}^{\infty} x(t)\psi_{a,b}^*(t)dt \qquad (7\text{-}6)$$

The wavelet families consist of a series of daughter wavelets obtained by dilatation and translation of a mother wavelet $\psi(t)$.

$$\psi_{a,b}(t) = \frac{1}{\sqrt{a}}\psi\left(\frac{t-b}{a}\right) \qquad (7\text{-}7)$$

Here is a is a scale parameter that determines the support width of the daughter wavelet, while b is the parameter that describes the translation in time. The effect of varying the scale parameter is to change in the frequency of the daughter wavelet. Thus the wavelet transform $W_\psi(a,b)$ describes the magnitude of a frequency component determined by a, at a point in time determined by b. For more on the wavelet transform see for example [58] and [59].

One application of wavelets that has recently emerged is in operational modal analysis. In contrast to traditional modal analysis wherein the input excitation and response are measured, operational modal analysis only involves measurement of the response of a structure to in service ambient excitation. This approach is particularly attractive for applications like slamming where the excitation is not fully understood. The wavelet transform offers a means for a time localized analysis of the response. Lardies [59] used the wavelet transform to extract the modal parameters of both a simulated system and a real tower structure instrumented with accelerometers and subjected to random wind loads. Damping ratios, natural frequencies and mode shapes were estimated from the experimental data and were shown to compare well with theoretical values.

In the present work, the continuous wavelet transform has been used on experimental data to firstly qualitatively describe the time-frequency domain features of the structural response in slamming. The natural frequencies and mode shapes are then estimated following the approach of Lardies. The mode shape χ_{ij} is the *j*th component of the mode associated with natural frequency *i*,

$$\chi_{ij} = W_{\psi}^{j}(a_i, b)/W_{\psi}^{r}(a_i, b) \quad (7\text{-}8)$$

Here W_{ψ}^{j} is the wavelet transform of the signal from the accelerometer at point j and W_{ψ}^{r}, the wavelet transform of a reference accelerometer signal.

Numerous wavelet functions have been developed, each with traits that make them suited to different types of analyses. In the present work, the common modified morlet wavelet is used. This wavelet is a slight variation of the traditional morlet wavelet that includes a parameter N for tuning of the time-frequency resolution balance. Larger values of N improve frequency resolution at the cost of temporal resolution.

$$\psi(t) = e^{j\omega_0 t} e^{-t^2/N} \quad (7\text{-}9)$$

Experimental Methods/Numerette

The slamming load test boat *Numerette* is a 9 meter long, 1.9 meter wide hybrid steel / composite boat designed by Grenestedt and manufactured at Lehigh University Composites Lab. The boat consists of a welded AL-6XN stainless steel skeleton and composite sandwich panels for the bottom, deck, sides, bulkheads and hatches. Composite panels were manufactured by vacuum infusion utilizing carbon and glass fiber reinforcements, PVC foam cores and epoxy or vinyl ester resin. Composite panels were bonded to the stainless steel frame with a structural epoxy.

Figure 7-2: Numerette slamming test boat

The layup of the 10 composite panels that make up the hull bottom were tailored specifically to the purpose of slamming analysis. At a given lengthwise position the port and starboard bottom panels use differing reinforcements or fiber orientation resulting in significant disparity in stiffness. For example the starboard and port bottom panels of bay 4 are constructed with the same Divinycell PVC foam core and Devold DBL700 triaxial (0°, ±45°) carbon reinforcement, but in the port panel the 0° fibers are oriented parallel to the keel, while in the starboard panel the 0° fibers are oriented perpendicular to the keel. As a result of the difference in layup and the long and narrow aspect ratio, the starboard panel is substantially stiffer.

A planform of the Numerette is shown in Figure 7-3. The indicated starboard panel near the bow was selected for detailed analysis. At this lengthwise location the slamming impacts are often the most severe (at relatively high speeds at relatively high sea states).

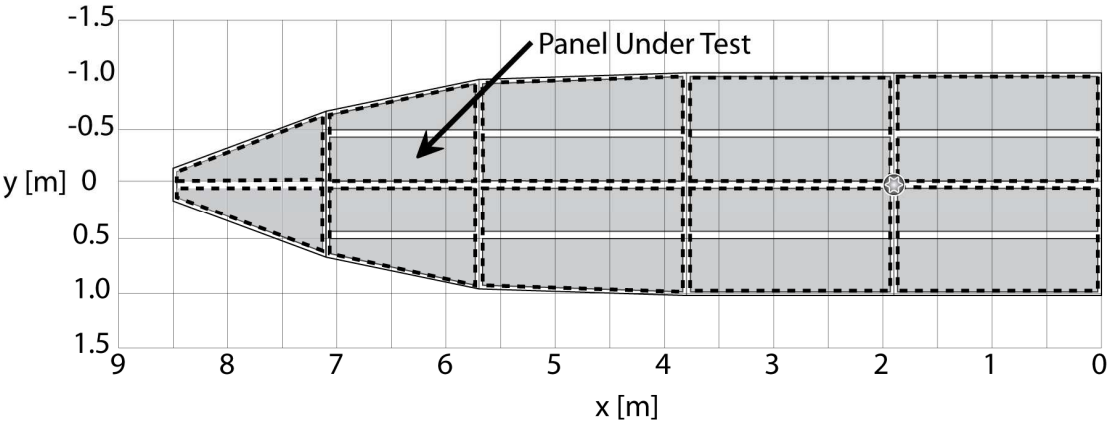

Figure 7-3: Location of panel under test

Instrumentation

The Numerette is equipped with extensive instrumentation to assess both the loads and structural responses involved in slamming. The steel skeleton and composite panels are equipped with strain gages. On bottom panels strain gages are located on both inner and outer skins and oriented both transverse and parallel to the keel. In total 27 gages are installed on the steel skeleton and 96 gages on the bottom panels. The bottom panels are also equipped with accelerometers. PCB model 352C04 +/-500g 0.5 to 10000 Hz accelerometers are installed to measure panel out-of-plane acceleration and displacement. PCB model 113B26 3.45 MPa pressure sensors were installed in the panels in a through-hole

configuration. A cross section of an instrumented composite sandwich panel is shown in Figure 7-4.

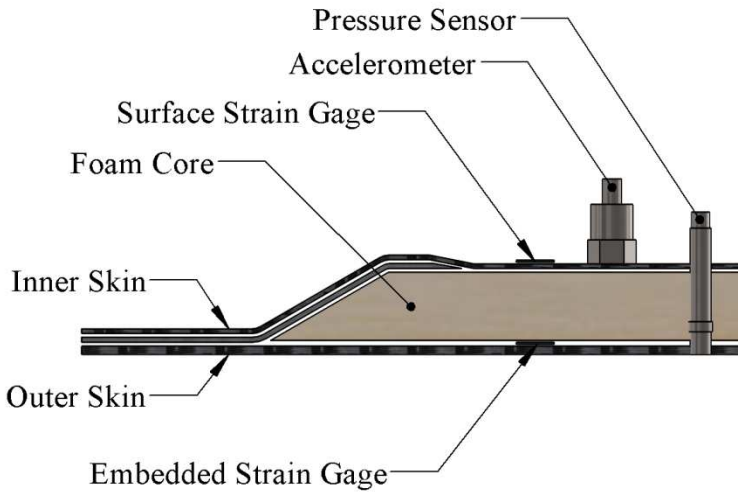

Figure 7-4: Sandwich panel cross section with sensor locations

The layout of the instrumentation of the panel under test is shown in Figure 7-5. The LVDTs were installed in an aluminum frame mounted between the keel and longeron, Figure 7-6. Omega LD320-15 AC LVDTs with +/-15mm range were used.

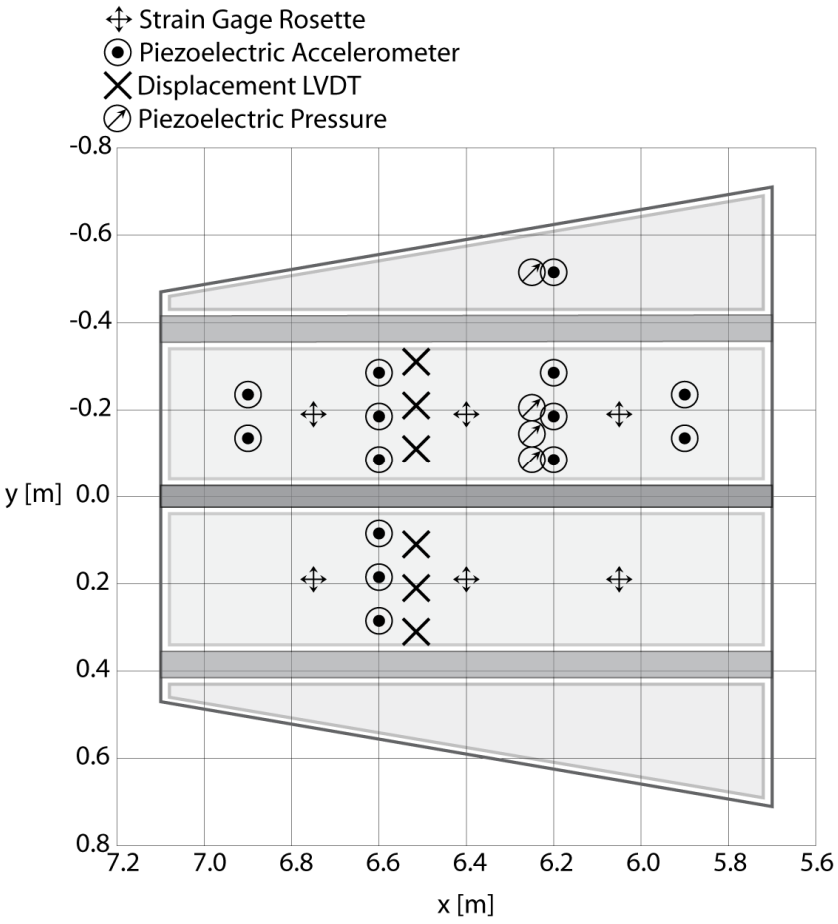

Figure 7-5: Test panel sensor locations

Figure 7-6: Test Panel

An onboard data acquisition system provided signal conditioning and recording of all sensor data. Strain gage signal conditioning and digital conversion was performed by National Instruments NI-9237 24 bit modules. National Instruments PXI-4472b 24 bit modules were used with IEPE pressure sensors and accelerometers. Custom Analog Devices AD698 based signal conditioners performed LVDT excitation and signal demodulation, while National Instruments PXI-6254 16 bit modules were used for analog to digital conversion. Two VectorNav VN-200 inertial navigation systems were mounted on a stiff bulkhead near the center of gravity to measure rigid body motions. Pressure, strain, displacement and acceleration were recorded at 25 kHz per channel, while INS solutions were recorded at 200Hz. All signals were synchronized at the start of acquisition.

Tests were conducted in the Atlantic Ocean near Barnegat Light NJ in sea state 3 conditions. The closest wave buoy NOAA 44091 indicated 0.8m significant wave height. A large number of slamming events were recorded and analyzed; one of these events was singled out and studied in detail as outlined below. In this 1.5 second time period, substantial roll to the heavily instrumented starboard side panel occurred, ensuring substantial wetting of the panel.

Dry Eigenfrequency Identification

In order to determine the resonance frequencies of the bottom panels, a modal test was devised to excite the panels and measure their response. The panel of interest was instrumented on the inner skin with a PCB Piezotronics model 352c04 +/-500g accelerometer with a -3 dB frequency range of 0.5 Hz to 10 kHz. The accelerometer was screw mounted to an aluminum base bonded to the inner surface of the panel with a cyanoacrylate adhesive. A

PCB piezotronics 086D05 22kN (5klbf) peak force impact hammer equipped with a medium stiffness impact cap (white) and vinyl cover was used to excite the structure and measure the force. Accelerations and load were recorded at 5 kHz per channel with a National Instruments PXI-4472B module signal conditioner.

The least squares complex exponential modal analysis method was used to identify the panel modes from experimental data. The panel was excited at 75 locations by the impact hammer and the response recorded by an accelerometer at a fixed location.

Results

Dry Modal Tests

A typical "accelerance" frequency response function from experimental modal analysis of the starboard bay 4 panel is shown in Figure 7-7. The synthesized FRF from identified modes is also plotted.

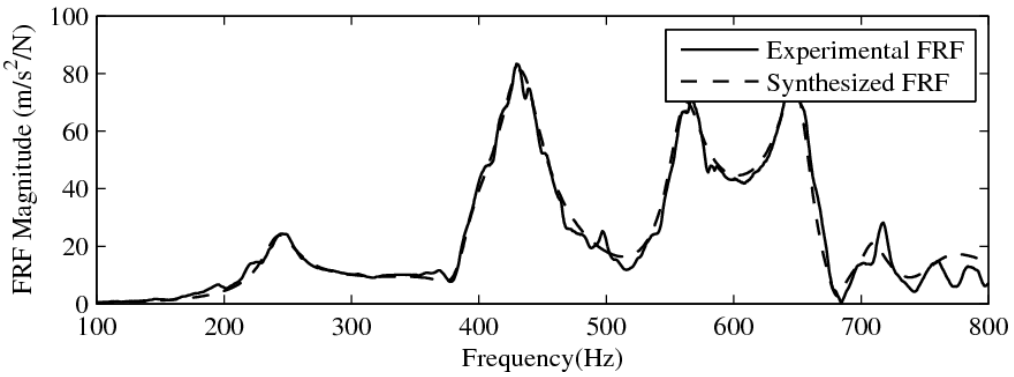

Figure 7-7: Dry accelerance frequency response function of mid panel accelerometer

The first mode of vibration is basically a longitudinal half sine wave deflection of the panel and longeron, Figure 7-8. The next three modes are pure panel modes with essentially no

deflection of the main longeron. These modes have a single transverse half bending wave and one, two or three longitudinal bending half-waves, respectively. Mode 5 consists of two transverse half waves and a single longitudinal bending wave. Mode 6 is four longitudinal half waves and a single transverse half wave. Table 7-1 summarizes the frequencies of these modes for the bay 4 starboard panel.

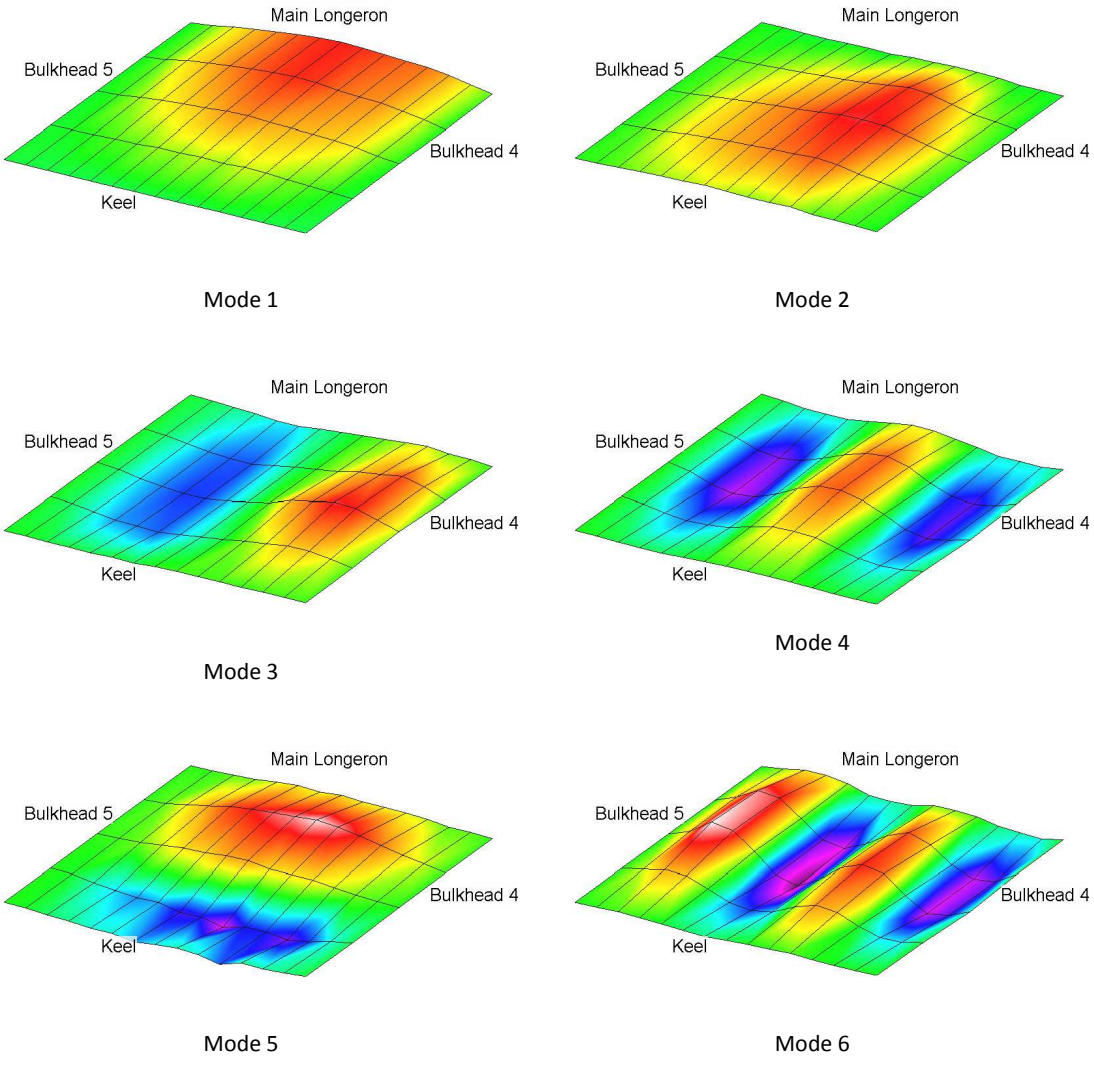

Figure 7-8: Dry panel modes

Table 7-1: Dry modal frequencies

	Bay 4 Starboard Panel
Mode 1 Frequency (Hz)	246
Mode 2 Frequency (Hz)	394
Mode 3 Frequency (Hz)	437
Mode 4 Frequency (Hz)	561
Mode 5 Frequency (Hz)	650
Mode 6 Frequency (Hz)	713

Slamming: Time Domain

The displacement, acceleration and pressure measured on the bay 4 starboard bottom panel during the selected slamming event are shown in Figure 7-9. At the time of this event the vessel was rolled to the starboard side 11.2 degrees, the peak vertical velocity was -2.2 m/s at bulkhead 5 and the forward speed was 16.9 m/s. The displacement plot indicates a maximum displacement of 0.34 mm, and rise time to peak displacement of 29 milliseconds. Peak pressure is 40.2 kPa with a rise time of just 2 milliseconds. Maximum mid panel acceleration is 62.7 m/s^2 but notably this occurs well before the rise of displacement or pressure.

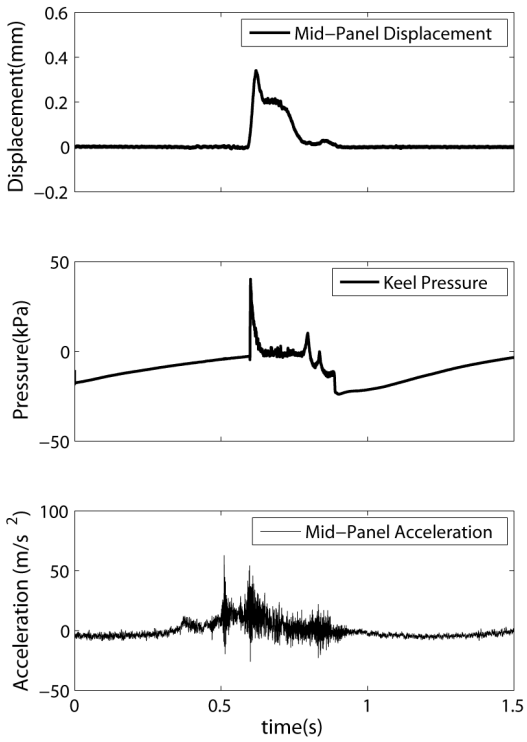

Figure 7-9: Displacement, pressure, and acceleration time histories

Transverse strains measured at the center of the bay 2, 3 and 4 panels are indicated in Figure 7-10 (bottom). This plot shows the correlation between the accelerations measured at the bay 4 panel (Figure 7-10, top) and loads on the hull. At 0.50s, the bay 3 panel strain rises sharply, coinciding with significant acceleration of the bay 4 panel. This acceleration quickly diminishes until there is a secondary peak coinciding with increased strain in the bay 4 panel.

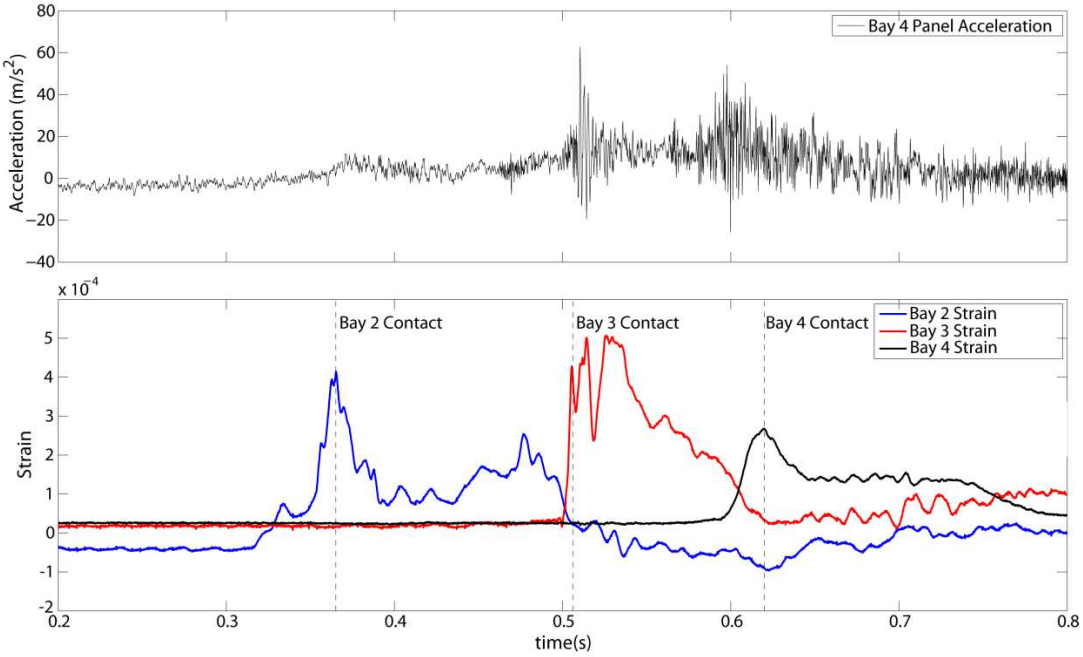

Figure 7-10: Bay 4 mid panel acceleration and bay 2,3,4 mid panel transverse strain time histories

The pressures recorded at two points close to the keel are shown in Figure 7-11. These sensors are separated by 60 mm in the transverse direction on the panel, and peaks are 5.8 milliseconds apart resulting in an estimated transverse speed of the pressure pulse along the bottom of 10.3 m/s.

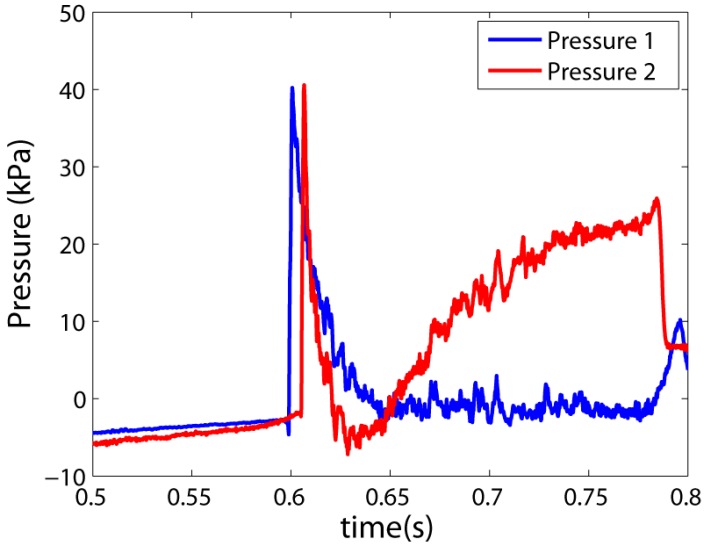

Figure 7-11: Pressure time histories at two locations

Slamming: Frequency Domain

The FFT of the panel acceleration from the 1.5 second time history is shown in Figure 7-12. This FFT is difficult to interpret; there are many closely spaced, sharp peaks but it is not clear which are important and all time localization is lost.

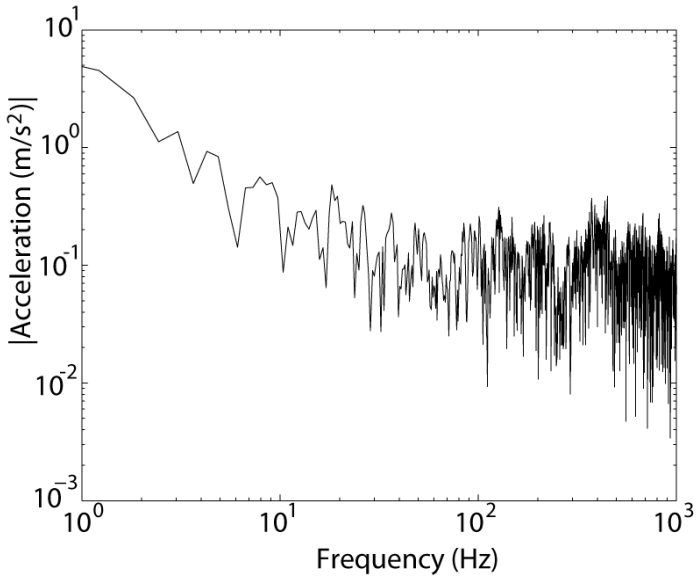

Figure 7-12: Fourier transform of mid panel acceleration

The wavelet transform of the same mid panel acceleration signal is shown in Figure 7-13. From this plot, some of the features become more identifiable. At the time of the panel 3 water impact identified from Figure 7-10 there are multiple, large magnitude peaks. Cross sections of the wavelet transform of the panel and bulkhead accelerations at this time (t=0.516s) are shown in Figure 7-14. From this figure it can be seen that much of the low frequency content below approximately 60 Hz correlates well with the presumed rigid body motion measured at the bulkhead. At higher frequencies, there are peaks at 87, 223, 346, 405, 446, 575, and 661 Hz. With the exception of the peaks at 87 and 346 Hz these are close to the observed dry eigenfrequencies.

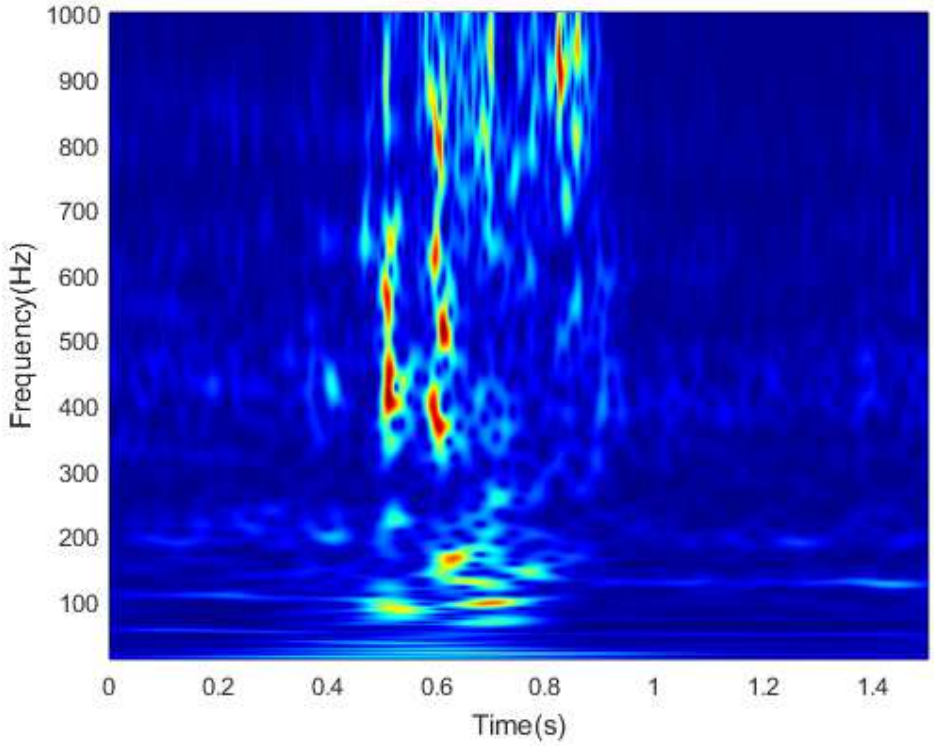

Figure 7-13: Continuous wavelet transform of mid panel acceleration signal

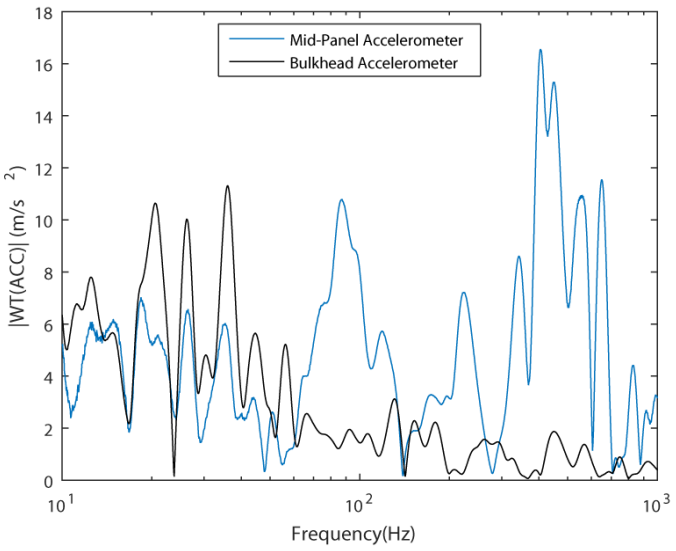

Figure 7-14: Cross sections of acceleration wavelet transforms at t=0.516s

Use of the complete array of accelerometers on the panel makes it possible to correlate these frequencies with mode shapes at this point in time. The individual components of the mode shapes, equation (7-8) are plotted at the locations of the measuring accelerometers. The extracted mode shapes are shown in Figure 7-15. Mode shapes 1, 2, 3, 4, and 6 show good agreement with the previous experimental results. The shape of mode 5 is not consistent with prior results and appears to be a combination of mode 4 and mode 5. This is likely due to the close spacing of these modal frequencies and the wide bandwidth of the wavelet. The significance of the 87 and 346 Hz frequency components is not clear. These may be global modes not described in the experimental modal analysis of the local panel structure.

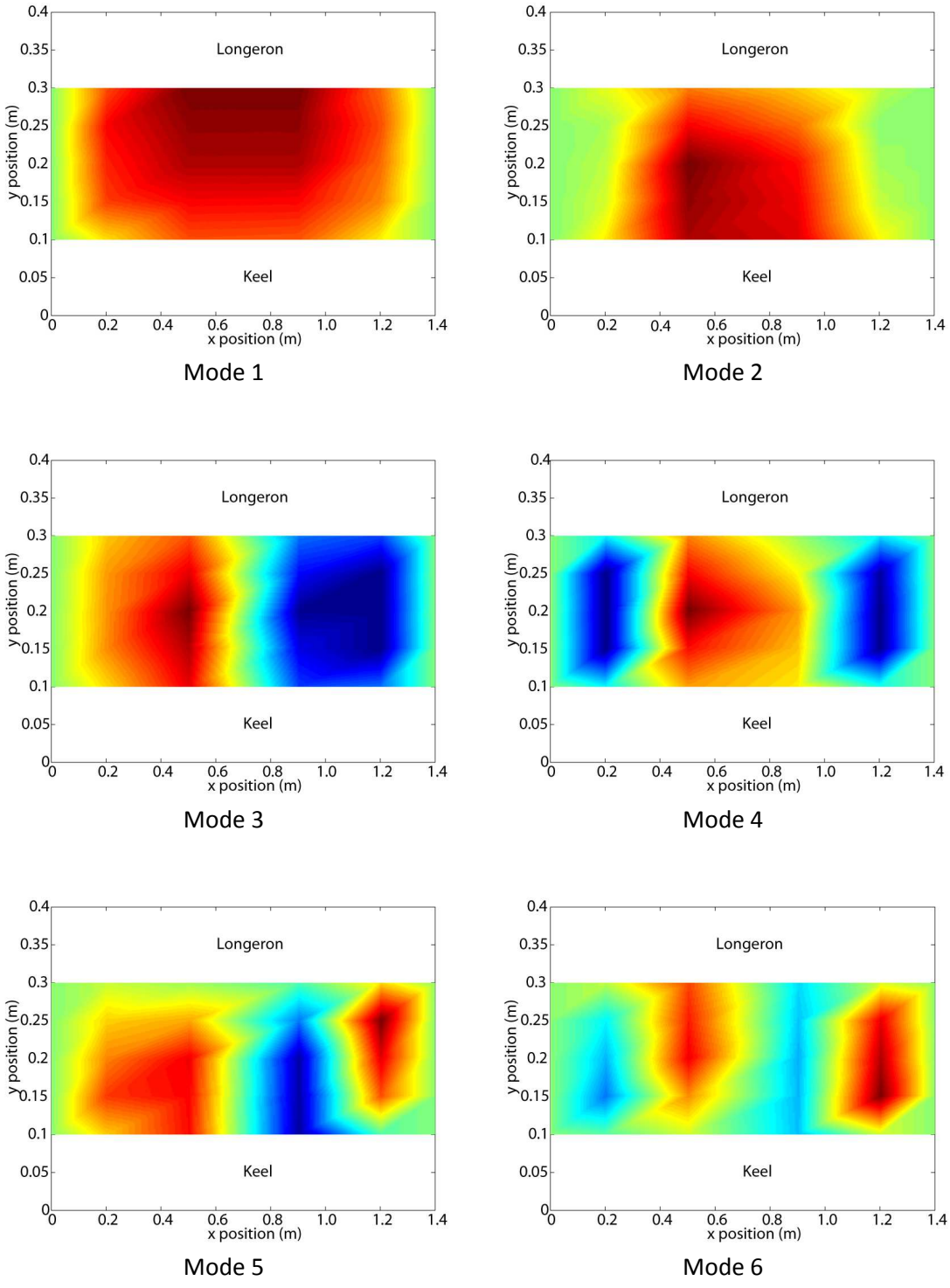

Figure 7-15: Mode shapes observed at t=0.516s

Approaching the second high vibration event of Figure 7-10 in the same manner as the first, a slice of the wavelet plot at t=0.7s is shown in Figure 7-16. Once again at low frequencies many of the frequencies from the mid panel accelerometer are correlated to vibration at the bulkhead. At higher frequencies a number of peaks can be observed including 64, 97,127, 180, 205 and 252Hz.

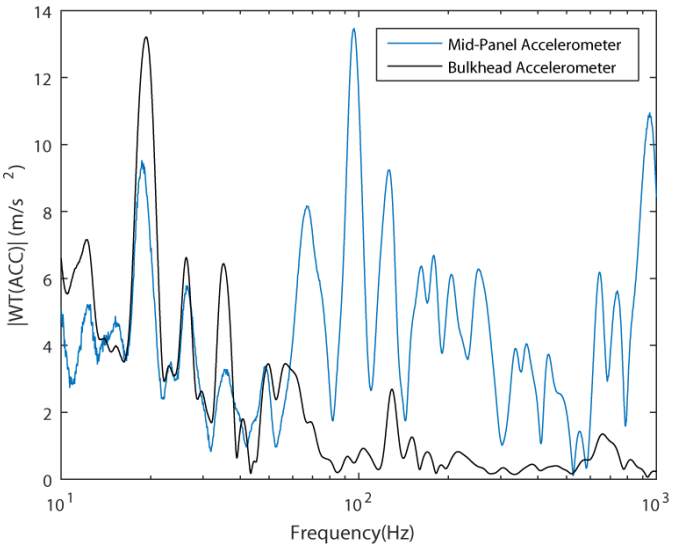

Figure 7-16: Cross section of wavelet transform at t=0.7s

Extracting displacement shapes from this set of frequencies reveals similar shapes to dry modes 2 through 5. The first displacement shape in this set is similar to dry mode 1 but does not show as much displacement of the longeron. The sixth mode is not consistent with the dry testing and once again may be the result of closely spaced modes and too wide wavelet bandwidth. The extracted displacement shapes are shown in Figure 7-17.

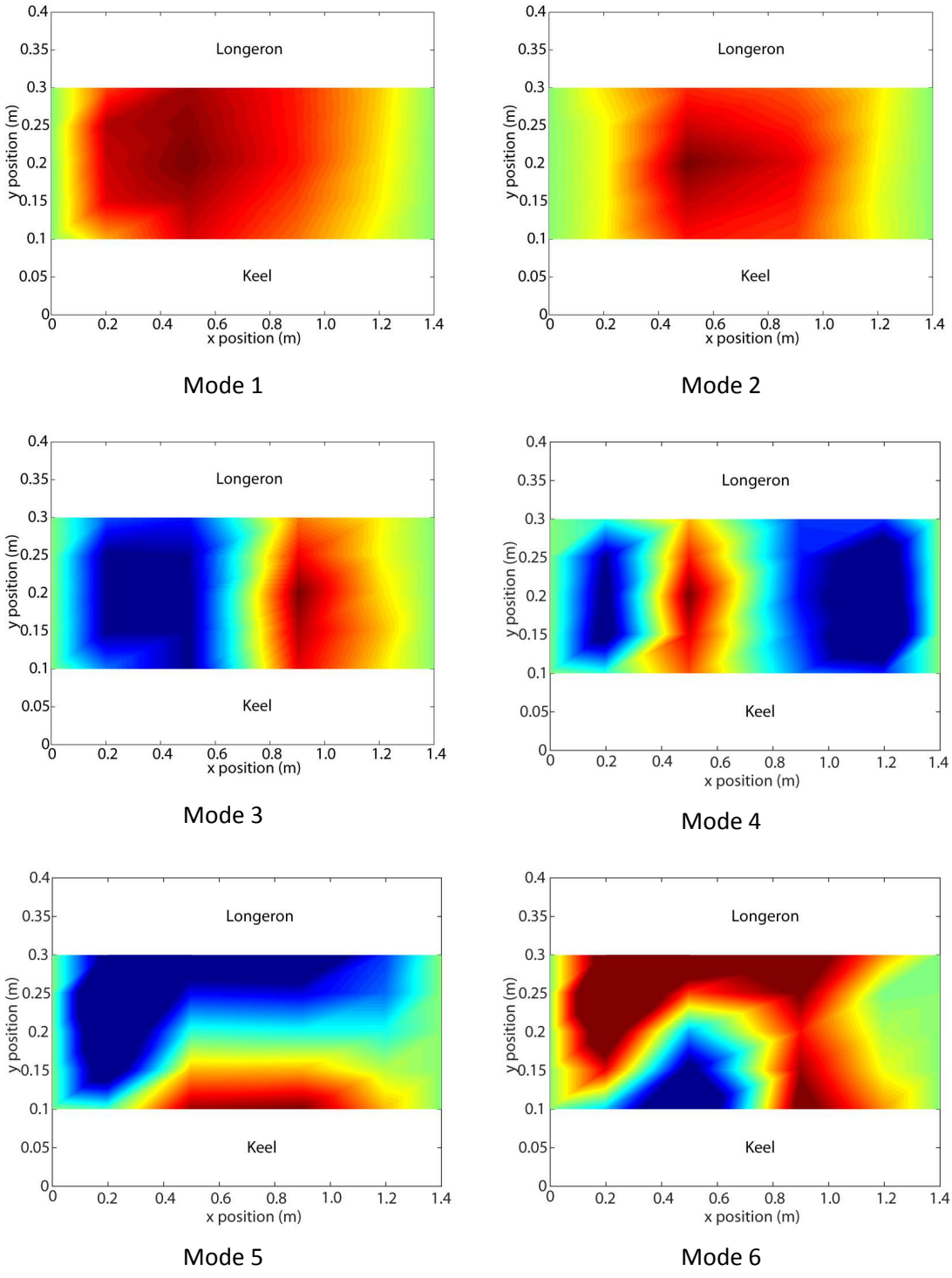

Figure 7-17: Mode shapes observed at t-0.7s

Wet Eigenfrequencies

Predicted wet mode eigenfrequencies are indicated in Table 7-2. Note the calculations are performed for a deadrise angle of 21 degrees to account for the roll angle measured at the time of impact. The predicted first mode frequencies do not agree well with the experimental result. This may be due to incorrect estimation of the coupled mass or the frequency peak in the experimental data may not be a true mode. The second experimental frequency is very close to the Lv wet mode 2.

Table 7-2: Predicted wet mode eigenfrequencies

	Starboard Bay 4 Panel Frequency (Hz)
Lv Wet Mode 1 (k=1)	50
Stenius Wet Mode 1 ($\beta = 21°$)	38
Observed Mode 1	64
Lv Wet Mode 2 (k=1)	96
Stenius Wet Mode 2 ($\beta = 21°$)	74
Observed Mode 2	97

The predicted eigenfrequencies indicate that when the wetting period is approximately 10-25 milliseconds, dynamic and hydroelastic effects will become significant. Considering the hull geometry and the measured propagation speed of 10 m/s, the behavior is expected to be largely quasi-static for this impact.

Conclusions

A single slamming event from an hour-long run in the Atlantic Ocean was studied in detail. The event consisted of two distinct phases; an initial impact with the starboard bay 3 panel followed by a secondary impact with the starboard bay 4 panel. During the initial impact, dry vibration modes were excited in the bay 4 panel. The frequencies and modes shapes observed agree well with previous vibration tests in free air. In the secondary impact, similar mode shapes occurred but at lower frequencies. These modes occurred after wetting of the bay 4 panels as evidenced by pressure sensors on the bay 4 starboard panel.

Pressure waveforms indicated a transverse propagation speed of 10 m/s and an excitation frequency well below the first wet natural frequency. In this case the maximum displacement and strain response occur in the initial phase of the impact. At higher impact speeds it is expected that a secondary wet vibration phase will dominate the response.

The loss of time localization makes the Fourier transform poorly suited for analyzing slamming impacts. The frequency components from the wet and dry vibrations as well as any transients occurring as the panel is progressively wetted all contribute to the Fourier transform, resulting in a plot that is difficult to interpret. In contrast, the wavelet transform allows for separate identification of the initial dry vibration as well as the later wet vibration. Further, this Wavelet analysis allows identification of mode shapes associated with the vibration frequencies. Lower order mode shapes were consistent with previous testing while the higher order modes were more difficult to resolve.

In this case the magnitude of the wet vibration is small, but work by Faltinsen [13], Lv and Grenestedt [15], Stenius [39] and others suggests that as the transverse wave propagation speed approaches a critical value, the wet vibrations will become significant.

8. Validation of High Fidelity CFD/FE FSI for Full-Scale High-Speed Planing Hull With Composite Bottom Panels Slamming

Silvia Volpi[*], *Hamid Sadat-Hosseini*[*], *Matteo Diez*[*§], *Dong-Hwan Kim*[*], *Frederick Stern*[*#], *Robert S. Thodal*[†], *and Joachim L. Grenestedt*[†]

[*]IIHR-Hydroscience & Engineering

The University of Iowa, Iowa City, IA 52242, USA

[§]National Research Council-Marine Technology Research Institute (CNR-INSEAN)

Rome, 00128, Italy

[†]Department of Mechanical Engineering and Mechanics

Lehigh University, Bethlehem, PA 18015, USA

[#]Corresponding author. Email: frederick-stern@uiowa.edu

Abstract. High fidelity CFD/FE FSI (Computational Fluid Dynamics/Finite Element Fluid-Structure Interaction) code development and validation by full-scale experiments is presented, for the analysis of hydrodynamic and structural slamming responses. A fully instrumented 9-meter high speed-planing hull with sterndrive is used. Starboard and port bottom panels are constructed with different composite materials and fiber orientations, allowing for the study of the relation between structural properties and slamming. The code CFDShip-Iowa is employed for CFD simulations and the commercial FE code ANSYS is used as structural solver. The hydrodynamic simulations include captive (2DOF without sterndrive) and 6DOF free running conditions for various Froude numbers in calm water and regular waves. Calm water simulations compares well with the experimental data and 1D empirical data provided by the sterndrive manufacturer for resistance, heave, pitch and roll motions. Numerical one-way coupling FSI is performed in head and following regular waves representative of sea-trial conditions, using FE models for two bottom panels. The resulting strains are compared with experimental data showing a good qualitative and quantitative agreement.

Introduction

Slamming impact loads are a critical factor in the structural design, performance and safety of ships, especially for high speed planing hulls. The complex physics of the fluid-structure interactions is not well understood. Experimental studies have primarily involved wedge drop tests, while model- or full-scale ship test data is limited. USNA model planing hull slamming pressures and accelerations are reported in [60]. Current prediction methods are largely empirical or use analytical [15] or potential flow-FE methods, often for 2D sections or idealized geometries. A collection of numerical studies of ship slamming is presented in Table 8-1. Studies have demonstrated the effectiveness of CFD in slamming analysis, including uncertainty quantification for regular/irregular waves using the Delft catamaran [61] and validation for regular/irregular waves for Fridsma model [62] and USNA model including slamming pressures [63]. Most slams show both primary re-entering (the bow enters the wave face) and secondary emerging (the bow impacts the wave crest) pressure peaks, whereas some show only re-entering pressure peaks, which is more typical of wedge drop and full-scale displacement ship test data. Extreme event slams (about twice standard deviation) correlate with three consecutive incoming wave lengths close to ship length with large steepness. Accelerations and pressure display Froude scaling.

The present collaborative research utilizes an instrumented slamming load test facility (high-speed planing hull - Numerette) for full-scale experimental validation of high-fidelity CFD/FE fluid-structure interaction.

The simulation environmental conditions model the experiments for head and following waves. Hydrodynamic calm water and seakeeping validation uses limited Numerette data

along with 1D Mercury Marine system based predictions and other planing hull data, respectively. Hydrodynamic regular wave validation uses Numerette pressure data; time-step verification is also performed. One-way coupling fluid-structure interaction validation uses Numerette strain data from strain gages embedded in bottom composite sandwich panels, collected by an onboard data acquisition system.

Computational methods

The FSI study is performed by means of CFD/FE coupling routines. One-way coupling is realized by application of the hydrodynamic loads on the structure. CFDShip-Iowa V4.5 [64] is used as high-fidelity solver for the flow field, whereas ANSYS Mechanical APDL V14.5 is used to solve the structural displacements and strains.

The CFDShip-Iowa is an overset, block structured CFD solver designed for ship applications. Absolute inertial earth-fixed coordinates are employed with turbulence model k-ε/k-ω based isotropic and anisotropic RANS. A single-phase level-set method is used for free-surface capturing. Dynamic overset grids use SUGGAR to compute the domain connectivity.

ANSYS Mechanical is a comprehensive commercial code for structural FE analysis. A fully transient dynamic analysis is used to determine the dynamic response of the structure under the action of time-dependent loads. It includes structural nonlinearities and utilizes the Newmark time integration method to solve the FE equations.

The one-way coupling method consists of computing the forces acting on the structure using CFD, assuming rigid-body motion of the entire ship, and then applying the forces on the elastic model of the panels. The response is determined in one way, since the deformed

geometry is not fed back into the CFD solver. In a two-way coupling approach, the flow field and the elastic deformations are computed by feeding back the elastic motions of the structure into the CFD solver. A tradeoff between one- and two-way coupling methods consists in extending the former, using the wet elastic modes of the structure. This requires the modeling of added mass and damping due to the elastic deformation of the body in water. The acceleration of the water due to the body deformation is not taken into account in the CFD solver. In general, the use of a feedback (two-way coupling) is required when large deformation significantly affects the flow field. In this work, the one-way coupling method with wet elastic structure modes is used for preliminary qualitative/quantitative analysis and comparison with experimental data.

Specifically, CFDShip-Iowa provides the hydrodynamic loads in terms of distribution of force per unit area over the ship hull surface. The force distribution is given for the CFD grid points and in the CFD coordinate system. A coordinate transformation is applied in order to provide the force distribution on the FE model, which has its own coordinate system. The interpolation of the loads on the FE grid points is carried out using Gaussian quadrature. The FE model is embedded in a fluid domain, modeled in ANSYS by acoustic elements. The structural problem is solved by ANSYS for displacements, strains and stresses. CFD/FE numerical results are validated by comparison with experimental strain data.

Experimental setup

The slamming load test facility is a 9 meter long 1.9 meter wide steel/composite boat designed and manufactured by Grenestedt [29]. The boat structure consists of a welded AL-

6XN stainless steel frame and composite sandwich panels. The boat has a top speed of approximately 27 m/s and a full load displacement of 2450kg.

To facilitate comparison of different panel constructions, the 10 bottom panels have varied composite layups. All bottom panels are vacuum infused with vinyl ester resin and use a Divinycell H250 foam core but vary in both reinforcement types and fiber direction. The results presented will focus on the behavior of panels in bay 4. The layup of these panels is given in Table 8-2.

Devold AMT DBL700 triaxial carbon and L(X) 440-C10 unidirectional carbon reinforcements are used in both port and starboard bay 4 panels, but the orientation of the DBL700 differs resulting in a large difference in stiffness.

The slamming load test facility is instrumented with strain gages on both inner and outer skins of the bay 4 bottom panels. Vishay CEA-06-250UN-350/P2 and CEA-06-250UT-350/P2 gages were used in quarter bridge configuration to measure strain parallel and perpendicular to the keel in the center of each panel. National Instruments NI-9237 signal conditioning and ADC modules were used to acquire 24 bit strain data at 50 kHz per channel. This data was filtered to 5 kHz in post processing. Pressure measurements are also available by AC coupled piezoelectric sensors (PCB 113b26).

Modal tests of the dry structure were conducted by exciting the panels at a number of grid points using an instrumented impact hammer and measuring the response with an accelerometer. The least squares complex exponential method was used to extract modal

parameters. A National Instruments NI-9234 signal conditioner was used with the PCB Piezotronics 086c03 modal analysis impact hammer and 352c04 accelerometer.

Sea trials were conducted in the Atlantic Ocean near the Barnegat Inlet in Barnegat Light, NJ. The strain gages were zeroed when the craft was at rest before each test sequence. Steering input was used to achieve as close to neutral roll angle as possible. The vessel has since been outfitted with a trim tab to control roll angle. Test segments consisted of nearly straight trajectories. The results presented will focus on head and following wave segments.

Computational setup

The total number of grid points for CFD simulations with sterndrive is 18.2 M (Figure 8-3). For bare hull simulations, symmetry with respect to the longitudinal plane is imposed; accordingly, the grid includes only the starboard side of bare hull and half-domain background with 6.94 M grid points.

During the experimental tests, the ship experiences irregular wave, variable heading, and variable speed. A CFD captive regular-wave simulation is used to model the irregular wave pertaining to real-sea conditions [61]. Available information about test conditions includes: sea state, wave direction, ship trajectory, and speed.

The head and following wave segments are used to model a regular head wave (S1) and following wave (S2) simulations and they are taken as a benchmark for validation. The speed used in S1 and S2 is the average speed $\bar{V}$ of the trial within the selected segments. The wave height is defined as the most probable condition associated to the Bretschneider spectrum, representing a fully-formed sea state 3 (see, e.g., [61]). The wave angular frequency ω is

derived by $\omega_e = \omega - (\omega^2 \bar{V}/g)cos\bar{\theta}$, where ω_e is the encounter angular frequency determined as the frequency associated with the FFT-peak of the experimental pressure and strain (Figure 8-4 and Figure 8-5), g is the gravity acceleration, and $\bar{\theta}$ is the heading angle ($\bar{\theta} = 0$ for following seas). The regular wave model parameters are given in Table 8-3.

Finite element models were developed for the slamming load test facility port and starboard bay 4 composite sandwich bottom panels extending from the keel to the chine and from the aft vertical bulkhead in bay 4 to the fore vertical bulkhead in bay 4 (Figure 8-6). The panel model consists of a sandwich cored region, a perimeter with only composite skins and the stainless steel longeron. All areas were modelled with Shell99 elements in ANSYS. The model is constrained in X,Y,Z displacement at the keel and chines, Y,Z displacement at the bulkheads and Y,Z displacement at the ends of the longerons. The total number of grid points is 51,648. The model was validated by comparison with experimental modal tests and static displacement tests.

Experimental analysis

Experimental data is presented here, which is collected from operation of the slamming load test facility. The position track and speed over the duration of the tests are shown in Figure 8-7 for the head wave segment and Figure 8-8 for the following; the average speed of the segments are 8.1 m/s (Fr=0.87) and 17 m/s (Fr=1.83), respectively. Wave conditions indicated the presence of sea state 3.

For each segment, port and starboard pressures, inner and outer skin transverse and longitudinal strains are measured at the center of the bottom panels (location P in Figure

8-2). Strains on the inner skins are primarily in tension (positive strain), while the outer skins are under compression (negative strain). The highest magnitude strains are seen on the inner skins transverse to the keel, which are herein the focus of the analysis.

Figure 8-9 (head wave) and Figure 8-10 (following wave) show the 1/3 highest port panel slamming pressures and inner skin/transverse strains. Slamming pressure and strain events are aligned in time by their re-entering peaks, which provide the expected value EV and standard deviation SD for the peak value and duration, and mean slamming strain. The event duration is defined by the re-entering peak and the signal drop below a given threshold (1% of the signal RMS). The strains are very irregular, however the mean strain is smooth and has a trend similar to typical slamming pressures.

Table 8-4 gives the average post/starboard EV and SD of the 1/3 highest peaks along with the average duration of the slamming event.

The inner skin transverse strains at the panel center will be used for validation, since more severe.

Hydrodynamic analysis

The calm water simulations are conducted for both a captive and a free running model. The captive simulations are conducted for a wide range of Fr for the bare hull model free to heave and pitch. The free running simulations are conducted at Fr=1.1, 1.9 and 2.7 for the model appended with sterndrive and body force propeller. The free running model has 6DOF.

Figure 8-11 shows the comparison of steady state values for both captive and free running simulations, compared with the experimental data. Heave and pitch motions are slightly larger for free running simulation, but the trends versus Fr are similar for both captive and free running simulations. The maximum pitch is for Fr=1.1 (3.6 and 4.2 deg for captive and free running simulations, respectively). Compared to the available experimental pitch data, the comparison errors E=(D-S)%D (where D and S are the experimental and simulation values, respectively) for captive and free running simulations are E=6.4 and -8.9%D, respectively. Roll motion is only predicted for the free running model. The roll angle increases by Fr and it is about 2.5 deg for the highest speed, very close to the available experimental value at Fr=2.7 (E=0.8%D). The propeller RPS shows the same trend as EFD, however, it is over predicted for high Fr (E=-12%D). Since the experimental resistance could not be measured for the full scale Numerette, it is estimated from the propeller input power computed using both the engine curve and propeller open water torque curve. The estimated experimental resistance based on engine curve shows similar resistance for low and high Fr, while open water curve estimates very small resistance at high speeds. The captive CFD simulations show E=58%, 49%, and 13% for Fr=1.1, 1.9, and 2.7, respectively. Corresponding errors for free running simulation are 49%, 36%, and -9%. The study of the free running results show that the pressure resistance of the sterndrive is comparable with the resistance of the bare hull. Therefore, captive simulations for the bare hull geometry with no sterndrive under predicted the resistance significantly. Figure 8-11 also shows the comparison of CFD results with 1D simulation results, provided by Mercury Marine. The propeller RPS, sterndrive resistance and total resistance show fairly good agreement with CFD free running simulations. However, the 1D simulation predicts larger trim angle as no

model was used for the stepped bottom of the boat. CFD free surface and pressure distribution on the hull are shown as example in Figure 8-12 for Fr = 2.1 and 2.7.

Figure 8-13 shows comparison of the captive simulations with the results for other ship hulls including USNA, USCG and Fridsma model. All geometries show similar non-dimensional resistance at high speed. The non-dimensional heave motion is smaller for Numerette, but it follows the same trend as for other geometries. The largest heave motion is for Fridsma, which has the shortest length among all geometries (L=4.5 ft). For pitch motion, Numerette and USNA show similar values for high speed and both show smaller values compared to those for USCG and Fridsma. The trends for pitch motion are the same for all geometries, i.e. there is a peak for pitch motion around Fv=$V/\sqrt{\Delta^{1/3}g}$=2.5-3.0.

The regular wave simulations S1 and S2 take the inputs as per Table 8-3. Simulations are performed over ten wave periods of encounter; force coefficients and motions indicate satisfactory convergence and a highly nonlinear response. S1 and S2 show a large airborne time; the ship impacts the wave face close to the crest in both head and following conditions. Figure 8-14 shows a superposition of slamming pressures probed at P, heave and pitch motions, wave elevation at P, and wave elevation at the ship center of gravity (CG). Pressure wave forms show a re-entering slam, associated to the first and largest pressure peak, and an emerging slam, associated to the second peak. Re-entering peaks approach 57 kPa for S1 and 68 kPa for S2. Figure 8-15 and Figure 8-16 display the pressure distribution over the hull (bottom view) corresponding to the re-entering and emerging phases. S1 shows bow re-entering slam in correspondence to minimum pitch, whereas S2 shows bow re-entering slam at minimum heave.

Time resolution is a critical factor in describing slamming by CFD simulation, since the characteristic time scale of the slam impact is significantly smaller than that of the ship motion. Therefore, time-step studies are conducted for S1 and S2. Figure 8-17 shows the slamming pressure using a time step equal to 1/400, 1/566, 1/800 of the wave encounter period, i.e. √2 ratio increments. Specifically, pressure are analyzed which are probed at three locations (Figure 8-2): center of the panel (P), keel (K), aft corner of bay 4 (C). For S1, discrepancy is displayed in predicting the peak pressure, while the trend is well captured even with the largest time step. For S2, by contrast, pressure peaks, wave forms and duration time differ significantly. Overall, in order to identify a typical slamming pressure shape, a time step as small as 1/800 times the encounter period is needed in the current study. For both S1 and S2, monotonic convergence of pressure peaks and duration is not achieved.

Experimental data include peak EV and SD, mean slamming event, 2.5%, 50%, and 97.5% of peak for 1/3 highest pressure peaks and associated duration time EV and SD. For both port and starboard panels, pressure peaks and duration are reasonable, and good agreement between CFD and mean experimental data is shown. Analogously, Figure 8-19 present the comparison for S2, showing a good quantitative and qualitative agreement in both port and starboard panels. The average absolute error versus 1/3 highest events is 28% with associated SD equal to 34%.

FSI analysis

Firstly, a modal analysis is performed in order to study modes and associated frequencies of the panels, as predicted by the FE model. The effects of the added mass are assessed by comparing dry conditions (vacuum) with fully wet conditions, using both air and water.

Figure 8-20, Figure 8-21, and Figure 8-22 show the first three modes in vacuum, air and water, respectively, of the port panel, while Figure 8-23, Figure 8-24, and Figure 8-25 show the modes of the starboard panel. The associated frequencies are collected in Table 8-5 for port panel and Table 8-6 for starboard panel. Coupling with air has a negligible effect; validation of frequencies in air is achieved by comparison with experiments which shows an average 4.7% and 5% error on the first three frequencies for port and starboard panels, respectively. Overall, coupling with water has a large effect on both modal shape and frequency; in particular, the latter results significantly reduced. Moreover, the modal analysis shows that the starboard panel is stiffer than the port one, and presents higher dry and wet frequencies.

Then, a transient analysis is performed by application of the CFD predicted hydrodynamic loads on the FE model. Figure 8-26 and Figure 8-27 show the CFD/FE slamming strains in vacuum and in water for S1 and S2. By superposition with the slamming pressures, as probed at P and C, the strain peak at the panel center is found corresponding with the pressure peak at the same location (P). The difference between dry and fully wet panels indicates that the effects of the added mass are significant; specifically, they increase the strain peak and introduce large oscillations at low frequency. The starboard panel is found stiffer that the port panel as it presents smaller peak and smaller oscillation amplitude. The average port/starboard panel peaks in slamming strain is given in Table 8-7. Results for S1 and S2 are analogous with generally larger peaks and shorter events in S2.

The CFD/FE slamming strains are validated for S1 and S2, following the approach used for validation of slamming pressures in [65]. The CFD/FE slamming strains are shown in Figure

8-28 and Figure 8-29 comparing with the experiments, as per Figure 8-18 and Figure 8-19. Strain peaks and duration show a reasonable agreement, especially in consideration of the simulation input approximation of the experimental conditions. The CFD/FE peaks are always greater than the experimental EV and close to the 95% upper bound. The duration of the event is well captured by both dry and wet simulations; note that the structural damping is not modelled in the current analysis. The average absolute error versus 1/3 highest events is 64% with associated SD equal to 34%. Overall, the trend of port versus starboard panel strains is well captured by CFD/FE.

The trend of S1 versus S2 depends on head versus following waves, which may be affected by surge and propeller controller, not considered (the CFD/FE model is towed at constant speed). Moreover, during the slamming event, the panels experience a transition from dry to wet conditions, therefore both fully dry and fully wet approximations result in a under- and over-estimation of the added mass effects, respectively.

Conclusions and future research

Hydrodynamic slamming on the bottom of a high-speed planing hull was studied experimentally and numerically (CFD/FE). A highly instrumented 9 meter long hull developed for slamming research was used. The bottom of this craft consists of ten separate carbon and glass fiber skin / foam core sandwich panels, each with its unique set of material combinations and fiber layup angles. This allows for study of the influence of bottom stiffness on slamming pressures and deformations. The code CFDShip-Iowa was employed for CFD simulations and the commercial FE code ANSYS was used as structural solver.

The hydrodynamic simulations included captive (2DOF without sterndrive) and 6DOF free running conditions for various Froude numbers in calm water and regular waves. Resistance, heave, pitch and roll motions correlated well between experimental operation and numerical simulations for calm water.

In offshore sea trials operating in head (S1) and following (S2) waves, pressure and strains in two different bottom panels were measured experimentally as well as calculated numerically using one-way coupling FSI routines (hydrodynamic loads from CFD of rigid hull, applied on dynamic FE model) with and without added mass effects. The average peak values and event duration in starboard and port panels were compared. CFD predicted pressure at the center of the panel correlated well with experimental data for both S1 and S2. CFD/FE predicted strains show reasonable agreement, especially with the 95% confidence upper bound of the experiments. Initial indications are that the numerical procedure correctly predicts which panel is straining more, although the absolute error may be on the order of 30-50%.

Future research will focus on: grid verification; semi-coupled two-phase free running irregular wave hydrodynamics simulations including sterndrive/propeller/controller and superstructure; trim tab and asymmetric pressure distribution effect on the slamming strains. The influence of bottom stiffness on slamming pressures will be studied experimentally and numerically; in particular, an attempt will be made to answer questions such as whether a more compliant bottom leads to lower slamming pressures. Further future developments include fully coupled (two-way) fluid-structure interaction analyses and multidisciplinary design optimization.

Acknowledgements

Research was sponsored by the Office of Naval Research (ONR) grants No. N00014-13-1-0616 and N00014-13-1-0617 administered by Dr. Roshdy Barsoum. The authors would like to thank Dr. Maysam Mousaviraad, assistant research scientist at University of Iowa, for assisting the comparison with other geometries and John Scherer, technical advisor at Mercury Marine, for providing the required information for CFD simulations and conducting 1D simulation.

Tables

Table 8-1 Literature review for slamming studies

	Subject of study	Structure model	Flow solver	Coupling and results
[32]	Wetdeck of a multi-hull	Euler beam	Potential	A matching of two solutions is used: (1) structural inertia phase (2) free-vibration phase.
[19]	Cylinder	Modal representation	RANS	Fluid and structure are coupled by including a source term in the fluid continuity equation to account for the deflection of the body.
[13]	Survey on plates and wedges			Relationship of the material and geometric properties of the structure, impact velocity, and relative angle between water and structure determine if hydro-elastic effect are significant.
[66]	Wedge	FE and finite number of Euler beams	Boundary element method	A coupled analysis is performed.
[65]	Wedge	FE		Ratio of the time duration of the impact stage (that is up to the time that the wedge fully wets) to the first natural period of the dry structure determines if hydro-elastic effects are significant; overall, the role of hydro-elasticity is to reduce the deflection of the structure
[67]	Wedge	Wagner impact theory and Euler beams with normal mode method		Body elasticity determines two effects: (1) added mass due to flexure, which appears as a matrix which couples all of the beam modes (2) change in speed of the spray root due to flexure.
[39]	Hull bottom panels	FE	FE	The analysis is based on an arbitrary Lagrangian-Eulerian formulation; inclusion of the added mass due to flexure in determining the natural period of the structure.
[20]	Ships	FE	RANS	CFD-predicted rigid-body fluid forces are applied to the structural model in a one-way manner; added mass due to flexure is accounted for using a two-dimensional approximation.
[18]	Wedge	FE for frequencies and mode shapes	RANS	The hydro-elastic impact is studied in a loose one-way coupling manner; added mass is accounted for using acoustic elements in the FE analysis.

Table 8-2 Slamming load test facility bay 4 bottom panel layup

	Bay 4 Port Panel	Bay 4 Starboard Panel
Top ↓ Bottom	2 layers DBL700 (0°, ±45°)* Divinycell H250 Foam core 3 layers DBL700 (0°, ±45°)* 1 layer L(X) 440-C10 (0°)*	2 layers DBL700 (0°, ±45°)** Divinycell H250 Foam core 3 layers DBL700 (0°, ±45°)** 1 layer L(X) 440-C10 (0°)*

* 0° parallel to keel

** 0° perpendicular to keel

Table 8-3 Regular wave model parameters

Parameter	S1	S2
f_{pitch} [Hz]	0.625	0.625
H [m]	0.75	0.75
T [s]	2.77	3.02
f [Hz]	0.36	0.33
λ [m]	12.0	14.3
λ/L	1.36	1.62
H/ λ	1/16	1/19
Fr	0.87	1.83
u [m/s]	8.10	17.0
f_e [Hz]	0.77	0.86
T_e [s]	1.31	1.16

Table 8-4 Average port/starboard 1/3 highest slamming events parameters (experiments)

Parameter	S1	S2
Pressure peak EV (SD) [kPa]	63.5 (37.9)	109.8 (47.5)
Strain peak EV (SD) [$x10^{-4}$]	3.3(2.3)	4.7 (1.8)
Duration time [s]	0.1	0.1

Table 8-5 Frequencies associated with the first three modes of the starboard panel

Frequency [Hz]	Air (experiments)	Vacuum (FE)	Air (FE)	Water (FE)
1^{st}	238	233	232 (-2.6%$_{exp.}$)	50
2^{nd}	373	337	333 (-11%$_{exp.}$)	97
3^{rd}	413	417	413 (0.5%$_{exp.}$)	120

Table 8-6 Frequencies associated with the first three modes of the port panel

Frequency [Hz]	Air (experiments)	Vacuum (FE)	Air (FE)	Water (FE)
1^{st}	246	237	235 (-4.5%$_{exp.}$)	484
2^{nd}	394	403	401 (-1.8%$_{exp.}$)	479
3^{rd}	437	484	479 (8.7%$_{exp.}$)	142

Table 8-7 Average port/starboard slamming strains (CFD/FE)

Parameter	S1	S2
Strain peak (vacuum) [x10^{-4}]	7	8
Strain peak (water) [x10^{-4}]	9	10

Figures

Figure 8-1: Slamming load test facility

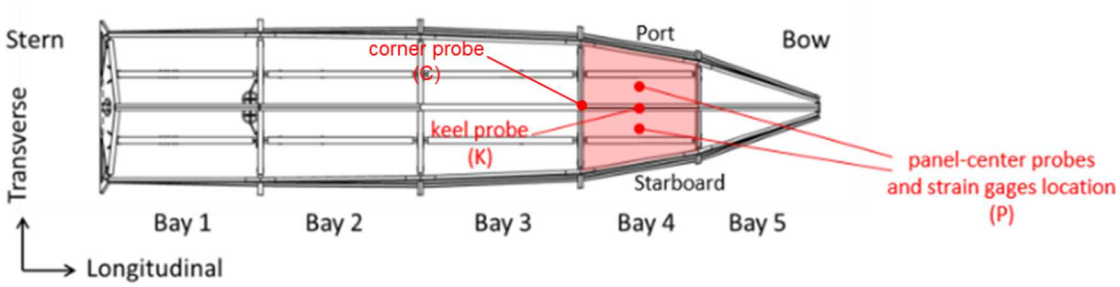

Figure 8-2: Slamming load test facility sensor layout

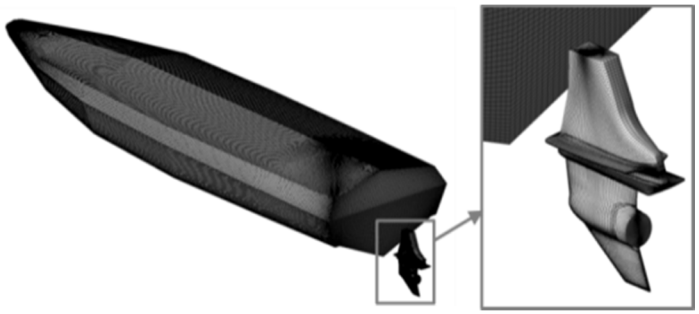

Figure 8-3: CFD model of Numerette with detailed view of the sterndrive

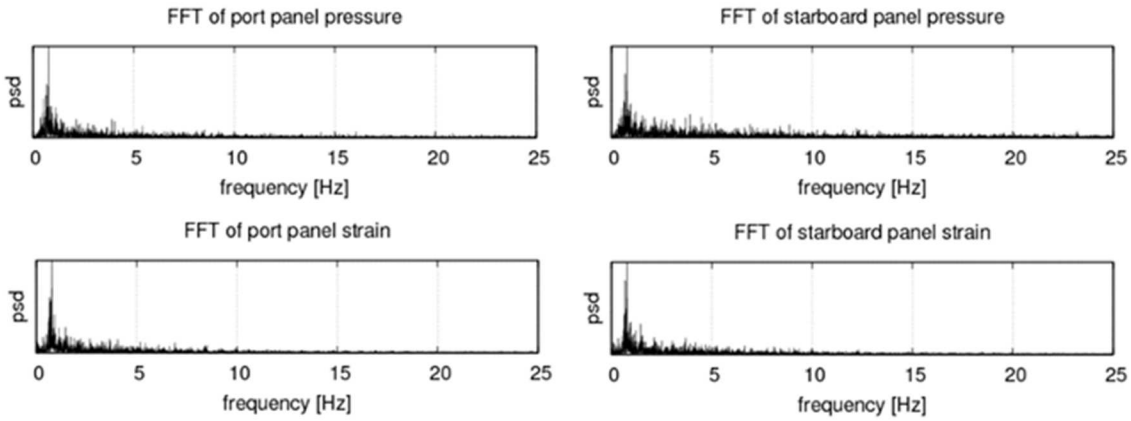

Figure 8-4 FFT of panel pressure and strain (S1)

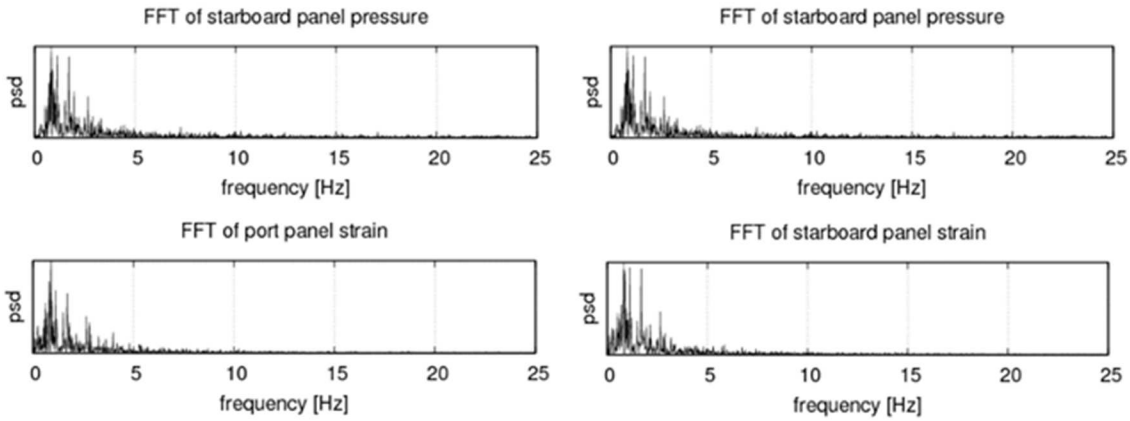

Figure 8-5 FFT of panel pressure and strain (S2)

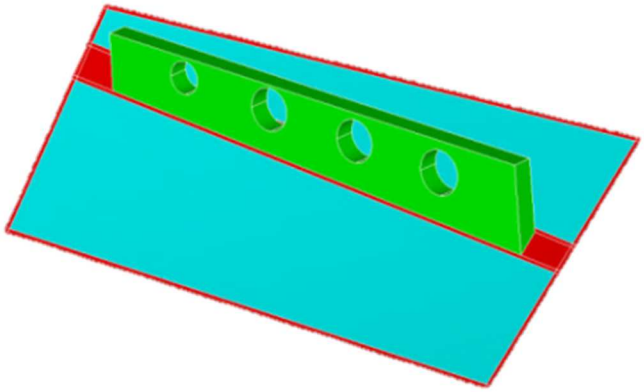

Figure 8-6: FE model of a Bay 4 panel showing cored sandwich areas (blue), single skin areas (red) and hollow steel longeron (green)

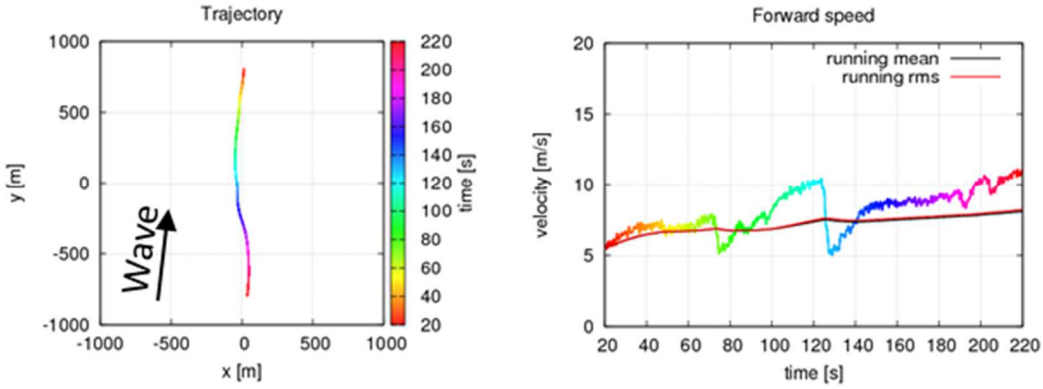

Figure 8-7 Sea trajectory and speed with color mapping for time of the head wave segment

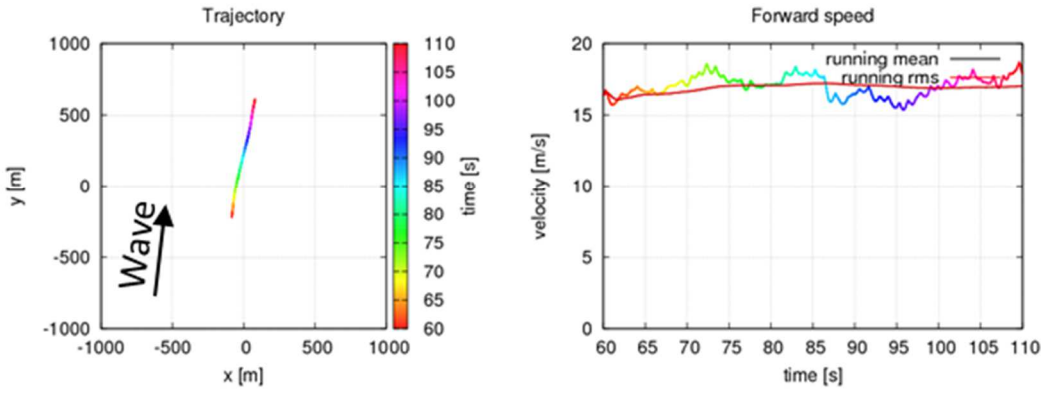

Figure 8-8 Sea trajectory and speed with color mapping for time of the following wave segment

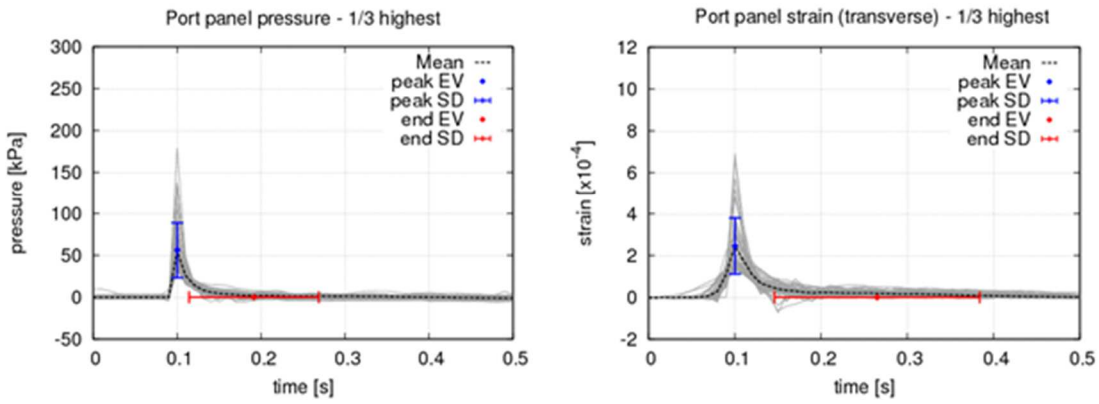

Figure 8-9 1/3 highest slamming event pressure and strain experienced at the port panel of the head wave segment

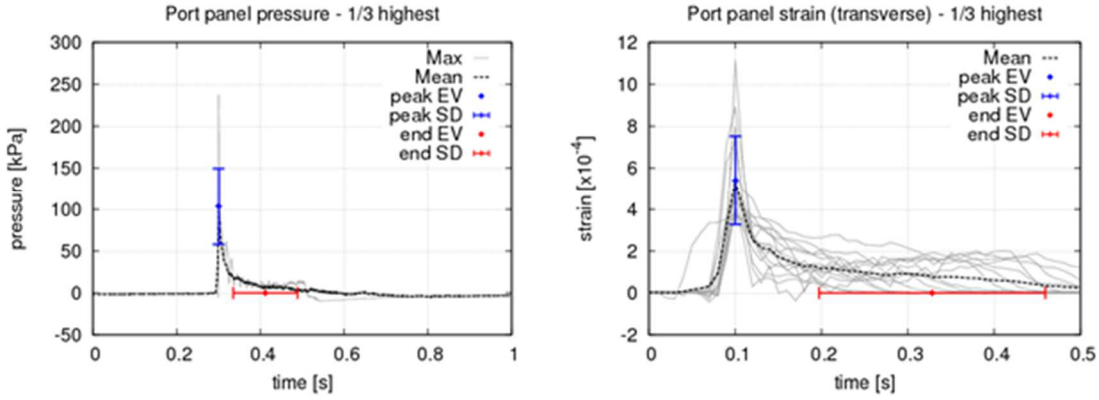

Figure 8-10 1/3 highest slamming event pressure and strain experienced by the port panel of the following wave segment

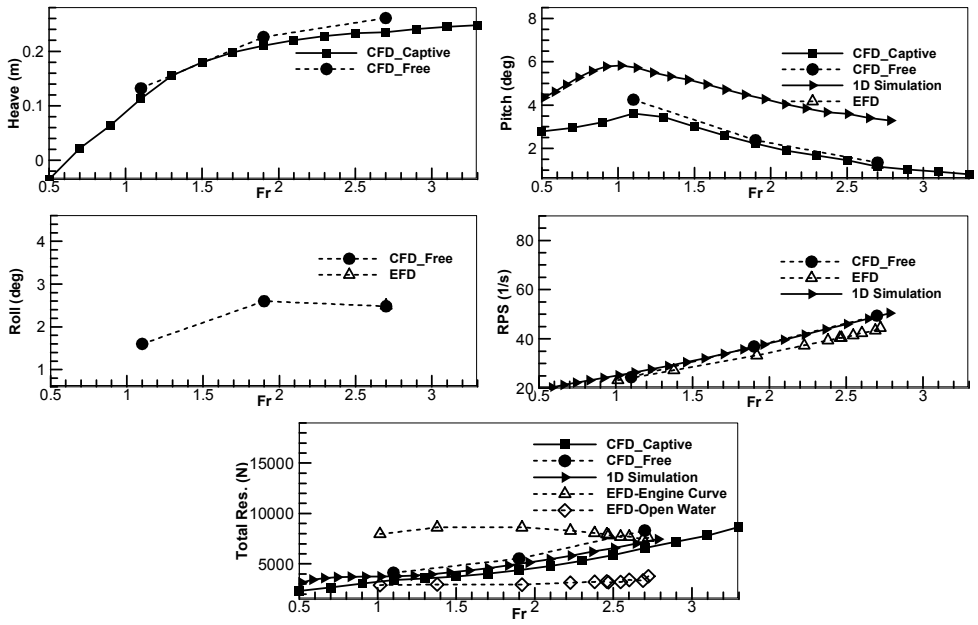

Figure 8-11: Comparison of CFD and EFD results in calm water

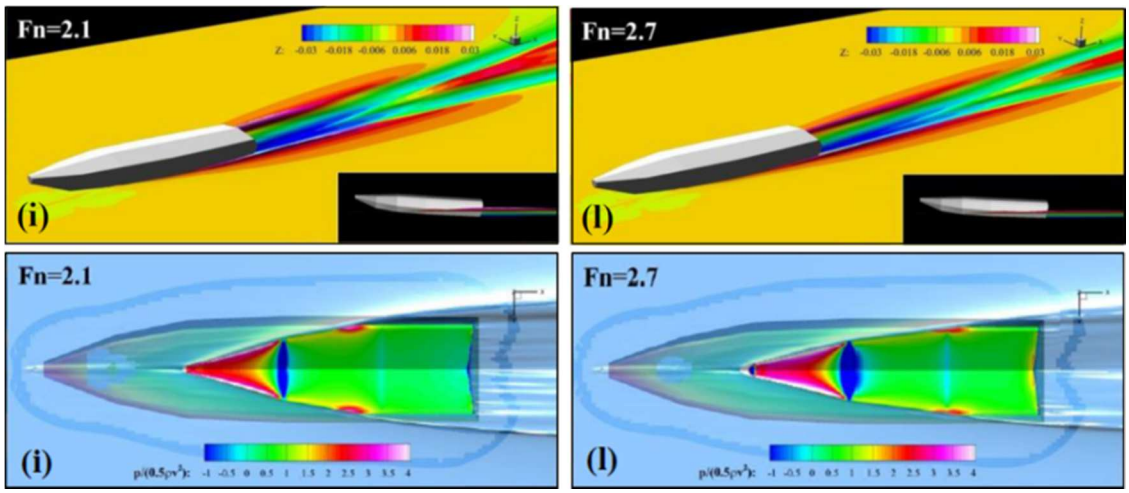

Figure 8-12: Free surface and pressure distribution for calm water simulation at Fr = 2.1 and 2.7

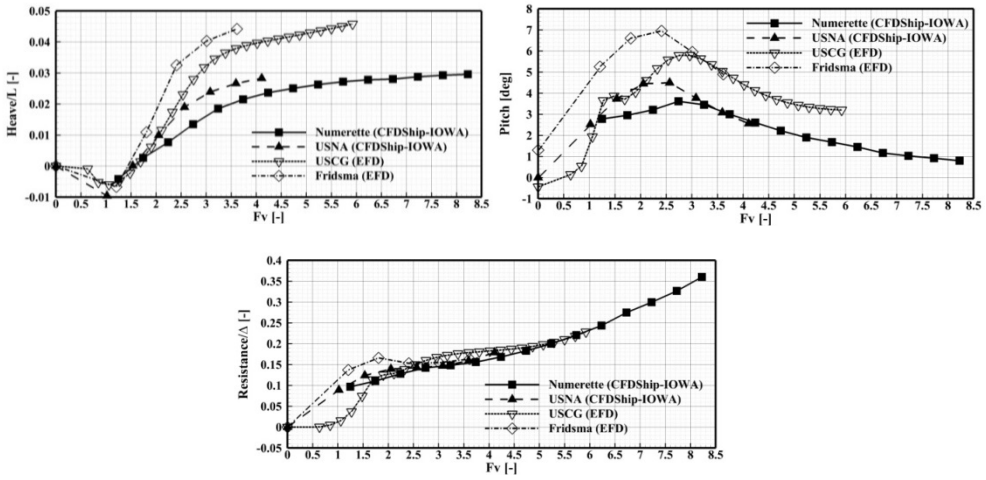

Figure 8-13: Comparison of motions and resistance against USNA (CFD), USCG (EFD) and Fridsma (EFD)

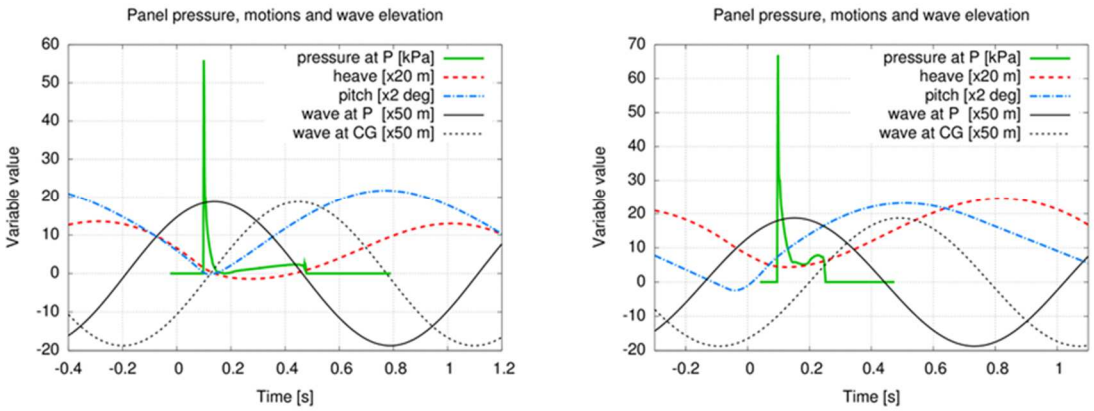

Figure 8-14 Pressure, motions and wave elevation: S1 (left) and S2 (right)

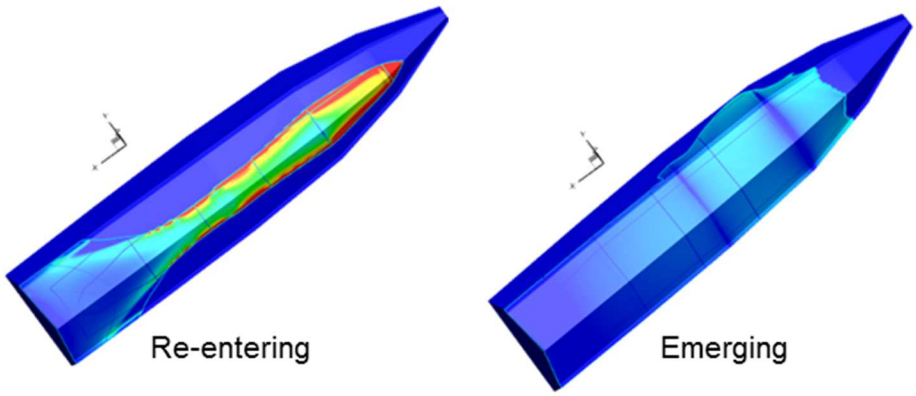

Figure 8-15 Pressure distribution for re-entering and emerging slams of S1

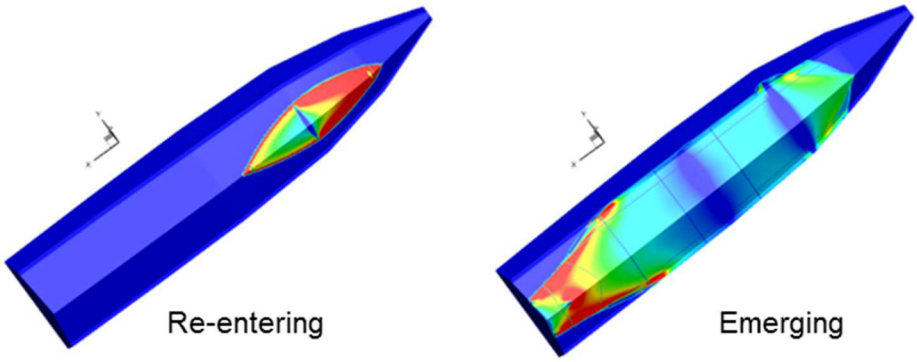

Figure 8-16 Pressure distribution for re-entering and emerging slams of S2

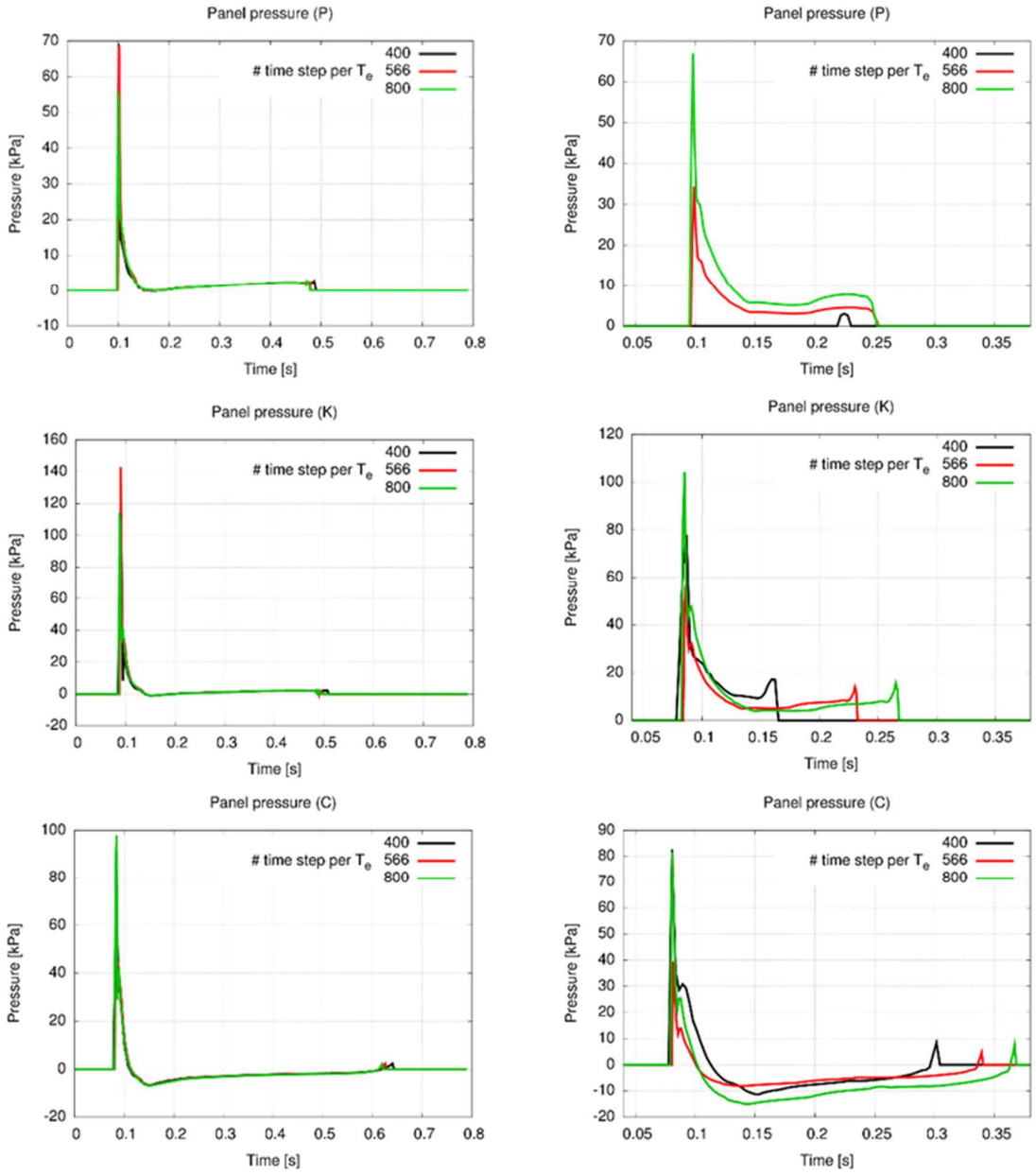

Figure 8-17 Time-step verification: S1 (left) and S2 (right)

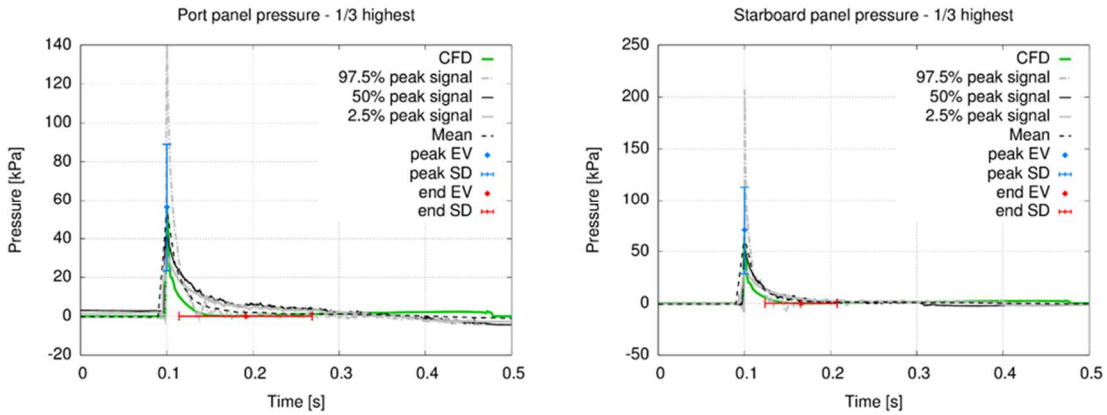

Figure 8-18 Comparison between CFD and experimental for S1

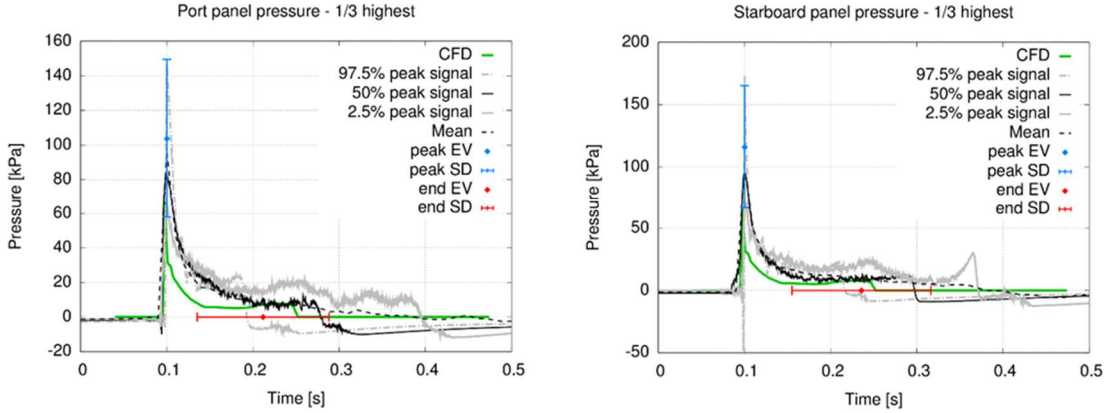

Figure 8-19 Comparison between CFD and experimental for S2

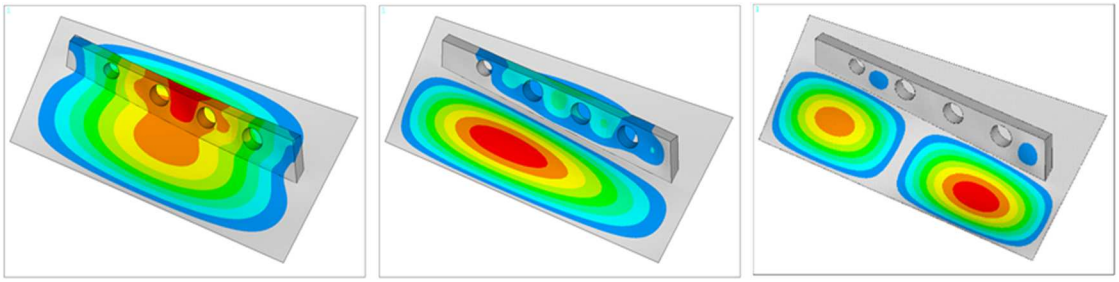

Figure 8-20 First three modes of the port panel in vacuum

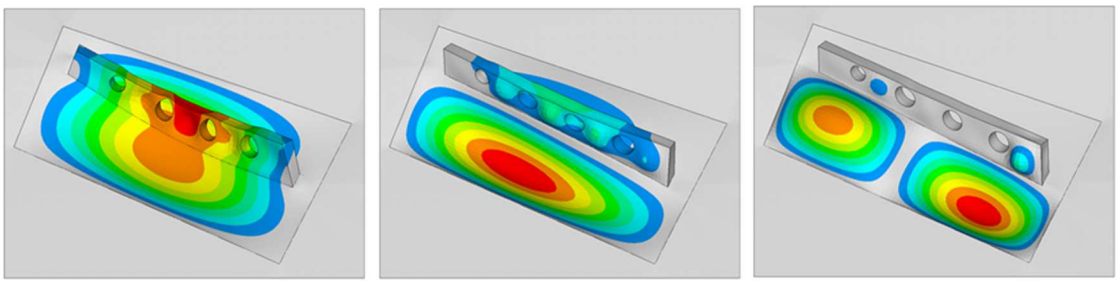

Figure 8-21 First three modes of the port panel in air

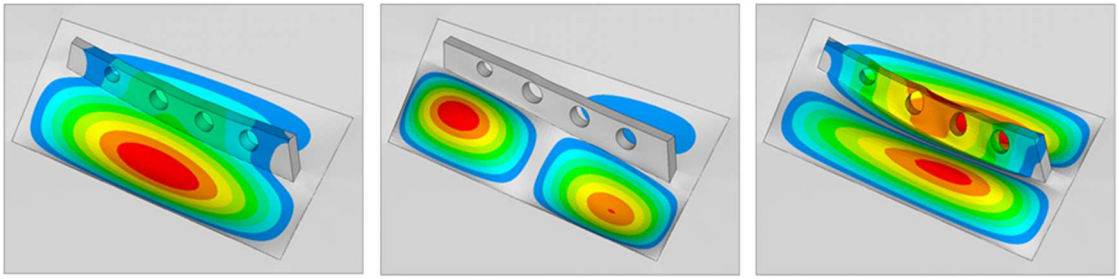

Figure 8-22 First three modes of the port panel in water

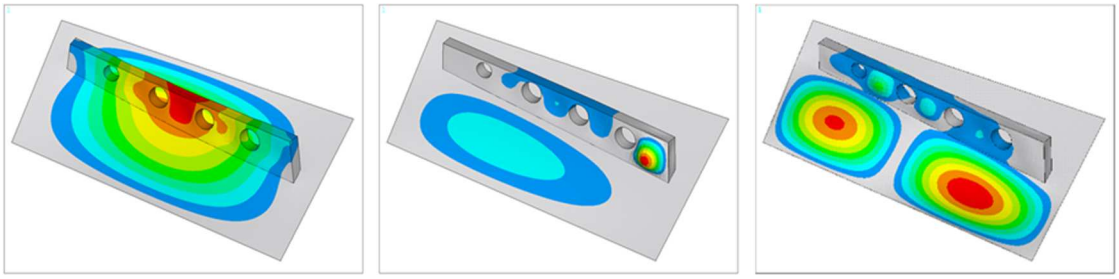

Figure 8-23 First three modes of the starboard panel in vacuum

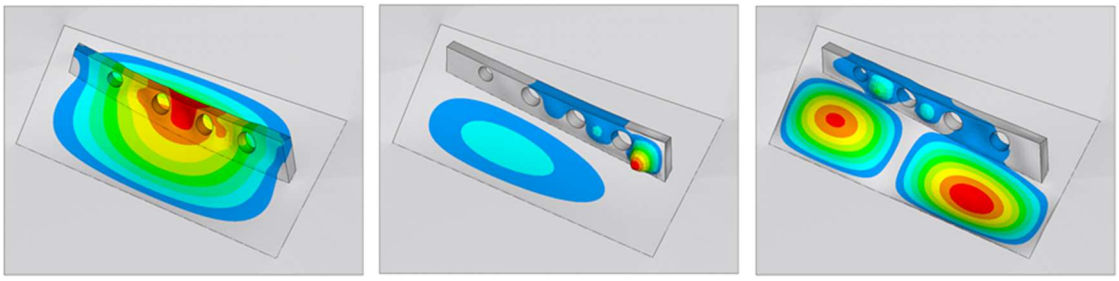

Figure 8-24 First three modes of the starboard panel in air

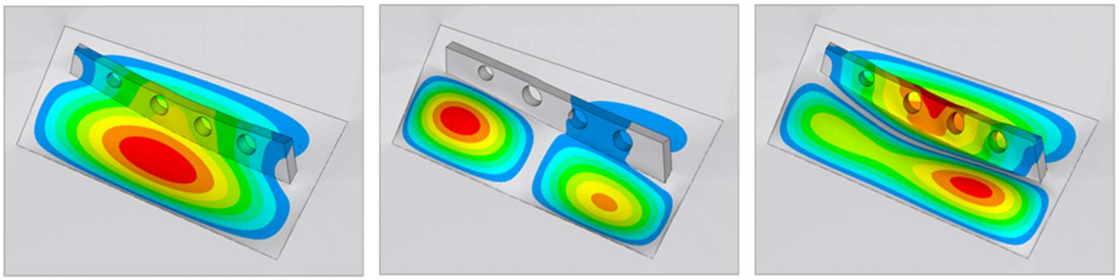

Figure 8-25 First three modes of the starboard panel in water

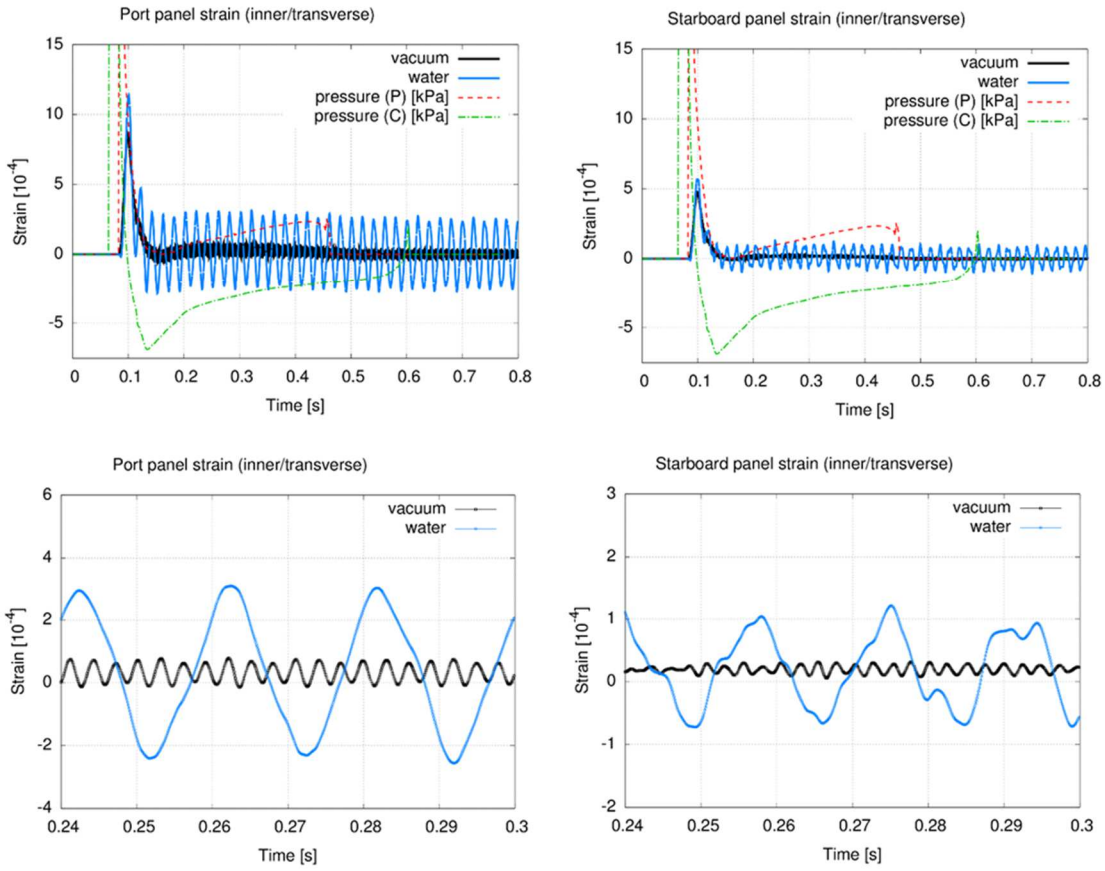

Figure 8-26 CFD/FE strains in vacuum and water for S1

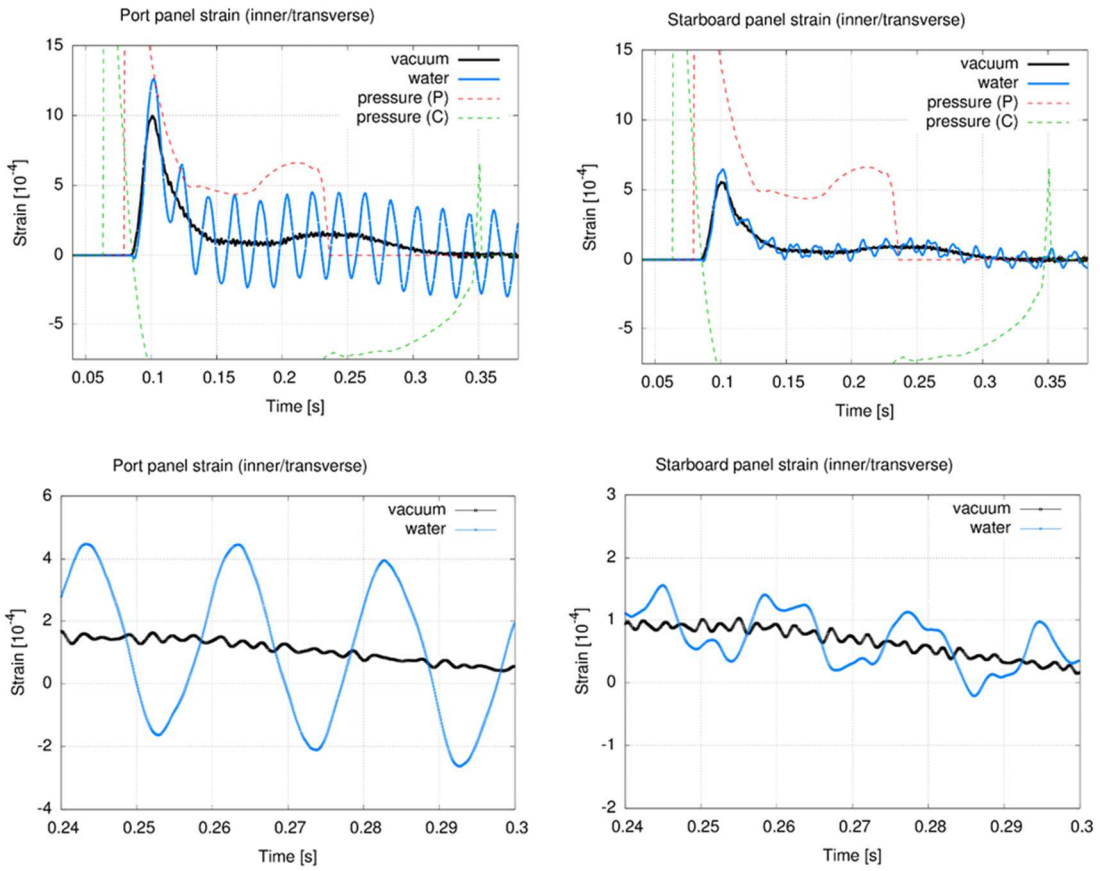

Figure 8-27 CFD/FE strains in vacuum and water for S2

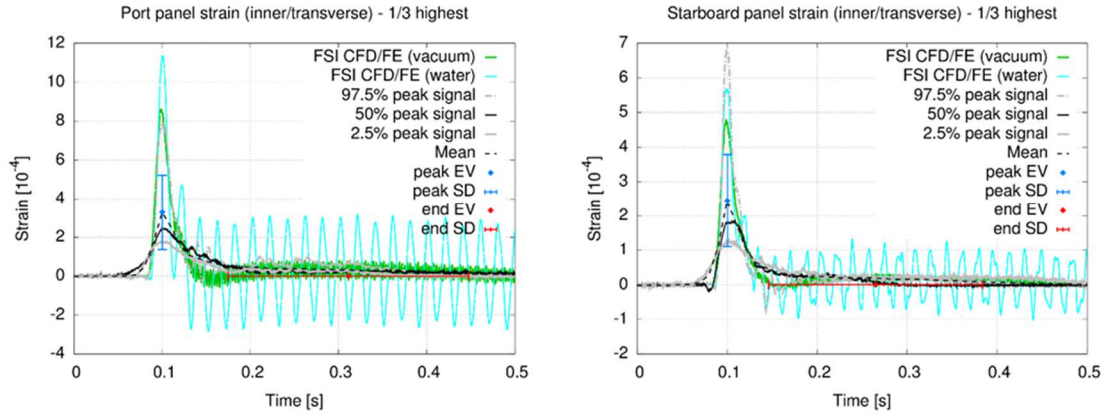

Figure 8-28 Comparison between CFD/FE and experimental strains for S1

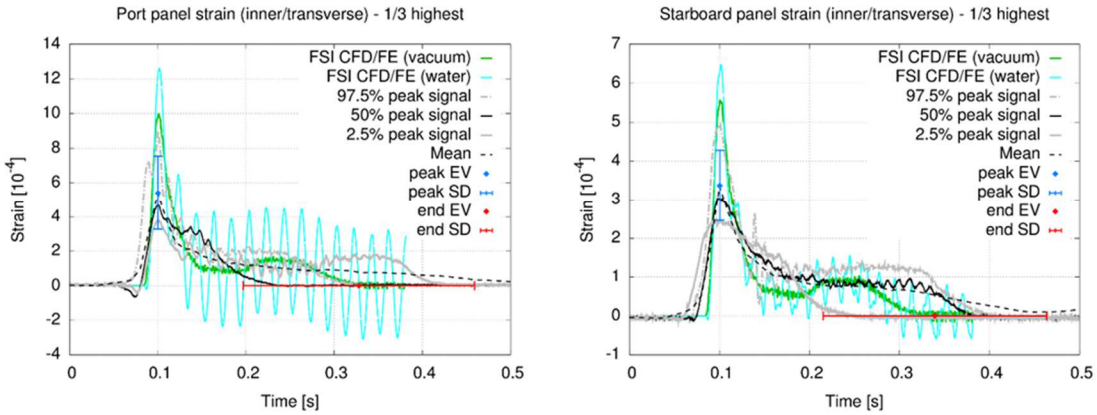

Figure 8-29 Comparison between CFD/FE and experimental strains for S2

9. Works Cited

[1] J. Aarsnes, "An experimental investigation of the effect of structural elasticity on slamming loads and structural response," Norwegian Maritime Technology Research Institute, 1994.

[2] J. Kvalsvold and O. M. Faltinsen, "Hydroelastic Modeling of Wet Deck Slamming on Multihull Vessels," *Journal of Ship Research,* vol. 39, no. 3, pp. 225-239, 1995.

[3] Det Norske Veritas, Rules for Classification of High Speed, Light Craft and Naval Surface Craft, 2012.

[4] R. Allen, R. Jones and D. W. Taylor, "A simplified method for determining structural design limit pressures on high performance marine vehicles," *Proceedings of AIAA/SNAME Advanced Marine Vehicle Conference San Diego,* 1978.

[5] American Bureau of Shipping, Rules for Building and Classing High-Speed Craft, 2015.

[6] Lloyd's Register, Rules and Regulations for the Classification of Ships, 2015.

[7] M. Razola, A. Rosen and K. Garme, "Allen and Jones revisited," *Ocean Engineering,* vol. 89, pp. 119-133, 2014.

[8] I. Stenius and J. Kuttenkeuler, "On Structural Design of Energy Efficient Small High Speed Craft," *Marine Structures,* vol. 38, pp. 371-381, 2011.

[9] T. von Karman, "The impact on seaplane floats during landing," *Technical report NACA 321,* 1929.

[10] H. Wagner, "Phenomena associated with Impacts and Sliding on liquid Surfaces," *Mathematik und Mechanik,* vol. 12, no. 4, pp. 193-215, 1932.

[11] I. Stenius, A. Rosen and J. Kuttenkeuler, "Hydroelastic interaction in panel-water impacts of high-speed craft," *Ocean Engineering,* vol. 38, pp. 371-381, 2011.

[12] J. Kvalsvold and O. Faltinsen, "Hydroelastic Modelling of Slamming against the wetdeck of a catamaran," in *Int. Conf. Hydroelasticity in Marine Technology*, Trondheim, 1993.

[13] O. Faltinsen, "Hydroelastic slamming," *Marine Science and Technology,* vol. 5, no. 2, pp.

49-65, 2000.

[14] J. Lv and J. Grenestedt, "Some Analytical Results for the Initial Phase of Bottom Slamming," *Marine Structures,* vol. 34, pp. 88-104, 2013.

[15] J. Lv and J. Grenestedt, "Analytical study of the responses of bottom panels to slamming loads," *Ocean Engineering,* vol. 94, pp. 116-125, 2015.

[16] G. Kapsenberg, "Slamming of ships: where are we now?," *Philosophical Transactions of The Royal Society,* pp. 2892-2919, 2011.

[17] M. Arai, L.-Y. Cheng and Y. Inoue, "A Computing Method for the Analysis of Water Impact of Arbitrary Shaped Bodies," *Journal of The Society of Naval Architects of Japan,* vol. 176, pp. 233-239, 1994.

[18] K. Maki, D. Lee, A. Troesch and N. Vlahopoulos, "Hydroelastic impact of a wedge-shaped body," *Ocean Engineering,* vol. 38, no. 4, pp. 621-629, 2011.

[19] M. Arai and T. Miyauchi, "Numerical study of the impact of water on cylindrical shells considering fluid-structure interactions," in *Conference on Practical Desing of Ships and Mobile Structure*, The Hague, Netherlands, 1998.

[20] J. Oberhagemann, M. Holtmann, O. el Moctar, T. Schellin and D. Kim, "Stern slamming of a LNG carrier," *Journal of Offshore Mechanics and Arctic Engineering,* vol. 131, no. 3, pp. 1-10, 2009.

[21] S. Chuang, "Experiments on slamming of wedge-shapped bodies," *Journal of Ship Research,* vol. 11, pp. 190-198, 1967.

[22] B. Hayman, T. Haug and S. Valsgard, "Slamming drop tests on a GRP sandwich hull model," *Proceedings 2nd international conference on sandwich construction Florida,* 1992.

[23] B. Hayman, T. Haug and S. Valsgard, "Response of Fast Craft Hull Structures to Slamming Loads," in *First International Conference on Fast Sea Transportation*, Trondheim, 1991.

[24] M. Battley and T. Allen, "Servo-hydraulic System for Controlled Velocity Water Impact of Marine Sandwich Panels," *Experimental Mechanics,* vol. 52, pp. 95-106, 2012.

[25] T. Allen and M. Battley, "Quantifiication of hydroelasticity in water impacts of flexible composite hull panels," *Ocean Engineering,* vol. 100, pp. 117-125, 2015.

[26] I. Stenius, A. Rosen, M. Battley, T. Allen and P. Pehrson, "Hydroelastic Effects in Slamming Loaded Panels," *11th International Conference on Fast Sea Transportation Honolulu,* pp. 644-652, 2011.

[27] A. Rosen, K. Garme and J. Kuttenkeuler, "Full Scale Design Evaluation of the Visby Class Corvette," in *Ninth International Conference on Fast Sea Transportation*, Shanghai, 2007.

[28] F. Stern, Z. Wang, J. Yang, H. Sadat-Hosseini, M. Mousaviraad, S. Bhushan, M. Diez, S.-H. Yoon, P.-C. Wu, S. Yeon, T. Dogan, D.-H. Kim, S. Volpi, M. Conger, T. Michael, T. Xing, R. Thodal and J. Grenestedt, "Recent Progressin CFD for naval architecture and ocean engineering," *Journal of Hydrodynamics,* vol. 27, no. 1, pp. 1-23, 2015.

[29] R. Thodal and J. Grenestedt, "Experimental Study of Slamming on High-Speed Craft Operating in the Atlantic (In Preparation)," 2015.

[30] D. Savitsky, "Hydrodynamic design of planing hulls," *Journal of Marine Technology,* vol. 1, no. 1, pp. 71-95, 1964.

[31] D. Savitsky and P. W. Brown, "Procedures for hydrodynamic evaluation of planing hulls in smooth and rough water," *Journal of Marine Technology,* vol. 13, no. 4, pp. 381-400, 1976.

[32] O. Faltinsen, "The effect of hydroelasticity on ship slamming," *Philosophical Transactins of The Royal Society of London A,* vol. 355, pp. 575-591, 1997.

[33] O. Faltinsen, J. Kvalsvold and J. Aarsnes, "Wave impact on a horizontal elastic plate," *Marine Science and Technology,* vol. 2, no. 2, pp. 87-100, 1997.

[34] E. Haugen, "Hydroelastic analysis of slamming on stiffened plates with application to catamaran wetdeck," *Thesis Deparment of Marine Hydrodynamics, Norwegian University of Science and Technology,* 1999.

[35] R. Zhao, O. Faltinsen and J. Aarnes, "Water entry of arbitrary two-dimensional bodies," *Journal of Fluid Mechanics,* vol. 246, pp. 593-612, 1993.

[36] A. Fairlie-Clarkea and T. Tveitnes, "Momentum and gravity effects during the constant velocity water entry of wedge-shaped sections," *Ocean Engineering,* vol. 35, no. 7, pp. 706-716, 2008.

[37] L. Olovsson and M. Souli, "Improved Fluid-Structure Capabilities in LS-DYNA,"

Proceedings of the 3rd European LS-DYNA Users Conference Paris, 2001.

[38] I. Stenius, A. Rosén and J. Kuttenkeuler, "Explicit FE-modelling of fluid-structure interaction in hull-water impacts," *International Shipbuilding Progress,* vol. 53, no. 2, pp. 103-121, 2006.

[39] I. Stenius, A. Rosén and J. Kuttenkeuler, "Explicit FE-Modelling of hydroelasticity in panel-water impacts," *International Shipbuilding Progress,* vol. 54, no. 2-3, pp. 111-127, 2007.

[40] J. Aarsnes and R. Hoff, "Full scale with Ulstein test vessel," *Technical Report MT60 F98-205,* 1998.

[41] J. Lee and P. A. Wilson, "Experimental Study of the hydro-impact of slamming in a modern racing sailboat," *Journal of Sailboat Technology,* 2010.

[42] M. Hentinen and G. Holm, "Load measurement on the 9.4m sailing yacht 'sail lab'," *Proceedings, 13th International Symposium on Yacht Design and Yacht Construction Amsterdam,* 1994.

[43] R. Reichard, "The structural response of small craft to dynamic loading," *Proceedings of the 14th AIAA Symposium on the Aero/Hydronautics of Sailing,* vol. 30, pp. 105-110, 1984.

[44] A. Rosen and K. Garme, "Slamming Studies on High Speed Planing Craft Thorugh Full-Scale Trials and Simulations," *Proceedings 5th International Conference on Fast Sea Transportation Seattle,* 1999.

[45] W. Sottorf, "Experiments with planing surfaces," *Technical Report NACA-TM-661,* 1932.

[46] T. Tveitnes, A. Fairlie-Clarke and K.Varyani, "An experimental investigation into the constant velocity water entry of wedge-shaped sections," *Ocean Engineering,* vol. 35, no. 14-15, pp. 1463-1478, 2008.

[47] R. Wraith, "Pressure Loads on Ship Hull Plating Caused by Slamming," *PhD Thesis Department of Mechanical and Manufacturing Engineering University of Melbourne,* 1998.

[48] M. Battley and S. Lake, "Designing Composite Structures for Slamming Loads," *2nd High Performance Yacht Design Conference Auckland,* pp. 177-184, 2006.

[49] M. Battley and S. Lake, "Dynamic Performance of Sandwich Core Materials," *16th International Conference on Composite Materials Kyoto,* pp. 1-10, 2008.

[50] M. Battley, T. Allen, J. Schierlink, S. Lake and P. Pehrson, "Hydroelastic Behaviour of Slam Loaded Composite Hull Panels," *3rd High Performance Yacht Design Conference Auckland,* pp. 37-46, 2008.

[51] M. Battley, "Effects of panel stiffness on slamming responses of composite hull panels," *17th International Conference on Composite Materials Edinburgh,* 2009.

[52] I. Stenius, A. Rosen, M. Battley and T. Allen, "Experimental Hydroelastic Characterization of Slamming Loaded Marine Panels," *Ocean Engineering,* vol. 74, pp. 1-15, 2013.

[53] O. Faltinsen, "Water entry of a wedge by hydroelastic orthotropic plate theory," *Journal of Ship Research,* vol. 43, pp. 180-193, 1999.

[54] M. Samuelides and G. Katsaounis, "Experimental modelling of wet deck slamming," in *4th International Conference on Fast Sea Transportation*, Sydney, 1997.

[55] D. Dessi, "Whipping-based criterion for the identification of slamming events," *International Journal of Naval Architecture and Ocean Engineering,* vol. 6, pp. 1082-1095, 2014.

[56] Y. Kim, J.-H. Kim and Y. Kim, "Identification of Whipping Response using Wavelet Cross-Correlation," *Journal of the Society of Naval Architects of Korea,* vol. 51, no. 2, pp. 122-129, 2014.

[57] W. Amin, M. Davis, G. Thomas and D. Holloway, "Analysis of wave slam induced hull vibrations using continuous wavelet transforms," *Ocean Engineering,* vol. 58, pp. 154-166, 2013.

[58] C. Torrence and G. P. Compo, "A Practical Guide to Wavelet Analysis," *Bulletin of the American Meteorological Society,* vol. 79, no. 1, pp. 61-78, 1998.

[59] J. Lardies and S. Gouttebroze, "Identification of modal parameters using the wavelet transform," *International Journal of Mechanical Sciences,* vol. 44, pp. 2263-2283, 2002.

[60] C. Ikeda and C. Judge, "Slamming Impacts of Hydrodynamically-Supported Craft," in *ASME 2014 33rd International Conference on Ocean, Offshore and Arctic Engineering*, 2014.

[61] W. He, M. Diez, Z. Zou, E. Campana and F. Stern, "URANS study of Delft catamaran total/added resistance, motions and slamming loads in head sea including irregular wave and uncertainty quantification for variable regular wave and geometry.," *Ocean Engineering,* vol. 74, pp. 189-217, 2013.

[62] S. M. Mousaviraad, Z. Wang and S. F., "URANS Studies of Hydrodynamic Performance and Slamming Loads on High-Speed Planing Hulls in Calm Water and Waves For Deep and Shallow Conditions," in *3rd International Conference on Ship Maneuvering in Shallow and Confined Water:Ship Behaviour in Locks*, Ghent, Belgium, 2013.

[63] T. Fu, K. Brucker, S. Mousaviraad, C. Ikead, E. Lee, T. O'Shea, Z. Wang, F. Stern and C. Judge, "An Assessment of Computational Fluid Dynamics Predictions of the Hydrodynamics of High-Speed Planing Craft in Calm Water and Waves," in *30th Symposium on Naval Hydrodynamics*, Hobart, Tasmania, Australia, 2014.

[64] J. Huang, P. Carrica and F. Stern, "Semi-coupled air/water immersed boundary approach for curvilinear dynamic overset grids with application to ship hydrodynamics," *International Journal Numerical Methods Fluids,* vol. 58, no. 6, pp. 591-624, 2008.

[65] A. Bereznitski, "Slamming: the role of hydroelasticity," *International Shipbuilding Progress,* vol. 48, no. 4, pp. 333-351, 2001.

[66] C. H. Lu, H. Y. S. and G. X. Wu, "Coupled analysis of nonlinear interaction between fluid and structure during impact," *Journal of fluids and structures,* vol. 14, no. 1, pp. 127-146, 2000.

[67] T. Khabakhpasheva and A. Korobkin, "Approximate models of elastic wedge impact," in *18th International Workshop on Water Waves and Floating BOdies*, Le Croisic, France, 2003.

10. Vita

Robert Thodal was born January 30, 1986 in Middlebury, Vemont to Sally and Richard Thodal. Robert attended Middlebury Union High School, graduating in May 2004. He began his studies at Lehigh University in the fall of 2004. As an undergraduate Robert was on the dean's list, a member of honor societies including Pi Tau Sigma and Tau Beta Pi and the recipient of the Victaulic Award in Mechanical Engineering and Mechanics. Robert worked as an undergraduate research assistant at the Lehigh Energy Research Center in the summer of 2007. He graduated with a Bachelor of Science Degree in Mechanical Engineering in May 2008, minoring in Aerospace Engineering and receiving highest honors. In the summer of 2008 he was employed as an engineering intern at Mack Trucks.

Robert started graduate studies in Mechanical Engineering at Lehigh University in the fall of 2008. He was a teaching assistant and recipient of awards including the Presidential Scholarship and the Excellence in Polymer Science and Engineering Award from the Society of Plastic Engineers Lehigh Valley Section. While working as a research assistant in the Lehigh Composites Lab under Professor Joachim Grenestedt, Robert conducted research in the field of composites and hydrodynamic impact of high speed craft. In September, 2010 he received a Master of Science Degree in Mechanical Engineering, continuing his studies as a Ph.D student. Robert began work as an Aero Structures and Composites Engineer at Joby Aviation in Santa Cruz, California in October, 2015.